Dissertation

zur Erlangung des Grades

"Doktor der Naturwissenschaften"

im Promotionsfach Chemie

am Fachbereich Chemie

der Johannes Gutenberg-Universitat Mainz

Superconductivity in hydrogen-rich materials at high pressures

Alexander Drozdov

geboren in Troitsk

Mainz, 2016

Zusammenfassung

Ein Raumtemperatur-Supraleiter ist wahrscheinlich eines der begehrtesten Systeme in der Festkörperphysik. Die höchste Sprungtemperatur (T_c) wurde bisher im Kupferoxid-System erreicht: 133 Kelvin (K) bei atmosphärischem Druck ([82]Schilling et al. 1993) und 160 K unter erhöhtem Druck ([42]Gao et al. 1994). Der Mechanismus der Supraleitung in den Kupraten und in der vor Kurzem entdeckten eisenbasierten Supraleiterfamilie (T_c = 57 K) ist noch immer nicht vollständig verstanden. Dem entgegen stehen die konventionellen Supraleiter, die gut durch die Bardeen-Cooper-Schrieffer-Theorie (BCS-Theorie) beschrieben werden. Mit großem Aufwand wurde daher nach konventionellen Hochtemperatur-Supraleitern (T_c > 77 K) gesucht, aber die höchste gefundene Sprungtemperatur beträgt nur 39 K in MgB_2 ([68]Nagamatsu et al. 2001).

Die BCS-Theorie beschränkt T_c nicht, wie aus Eliashbergs Erweiterung der BCS-Theorie folgt. T_c kann hoch sein, wenn eine günstige Kombination aus hochfrequenten Phononen, starker Elektron-Phonon-Kupplung und einer großen Zustandsdichte zustande kommt. Die Theorie sagt allerdings nicht voraus, in welchen Materialien diese drei Parameter hoch sind. Klar ist zumindest, dass Materialien aus leichten Elementen hohe Frequenzen in ihren Phonon-Spektren aufweisen.

Das leichteste Element ist Wasserstoff und Ashcroft sagte als erster voraus, dass metallischer Wasserstoff ein Hochtemperatur-Supraleiter sein würde ([6]Ashcroft 1968). Da der zur Metallisierung von Wasserstoff benötigte Druck (etwa 400-500 GPa) für die damals verfügbaren experimentellen Techniken noch zu hoch war, schlug er vor, dass durch Wasserstoff dominierte Verbindungen (Hydride) auch gute Hochtemperatur-Supraleiter sein könnten.

Viele darauffolgende Berechnungen unterstützten diese Idee. T_c im Bereich von 50-235 Kelvin wurde für viele Hydride vorhergesagt. Leider wurde bisher nur eine moderate T_c von 17 Kelvin experimentell beobachtet ([27]Eremets et al. 2008). Ein Ziel der vorliegenden Arbeit ist es, ein Wasserstoff-dominiertes Material mit einer höheren T_c zu finden.

Contents

Introduction

A room temperature superconductor is probably one of the most desired systems in solid state physics. The highest critical temperature (T_c) that has been achieved so far is in the copper oxide system: 133 kelvin (K) at ambient pressure ([82]Schilling et al. 1993) and 160 K under pressure ([42]Gao et al. 1994). The nature of superconductivity in the cuprates and in the recently discovered iron-based supercondutor family (T_c=57 K) is still not fully understood. In contrast, there is a class of superconductors which is well-described by the Bardeen, Cooper, Schrieffer (BCS) theory - convetional superconductors. Great efforts were spent in searching for high-temperature (T_c > 77 K) conventional superconductor but only T_c = 39 K has been reached in MgB_2 ([68]Nagamatsu et al. 2001).

BCS theory puts no bounds for T_c as follows from Eliashberg's formulation of BCS theory. T_c can be high, if there is a favorable combination of high-frequency phonons, strong electron–phonon coupling, and a high density of states. It does not predict however in which materials all three parameters are large. At least it gives a clear indication that materials with light elements are favorable as light elements provide high frequencies in the phonon spectrum.

The lightest element is hydrogen, and Ashcroft made a first prediction that metallic hydrogen will be a high-temperature superconductor ([6]Ashcroft 1968). As pressure of hydrogen metallization was too high (about 400-500 GPa) for experimental techniques then he proposed that compounds dominated by hydrogen (hydrides) also might be good high temperature superconductors ([6]Ashcroft 1968; [7]Ashcroft 2004).

A lot of the followed calculations supported this idea. T_c in the range of 50–235 kelvin was predicted for many hydrides. Unfortunately, only a moderate T_c of 17 kelvin has been observed experimentally ([27]Eremets et al. 2008) so far. A goal of the present work is to find a hydrogen-dominant material with higher T_c.

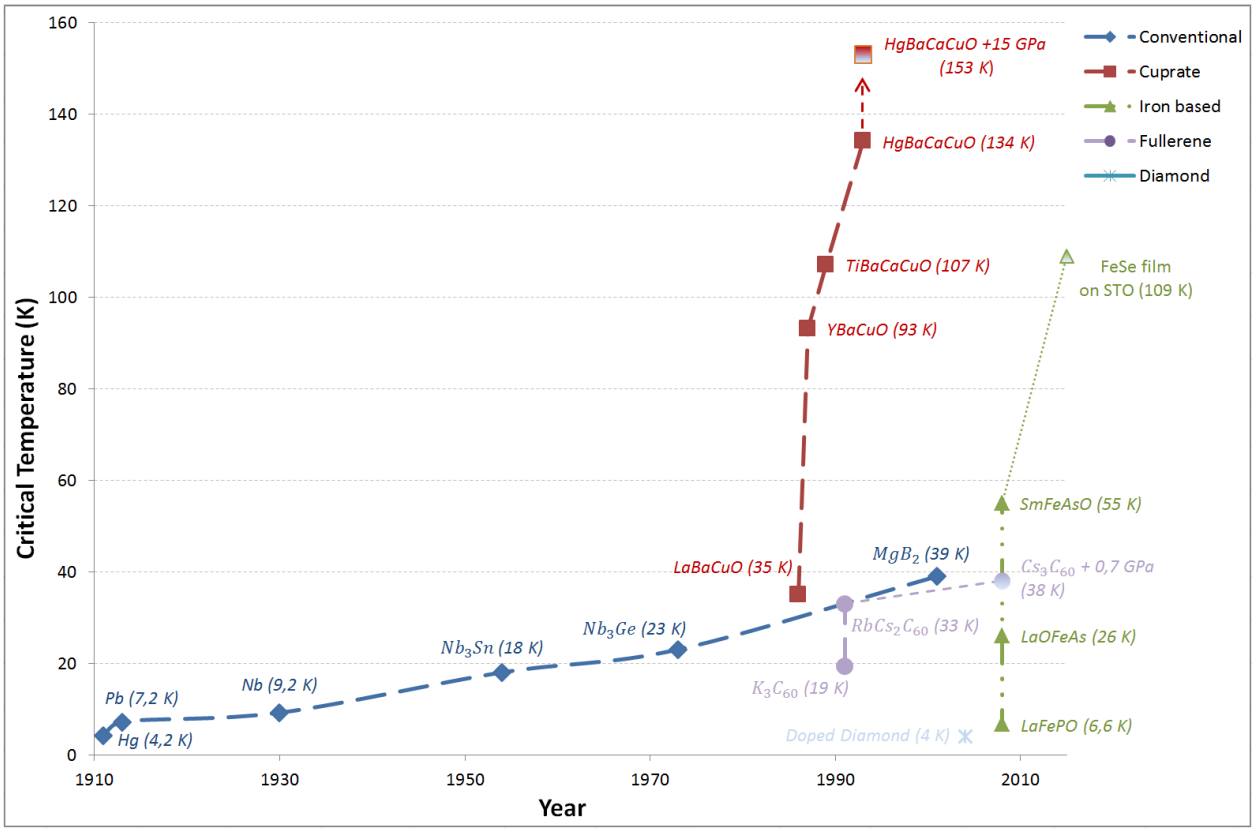

Figure 0.1 – Main discovered superconducting critical temperatures for different materials

Figure 0.1 shows a timeline of discovered superconductors. Blue rhombuses show conventional superconductors that are described by BCS theory. Red shaded squares show copper oxide systems (cuprate). Red open square shows cuprate superconductors under pressure. Green triangles show iron-based superconductors.

	Category	Material class	Year	Max Tc material	T_c (K)	ξ (Å)	$2\Delta/k_B T_c$	λ_L(Å)	dT_c/dP
C1	conv	Elements, alloys and simple compounds	1911	Nb	9,5	380	390	3,8	+/–
	conv		1912	NbN	17	50	2000	4,1	+/–
C2	conv	A15's	1954	Nb_3Ge	23,2	55	1000	4,2	+
C3	conv	Doped semiconductors	1964	CB_x	10	950	720	3,5	–
C4	conv	Insul. elements under pressure	1964	S	17				+
C5	conv	Intercalated graphite	1965	C_6Ca	11,5	380	720	3,6	+
C6	conv	Metallic elements under pressure	1968	Ca	25				+/–
C7	conv	Hydrogen-rich materials	1970	PdD	10,7	400		3,8	+/–
C8	conv.	Layered t. m. dichalcogenides	1970	NbS_2	7,2	100	1250	3,7	–
C9	conv	Chevrel phases	1971	$PbMo_6S_8$	15	30	3000	4,7	+/–
C10	conv	Magnetic superconductors	1972	$ErRh_4B_4$	8,7	180	830	4	+/–
C11	conv	Thin films	1978						
C12	conv	Magnesium diboride	2001	MgB_2	39	52	1400	4,5	–
P1	poss unc	Bismuthates	1975	$Ba_{1-x}K_xBiO_3$	34	50	5500	4	–
P2	poss unc	Fullerenes	1991	$RbCs_2C_{60}$	33	30	4500	3,5 - 5,0	–
P3	poss unc	Borocarbides	1993	$YPd_5B_3C_{0,3}$	23	100	1000	4	+/–
P4	poss unc	Plutonium compounds	2002	$PuCoGa_5$	18,5	16	2400	5–8	+/–
P5	poss unc	Interface superconductivity	2007	$LaAlO_3/SrTiO_2$	0,35	600			
P6	poss unc	Aromatic hydrocarbons	2010	$K-doped\ DBP$	33	180	770		+/–
P7	poss unc	Doped top. ins.	2010	$Cu_x(PbSe)_5(Bi_2Se_3)_6$	3	110	13 000		
P8	poss unc	*BIS2* - based materials	2012	$YbO_{0,5}F_{0,5}BiS_2$	5,4	53	5000	7,2	+/–
P9	poss unc	Unstable/elusive sc	1946	$C-S$	300?				
U1	unconv	Heavy fermions	1979	UPd_2Al_3	2	50	4000		+/–
U2	unconv	Organic charge-transfer	1980	$(BEDT-TTF)_2X$	13,4	100	5000	4,4	–
U3	unconv	Cuprates hole-doped	1986	$HgBa_2Ca_2Cu_3O_9$	134	20	1200	4,3	+
U4	unconv	Cuprates e-doped	1989	$Sr_{0,9}La_xCuO_2$	40	50	2500	3,5	–
U5	unconv	Strontium ruthenate	1994	Sr_2RuO_4	1,5	660	1500		–
U6	unconv	Layered nitrides	1996	$Ca(THF)HfNCl$	26	60	4700	2,9–10	–
U7	unconv	Ferromagnetic sc	2000	UGe_2	0,8	100		$\sim 10^4$	+/–
U8	unconv	Cobalt oxyde hydrate	2003	$Na_x(H_3O)_2CoO_2 \cdot yH_2O$	4,7	100	7000	4,3–4,6	–
U9	unconv	Non-centro-symmetric	2004	$SrPtSi_3$	2	60	8000		
U10	unconv	Iron pnictides	2008	$SmFeAsO_{0,85}$	55	10–50	2000	7,5	+/–
U11	unconv	Iron chalcogenides	2008	$Na_xFe_2Se_2$	46	20	2000	3,8	+

Table 0-1 Classes of superconducting materials ([48]Hirsch et al. 2015)

- C – Conventional
- P - possibly unconventional
- U - unconventional.

Table 1-1 shows an existing classes of superconductors. T_c column shows the highest achieved critical temperature in the class. Typical values of the coherence length ξ, penetration depth λ_L and gap ratio are given.

Chapter 1
Superconductivity

1.1 Brief history

Superconductivity was discovered in 1911-year by the Dutch physicist Kamerlingh Onnes. At that time it was already known that: electrons are responsible for conductivity; scattering of electrons on the ions is a source of resistance and that resistance of the metals decreases with temperature decreasing. Physicists were interested what will happen when the temperature approaches zero. There were three different theories (Fig. 1.1):

- Resistance will increase to infinity cause electrons will be frozen (Kelvin)
- Resistance will approach zero with temperature (Dewar)
- Resistance will flatten at some finite point because of impurities in sample (Matthiessen)

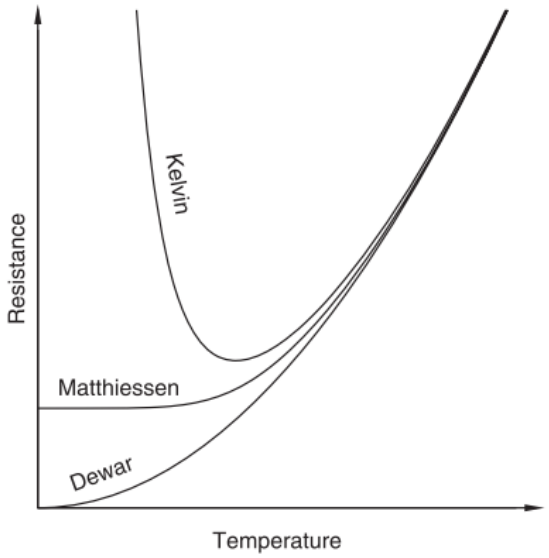

Figure 1.1 - Three theories of resistance behavior near zero temperature

Experiments with gold and platinum were showing that Matthiessen's theory was right, and purity of the sample defines its residual resistance. Kamerlingh Onnes believed in Dewar's theory that resistance should approach zero. He believed that residual resistance in all experiments can be explained by the not pure enough samples, and the supremely pure sample

will have zero resistance at zero temperature. Metal for which Onnes could get the purest sample was mercury, and he decided to study what lowest resistance can be obtained. In 1911, Onnes and his student Gilles Holst cooled down the sample of mercury and the resistance dropped to zero at T=4.2 K - it was the first observation of a superconducting transition (Fig. 1.2). In fact in the same experiment they also for the first time in the world saw a superfluid transition of helium. At 1.8K a boiling of the helium stopped and its level begin to decrease very fast. They didn't realize a reason of this phenomenon and focused on the zero resistance because it was much more catching.

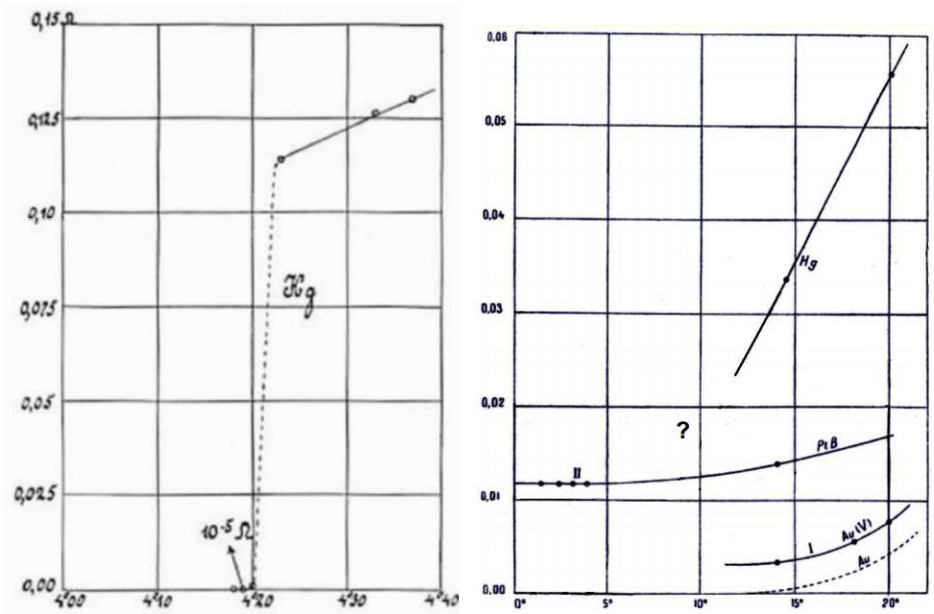

Figure 1.2
a) The historical plot of the temperature dependence of Hg resistance (Onnes notebook). b) Resistance dependence on temperature of Hg, Pt and Au. Pt doesn't have a superconductive transition at helium temperatures

In contrast to the expectations of Onnes that the resistance of the mercury would go smoothly to zero, it abruptly dropped at some temperature. The purity of the sample, however, effects on the sharpness of resistance drop. In the contaminated samples, the superconductive transition is smother and shifts to the higher temperatures. In the purest samples, the resistance drop can be within 10^{-5} K. Discovering of other superconducting metals wasn't fast. One of the reasons was that very low temperature was required while only Onnes's laboratory could liquefy helium for fifteen years after discovery of superconductivity.

In 1914, Kamerlingh Onnes discovered that magnetic field shifts a critical temperature to the lower values. Very important step to understanding the nature of superconductivity has been done by Hans Meissner and Robert Ochsenfeld in 1933: they discovered that superconductor expels the magnetic flux at the temperatures lower than critical.

The first theoretical explanation of magnetic flux behavior in the superconductors was done in 1935 in England by two immigrated German physicists - Fritz London and Heinz London. In 1950, Ginzburg and Landau published their phenomenological theory of superconductivity.

Microscopic mechanism of superconductivity remained to be elusive. An apparent similarity of superconductivity and superfluidity indicated that superconductivity caused by boson particles as first was proposed by Ogg in 1946 ([72]Ogg 1946). He was trying to explain his discovering of high-temperature superconductivity (180-190 kelvin) in the sample of dissolved sodium in the liquid anhydrous ammonia and hypothesized that the pairing electrons (bosons) are responsible for the superconductivity. But in the later experiments superconductivity was not confirmed (this key issue has not yet been finally settled). Because of this his great insight about pairing electrons was discredited.

During many years of intensive work a lot of experimental facts were accumulated. The most important apparently is the isotope effect in Hg ([64]Maxwell 1950): T_c depends as square root of the mass of the atom. This result clearly indicates that an interaction with the lattice is involved into the phenomenon of superconductivity.

Almost ten years later in 1957 year Bardeen, Cooper and Schrieffer published a microscopic theory of superconductivity (BCS theory) which very successfully explained all the accumulated experimental data and gave a deep insight to the phenomenon of superconductivity. The key idea was a pairing of electrons.BCS theory states that below critical temperature it's energetically more preferable that two electrons with opposite spin and momenta will form a pair. Such pair of electrons can be considered as a new particle, and it's called Cooper pair. Cooper pair has a zero spin and appears to be a boson. The distance between two paired electrons is very large: Cooper pair's size can be few hundred of lattice spaces. One Cooper pair «contains» a lot of electrons which also form another Cooper pairs. All these merged bosons (Cooper pairs) exist on the same energy level (ground level) and form collective quantum wave called a Bose-Einstein condensate (Fig. 1.3). This collective quantum wave responses on the externally applied influence (voltage or magnetic field) and transmits excitation (current) through the material without resistance. Thus, superconductivity becomes possible. Good presentation of the Bose-Einstein condensation can be seen here: https://youtu.be/shdLjIkRaS8

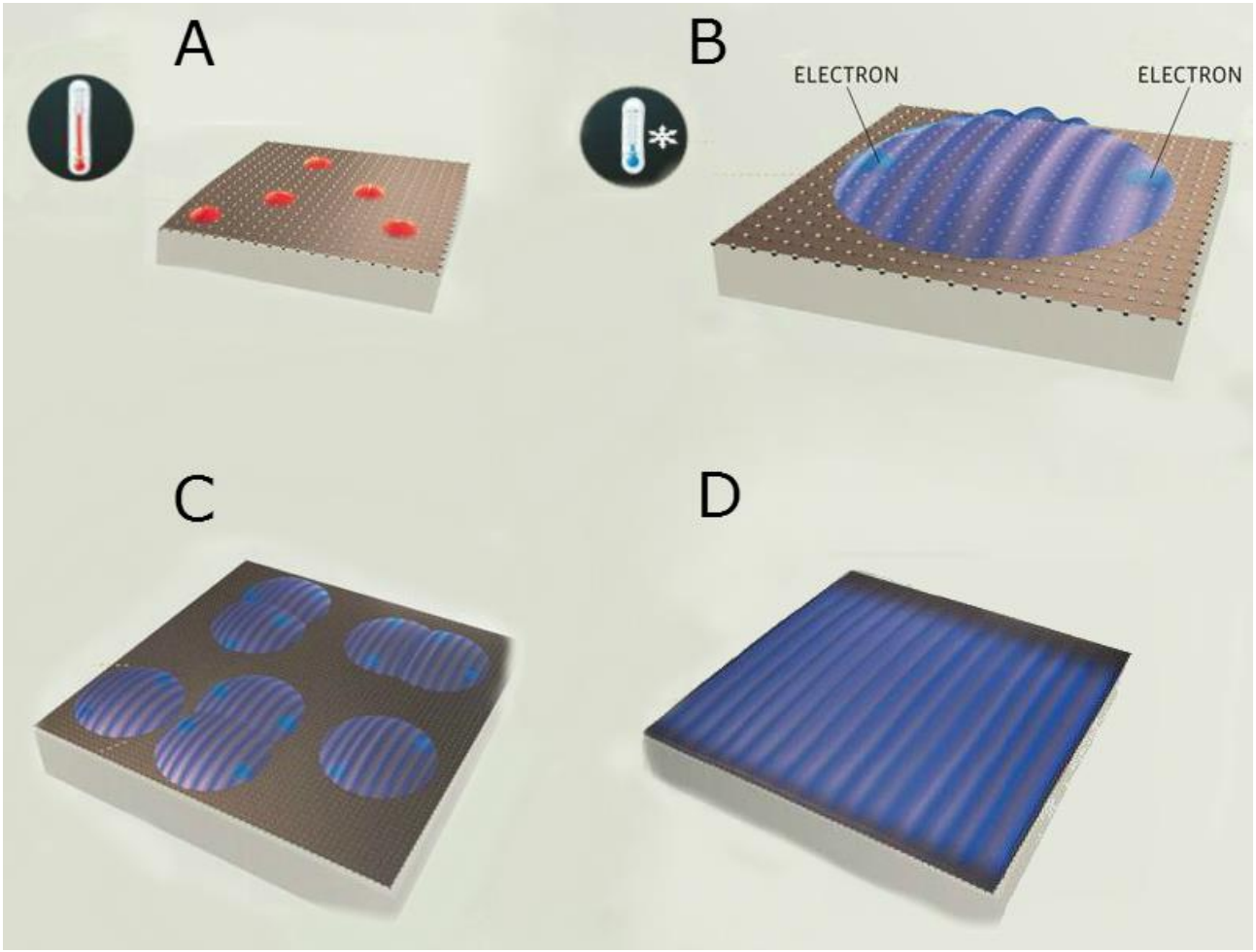

Figure 1.3– Superconductivity appearing
a) At the temperature higher than critical electrons move freely in the lattice
b) After cooling below the critical temperature electrons form a Cooper pair
c) There is a lot intersected Cooper pairs
d) All merged Cooper pairs form a collective quantum wave – Bose-Einstein condensate

High importance for the understanding of superconductivity was a work of Abrikosov in 1957 year ([1]Abrikosov 1957) who explained the difference between superconductors of types I and II and predicted vortexes of magnetic field in the type II superconductors.

The understanding of the phenomenon of superconductivity did not lead to a quick progress in finding of materials with higher T_c. The BCS theory does not have a real predicted power – superconductivity depends on several parameters. Highest superconductive temperature from 1954 till 1979 year was 18 K in Nb_3Sn and from 1979 till 1986 it was Nb_3Ge with 23,2 K.

Superconductivity in MgB_2 at 39 K was discovered only in 2001 year by Nagamatsu ([68]Nagamatsu et al. 2001) and now it is used as superconductive wires in MRI scanners. It's interesting that in the same 1957 year with BCS theory heat capacity measurement of MgB_2 from

18 to 304 kelvin was published ([89]Swift, White 1957), but no signs of superconductivity were recognized. Over than forty years this material was laying on the shelves.

A real breakthrough, but in completely another class of materials has been done 1 June 1986 by Bednorz and Muller. They reported about possible superconductivity at 30 K in ceramic material – barium doped oxide of copper and lanthanum ([8]Bednorz, Muller 1986).

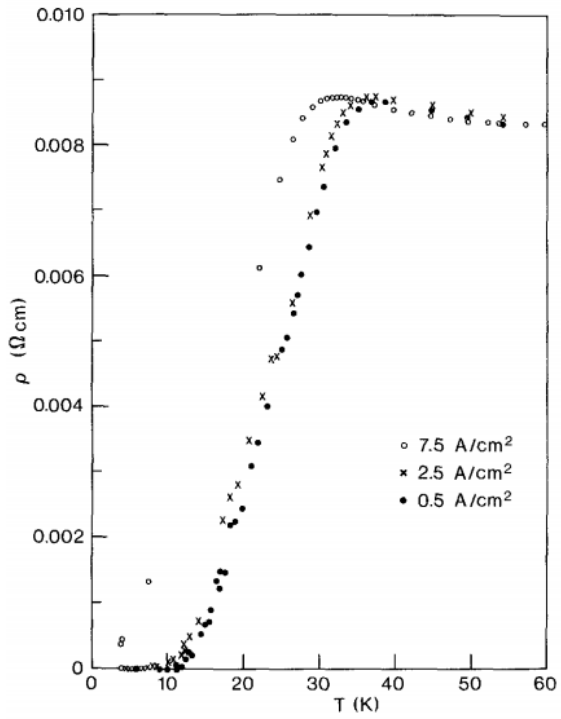

Figure 1.4 - Historical graph of temperature resistivity dependence with different currents in Ba−La−Cu−O system.

This result induced very high interest to this type of materials. In less than one year, to the end of January 1987, the highest superconducting temperature already was 93 kelvin – more than the temperature of liquid nitrogen (and therefore these superconductors are called high temperature superconductors - HTSC). Today the highest superconductive temperature reached in cuprate systems is 133 K at ambient pressure ([82]Schilling et al. 1993) and 160 K under pressure ([42]Gao et al. 1994).

It is interesting to notice hystorically that cuprate system was synthesized and described by Shaplygin in 1979 ([84]Shaplygin et al. 1979), but resistance was not measured till helium temperatures cause they didn't have helium in the lab. Independently, group of Reveau ([70]Nguyen et al. 1981) synthesized and studied cuprate system but also didn't measure its resistivity below liquid nitogen temperatures ([69]Nguyen et al. 1983). Good review of the existing superconducting materials and classes was done by Hirsch ([48]Hirsch et al. 2015).

1.2 Properties of superconductivity

Zero Resistance

One of the main properties of superconductivity is zero resistance. However, the measurement of the zero resistance takes some precaution. There were quite a lot of cases when zero resistance was measured but afterward superconductivity wasn't proven. One of a typical mistake is the following. If below a certain temperature the current stops to flow for some reason (for instance, the resiatance of the electrodes became too high) the measured difference of the potentials is zero – the same as in the case of superconductivity.

The most impressive demonstration of the free current flow is with the aid of the superconducting loop. In 1914, Kamerlingh Onnes conducted such an experiment. In the presence of magnetic field, a small loop made from lead was placed into the helium temperatures (1,8 K) then a superconducting current was induced in the loop by removing the magnetic field. The loop produced its own magnetic field which was detected by a compass placed near the cryostat, and thus Onnes was able to monitor the changing of the superconducting current in the loop. He had an opportunity to conduct measurements for about one hour until liquid helium didn't evaporate, and he didn't observe any changes in the current. Later the same experiment was repeated, but the duration of monitoring was more than one year, and the result was the same – no changes of the current.

Superconducting transition in magnetic field

Another crucial property of superconductors is expulsion of a magnetic field after the superconducting transition. When the temperature of a superconductor is higher than the critical temperature magnetic field will penetrate into the material. At the temperatures lower than T_c surface current will appear inside the superconductor, and it will screen the superconductor from the external magnetic field.

In the presence of a magnetic field critical temperature T_c decreases. Each superconducting material has each own limit of the critical magnetic field (H_c) at which superconductivity can exist. After magnetic field exceeds this limit, material behaves as a normal metal.

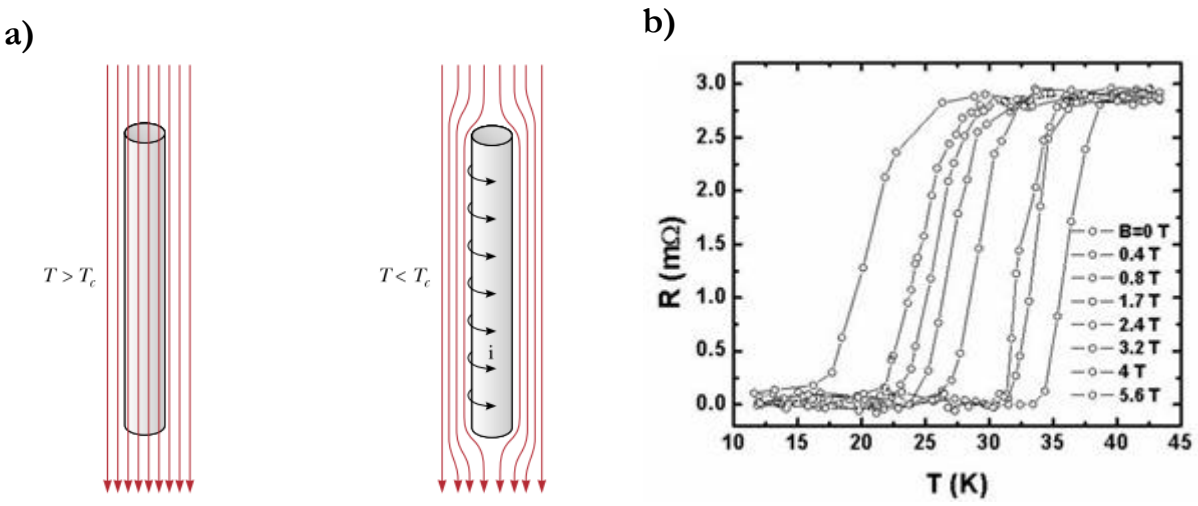

Figure 1.5
a) Type I superconductors in the presence of magnetic field at temperatures below T_c and higher than T_c
b) Shift of T_c in presence of magnetic field in MgB_2

Approximate dependence of H_c on temperature is:

$$H_c(\mathrm{T}) = H(0)\left[1 - \left(\frac{T}{T_c}\right)^2\right]$$

Typical critical magnetic field of elemental superconductors is presented in table:

Superconductor	T_c, K	$H_c(0)$, Oe
Hg	4.15	411
Pb	7.19	800
Al	1.19	105
Ta	4.47	830
Ga	1.08	58

Table 1-1 Typical critical magnetic field of elemental superconductors

For comparing: the magnetic field of the Earth is 0.5 oersted. The magnetic field produced by the wire of an electrical teapot is about 10 oersted.

Type I superconductors: critical currents, depth of penetration of magnetic field

A current of a high density also can destroy superconductivity because current in the superconductor induces a magnetic field. When this magnetic field will exceed critical value H_c - superconductivity will disappear.

In the type I superconductor magnetic field does not penetrate into the bulk and current flows in the thin volume near the surface of the superconductor. A magnetic field also exists in this thin layer and decreases exponentially from external value to zero.

$$H(x) = H_0 e^{-x/\lambda}$$

Figure 1.6 shows magnetic field and current density dependence on the distance from the edge of the superconducting wire. Penetration depth is taken as depth on which magnetic field decreases in e times. It's called London penetration depth - λ_L .

a)

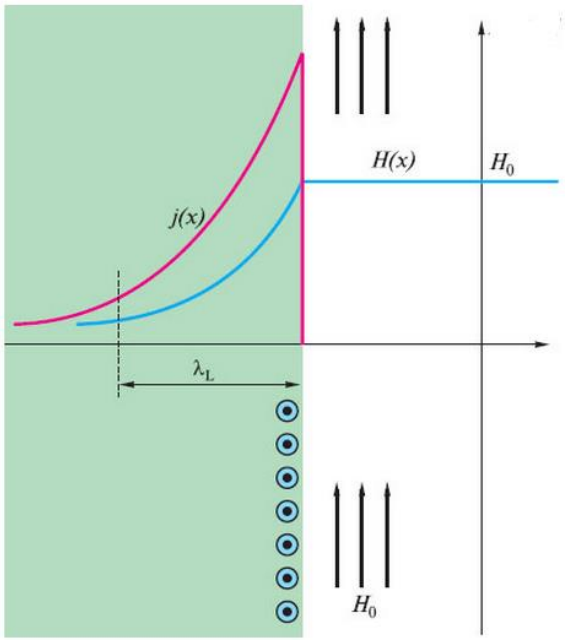

b)

Superconductor	T_c, K	λ_L (0), nm	Atomic distance, nm
Hg	4.15	41	0.3
Pb	7.19	39	0.34
Nb	9.26	47	0.286
Al	1.19	50	
MgB_2	39	140	
V	5.3	110	0.26
Nb_3Ge	23	100	

Figure 1.6
a) Magnetic field and current density inside superconducting wire
b) Typical values of London penetration depth and atomic distance for comparing. In type I superconductors currents flow in the depth of few hundreds atomic layers.

London penetration depth changes with temperature:

$$\lambda(T) = \lambda_0 \left[1 - \left(\frac{T}{T_c}\right)^2\right]^{-1/2}$$

The penetration of magnetic field increases with temperature increasing. At the critical temperature it becomes infinite, and sample becomes a normal metal.

Type II superconductors

Type I superconductors expel magnetic field until it doesn't exceed some critical value H_c. In the magnetic field higher than H_c sample becomes a normal metal.

There is another type of behavior of superconductor in a magnetic field which corresponds to type II superconductors.

Type II superconductors also expel magnetic field till some critical value H_{c1}. After magnetic field exceeds H_{c1} it doesn't destroy superconductivity. The magnetic field can penetrate into the type II superconductor and material still conducts with zero resistance until magnetic field will not exceed another critical value H_{c2}. The state between H_{c1} and H_{c2} is called mixed state or vortex state.

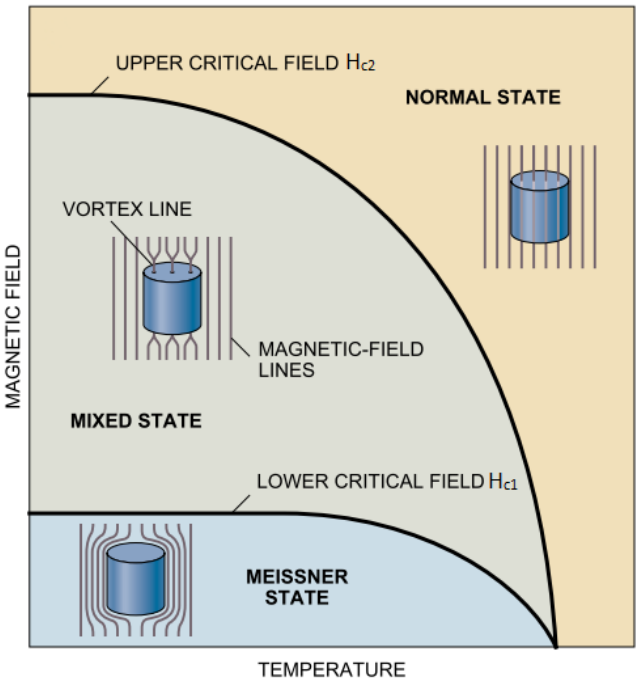

Figure 1.7 The magnetic field - temperature diagram of type-II superconductor.

A vortex state of superconductors was theoretically predicted and described by Abrikosov ([1]Abrikosov 1957). In this mixed state cylindrical swirls of supercurrents are induced in the material. These superconductive swirls form strings of normal metal in the material through which magnetic field can pass. The typical diameter of such vortex is about 100 nm.

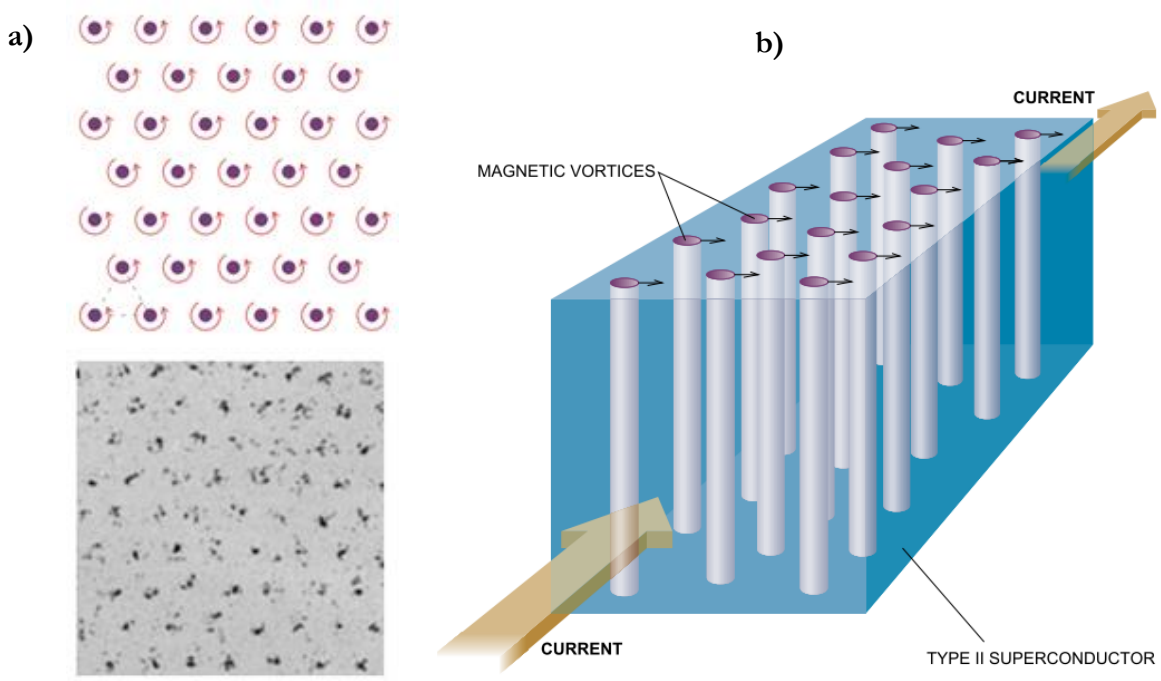

Figure 1.8 – Vortices in type II superconductor

Increasing of the magnetic field value doesn't impact on the diameter of vortices, but the number of vortices increases, and the distance between them decreases.

Superconducting currents which surround vortices repel from each other and vortices find places with a maximum distance from each other. They form a triangular lattice which can be seen on Figure 1.8a.

A typical value of H_{c1} in the type II superconductor is smaller than H_c in the type I superconductor, but H_{c2} is much higher than H_c.

Superconductor	Type	T_c, K	$H_c(0)$, Oe
Hg	Type I	4.15	411
Pb	Type I	7.19	800
Ga	Type I	1.08	58
Al	Type I	1.19	105
Ta	Type I	4.47	830
Nb_3Sn	Type II	18.3	300 000 (H_{c2})
Nb_3Ge	Type II	20.3	370 000 (H_{c2})
MgB_2	Type II	39	740 000 (H_{c2})

Magnetic flux quantization

If to place a ring from a superconducting material to the magnetic field at the temperature higher than T_c, the magnetic field will go through the material of the ring and through the hole. If $T<T_c$ the magnetic field will be expelled from the ring's material, and superconductive current will appear in the ring. Then, after turning off the magnetic field, the superconductive current will still flow through the ring, and we will get a "captured" magnetic field in the hole.

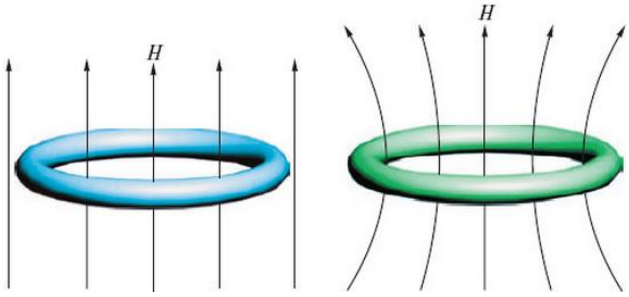

Figure 1.9 Capture of magnetic field by the superconductive ring

It's predicted by London theory and experimentally proved that magnetic flux through such ring is quantized, and quantum of magnetic flux is $\Phi_0 = {}^{h}/_{2e} = 2{,}07 * 10^{-15} Wb$.

This equation shows that superconducting current is transported by particles with charge equal to $2e$.

Value Φ_0 is the same for any superconductor and one vortex in a type II superconductor transmits one quantum of magnetic flux Φ_0. For illustration - magnetic flux from Earth's magnetic field through the wedding ring contain about 5 million quanta Φ_0.Flux quantization was experimentally proved by two groups in 1961 ([16]Deaver, Fairbank 1961; [17]Doll, Näbauer 1961).

Bardeen-Cooper-Schrieffer theory

Besides the above described properties of superconductors numerous important experimental and theoretical results were obtained and lead to the work of Bardeen, Cooper and Schrieffer in 1957. Among these results following can be emphasized:

- Survey of superconductor's crystal lattice structure
- Evidence of band gap which separates superconducting electrons with normal ones
- Isotopic effect in superconductors

Survey of superconductor's crystal lattice structure

X-ray crystallographic surveys showed that there is no any special "superconductive structure". Changing of the structure was not observed during the superconducting transition. Another idea was that superconductivity is a property of specific atoms. But this idea also appeared to be wrong. The materials which consist of the same atoms can have or don't have a superconducting transition depending on the structure of the lattice. However, it was shown that structure arrangement of the atoms is important. For example, white tin with tetragonal structure has a superconducting transition at 3.72 K, but gray tin with the diamond cubic structure doesn't have a superconductivity.

Band Gap

Heat capacity measurements of Niobium ([11]Brown et al. 1953) and Vanadium ([13]Corak et al. 1954) was first solid evidence of energy gap existence near the Fermi level. Afterward, band gap existence was confirmed by absorption measurements in far infrared – microwave spectra range ([10]Blevins et al. 1955).

Heat capacity in metals has the following dependence on temperature:

$$C = \gamma T + \beta T^3$$

The first term γT is a contribution due to electrons thermal excitations. In normal metals at low temperatures second term βT^3 (phonon contribution) can be neglected and dependence of the heat capacity on the temperature is almost linear. For superconductors heat capacity has an exponential dependence in the temperature interval from zero to T_c and at higher temperatures it sharply drops to normal value. Such exponential dependence is a strong proof of the model with energy gap between electrons on normal and superconducting states.

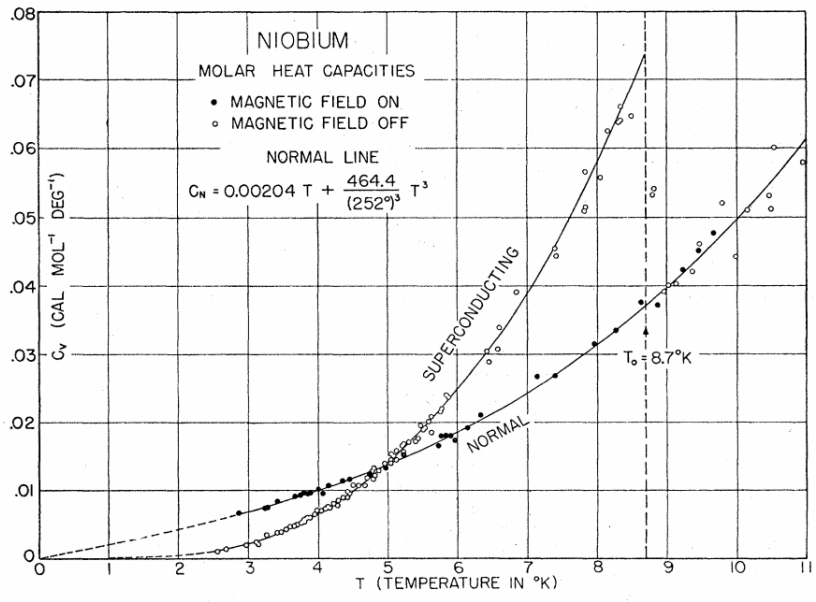

Figure 1.10 Temperature dependence of the heat capacities of niobium. ([12]Brown et al. 1953)

Isotopic effect in superconductors

It was found that different isotopes of mercury have slightly different critical temperatures ([64]Maxwell 1950; [78]Reynolds et al. 1950): This discovery showed that not only electrons but the lattice also is involved in the superconductivity. The dependence of critical temperature on the isotope mass for Hg was established as:

$$T_c \sim \frac{1}{\sqrt{M}}$$

And since Debye temperature has the same dependence on the mass it was obvious hint that the phonons are participating in the superconductivity process.

Later, dependence of the critical temperature on isotope mass was studied for other superconductors, and it's turned out that T_c not necessarily exactly depends on the square root of the mass:, but rather can be presented as:

$$T_c \sim \frac{1}{M^{\alpha}}$$

Metal	Tc	θD	α
Pb	7,2	105	0,48
Hg	4,15	72	0,5
Sn	3,7	200	0,46
Tl	2,4	78,5	0,5
Re	1,7	430	0,38
U	1,3	207	-2
Mo	0,92	450	0,37
Zn	0,85	327	0,3
Os	0,7	500	0,21
Zr	0,6	291	0
Cd	0,52	209	0,5
Ru	0,5	600	0

Figure 1.11 Relationship of T_c, Debye temperature and isotopic coefficient in elemental materials

Where coefficient α is different for different superconductors and can be even equal to 0 for Ruthenium (Ru) or -2 for Uranium.

Deviations of α from the value of 0.5 for the particular materials were explained lately.

Interaction of two electrons (Electron-phonon interaction)

The experimental studies were showing that interaction between electrons and ions in the crystal lattice likely relates to superconductivity. In 1950 Fröhlich first time showed that interaction of electrons with lattice can create an attraction between two negatively charged electrons ([36]Fröhlich 1950). As the result of this attraction two electrons can form a pair. Creation of these Cooper pairs of electrons is a key of understanding of the phenomenon of superconductivity.

To understand the attraction between two electrons let's firstly describe an interaction between two electrons through the phonon. Consider a free electron in the metal at zero temperature with momentum $\overrightarrow{p_1}$. At some moment electron interacts with ion in the lattice and this leads to the occurrence of oscillations in the lattice with frequency ω_{ph}. Occurrence of the oscillations is the same as a born of the phonon with energy $E = \hbar\omega_{ph}$ and momentum $\overrightarrow{q}$. In

the accordance with the law of conservation of momentum electron will change its momentum on $\overrightarrow{\Delta p} = -\vec{q}$ and will have momentum after interaction:

$$\overrightarrow{p_1'} = \overrightarrow{p_1} + \overrightarrow{\Delta p}$$

This electron will also change its energy:

$$\Delta E_1 = E_1' - E_1 = \frac{{p_1'}^2}{2m} - \frac{{p_1}^2}{2m}$$

Another electron can lately absorb the phonon which occurred after interaction of the first electron with the lattice. This absorption of the phonon will change the electron's momentum and energy. By this way an interaction between two electrons occurs through their interaction with the lattice. This interaction of two electrons obey the law of conservation of momentum and energy.

$$\overrightarrow{p_2'} = \overrightarrow{p_2} - \overrightarrow{\Delta p} \qquad \Delta E_2 = E_2' - E_2 = -\Delta E_1$$

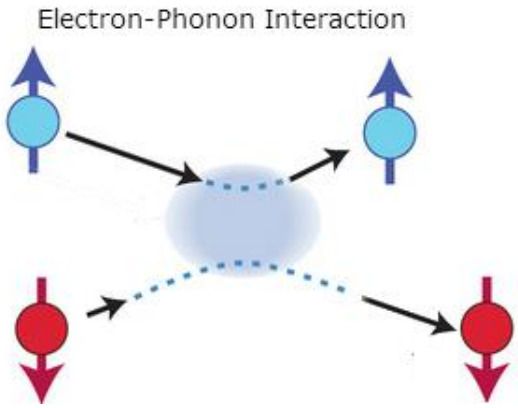

Figure 1.12 Schematic representation of electron-phonon interaction

Attraction of electrons

How attraction can occur as a result of such interaction? Coulomb repulsion can be neglected as the electron can be considered as a quasiparticle of Fermi sea (polaron). The charge of the electron is shielded by surrounding positive excitations.

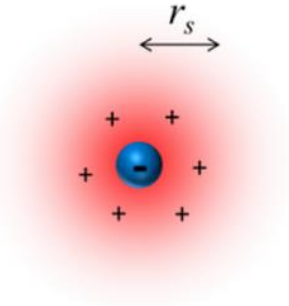

Figure 1.13 Polaron in Fermi sea

Change of the kinetic energy of the 1st electron causes an oscillation of electron density and can be described as:

$$\Delta E_1 = \hbar\omega_e$$

Frequency of the electron density oscillation ω doesn't necessary coincides with frequency of the lattice vibrations ω_{ph}. This means that phonon energy $\hbar\omega_{ph}$ is not equal to change of energy of electron $\Delta E_1 = \hbar\omega_e$. This is prohibited by the law of conservation of energy but Heisenberg's uncertainty principle allows violating it if lifetime of the phonon is very short. Energy of phonon is uncertain if its lifetime is short:

$$\Delta E \Delta t \geq \frac{\hbar}{2}$$

Motion of the ion in the lattice can be described as an oscillator (vibration of the lattice) driven by external sinusoidal force (vibration of electron density):

$$\ddot{x} + \omega_{ph} x = A \sin(\omega_e t)$$

Solution will be:

$$x = \frac{A}{{\omega_{ph}}^2 - {\omega_e}^2} \sin(\omega_e t)$$

If $\omega_e > \omega_{ph}$ than coefficient $\frac{A}{{\omega_{ph}}^2 - {\omega_e}^2}$ is negative and oscillation of electron density is not in phase with vibration of ions. Positive charge will be expelled from the area of excessive charge which was created by the first electron and total interaction between two electrons will be repulsive.

If $\omega_e < \omega_{\mathrm{ph}}$ than oscillation of the electron density is in the phase with vibration of the ions, positive charge will be attracted to the area of excessive charge and total interaction between two electrons will be attractive.

Thus, the attraction of two electrons is possible only if energy which is transferred in the process of the interaction is less than the energy of the phonon which participates in the interaction.

Cooper pair

We've discussed how attraction between two electrons can appear. Cooper described that this small atraction can lead to bounded state of two electrons. Such bounded electrons are called Cooper pair. Two bounded electrons has an integer spin (0 or 1) and form a boson particle. Lower than some specific temperature boson particles can form a collective state - superfluid Bose-Einstein condensate wich can

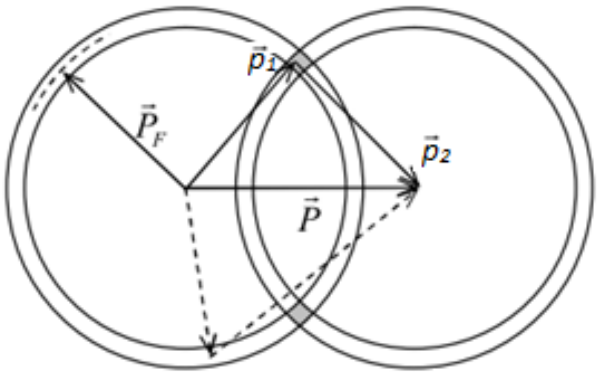

Figure 1.14 Cooper pair in Fermi sphere

transfer through the crystal lattice without interaction with it (resistance).

Not all electrons are participating in the superconductivity.

The maximum energy of the virtual phonon which mediates energy between two electrons is limited by the Debye energy. Thus, in the process of electron-electron interaction one electron can change its energy on the value which is less than the Debye energy. Debye energy is significantly less than Fermi level thus **superconductive electrons can exist only in the thin shell near the Fermi level**. Interaction of electrons on the levels which are deeper than Debye energy from a Fermi sphere is prohibited by the Pauli Exclusion Principle.

Let's return to two interacting electrons with momenta $\overrightarrow{p_1}$ and $\overrightarrow{p_2}$. These momenta lie in the thin shell near Fermi sphere (Fig 1.14). Interaction of two electrons should obey the law of conservation of momentum and momentums after interaction $\overrightarrow{p_1'}$ and $\overrightarrow{p_2'}$ should also be in the thin shell near Fermi sphere. Thus attraction of electrons is possible only for electrons from intersection of two circles (dashed areas on Fig 1.14). This dashed area is maximized (and total energy of the system is minimized) when total momenta $\vec{P} = \overrightarrow{p_1} + \overrightarrow{p_2} = 0$ and circles are fully intersected. Thus $\overrightarrow{p_1} = -\overrightarrow{p_2}$.

Momenta of superconducting electrons are equal and have opposite direction.

Characteristic values of BCS theory

Important parameter which characterizes Cooper pair is coherence length ξ_0 (the size of the Cooper pair).

$$\xi_0 = \frac{2\hbar v_F}{\pi \Delta}$$

- v_F - electron velocity near Fermi level
- Δ - superconducting energy gap

For elemental superconductors the characteristic length of Cooper pair is about 10^{-7} m (100 nm). Distance between ions in the lattice is about ~ 10^{-10} m (0.1 nm). Between two paired electrons there are thousands of other free electrons which don't influence on this interaction.

The size of the energy gap depends on temperature and can be described as follows:

$$\Delta(T) = 1.76 k_B T_c \left(1 - \frac{T}{T_c}\right)^{1/2}$$

For superconductor with $T_c = 10K$ energy gap at absolute zero is $\Delta \sim 3 \cdot 10^{-3}\ eV$.

Fermi energy has values about few eV thus only a thin layer of the Fermi surface participates in the superconductivity.

Description of BCS theory was made in the assumption of weak electron-phonon coupling and gives T_c as:

$$\boldsymbol{T_c = 1.14 \left(\frac{\hbar\omega_D}{k_B}\right) \exp\left[-\frac{1}{N(E_F)V_{eff}}\right]} \quad (1)$$

Where:

- ω_D – Debye frequency
- $N(E_F)$ – density of states at Fermi level
- V_{eff} - net attractive potential between electrons

In 1960 Eliashberg ([23]Eliashberg G.M. 1960) developed a generalized theory of superconductivity. He took into account retardation – the second electron interacts with the polarized lattice, and this polarization takes a time – it is quick for light atoms and slow for heavy atoms. Coupling constant λ represents the strength of electron-phonon interaction and can be calculated:

$$\lambda = 2\int_0^\infty \frac{\alpha^2(\omega)F(\omega)}{\omega} d\omega$$

Where:

- $F(\omega)$ – phonon density of states
- $\alpha^2(\omega)$ – represents average electron-phonon interaction

$\lambda \ll 1$ corresponds to **weak** electron-phonon interactions.

$\lambda \sim 1$ corresponds to **intermediate** electron-phonon interactions.

$\lambda > 1$ corresponds to **strong** electron-phonon interactions.

Analytical and numerical solutions of Eliashberg theory was made by McMillan ([66]McMillan 1968) and reexamined by the Allen-Dynes ([5]Allen, Dynes 1975). Generalized equation for T_c is:

$$\boldsymbol{T_c = \frac{\langle\omega\rangle}{1.2} exp\left(-\frac{1.04(1+\lambda)}{\lambda-\mu^*(1+0.62\lambda)}\right)} \quad (2)$$

Where:

- $\boldsymbol{\langle\omega\rangle}$ **-** weighted average over the phonon frequency spectra
- μ^* - Coulomb pseudopotential which takes into account the Coulomb repulsion between the electrons.

In the BCS theory density of states $N(E_F)$ and attractive potential V_{eff} are not depended on the mass M and equation (1) for a T_c will give:

$$T_c \sim \langle \boldsymbol{\omega} \rangle \sim const * M^{-\alpha}$$

α can be described by:

$$\alpha = -\frac{\partial \ln T_c}{\partial \ln M}$$

Debye frequency is inversely proportional to square root of mass:

$$\omega_D \sim \frac{1}{\sqrt{M}}$$

So

$$T_c \sim \langle \boldsymbol{\omega} \rangle \sim \frac{1}{\sqrt{M}}$$

So BCS theory gives $T_c \sim \frac{1}{\sqrt{M}}$ and $\alpha \approx 0.5$. This value coincides with known at 1957 experimental value of α for mercury.

If we will look at others elemental superconductors we can see that coefficient α often differs from 0.5. BCS makes an assumption Coulomb repulsion is weak ($\mu^* = 0$). If $\mu^*(\boldsymbol{\omega})$ is not a zero than from McMillan equation (2) isotope effect exponent α depends on the electron coupling like:

$$\alpha = \frac{1}{2}\left[1 - \frac{1.04(\mathbf{1}+\boldsymbol{\lambda})(\mathbf{1}+\mathbf{0.62}\boldsymbol{\lambda})}{[\boldsymbol{\lambda} - \boldsymbol{\mu}^*(\mathbf{1}+\mathbf{0.62}\boldsymbol{\lambda})]^2}\boldsymbol{\mu}^{*\mathbf{2}}\right]$$

If $\boldsymbol{\mu}^* = \mathbf{0}$ than α reduces to 0.5.

1.3 High Pressure effects on superconductivity

The presence of the superconductivity in the specific material is determined by its phonon and electronic structure. Changing of temperature of material leads to changing in the occupation of energy levels. Pressure changing leads to modification of energy levels and electronic configuration. Eliashberg theory and McMillan expression for T_c can only tell us that dependence of T_c on pressure is very complicated and can be different for different materials. If we assume that Coulomb pseudopotential doesn't depend on pressure than from Eliashberg formulation we can get:

$$\frac{d \ln T_c}{dP} = \frac{1}{B}\left\{\gamma + \left[\frac{1.04\boldsymbol{\lambda}}{\boldsymbol{\lambda} - \boldsymbol{\mu}^*(\mathbf{1}+\mathbf{0.62}\boldsymbol{\lambda})} - \frac{1.04\boldsymbol{\lambda}(\mathbf{1}+\boldsymbol{\lambda})(\mathbf{1}-\mathbf{0.62}\boldsymbol{\mu}^*)}{[\boldsymbol{\lambda} - \boldsymbol{\mu}^*(\mathbf{1}+\mathbf{0.62}\boldsymbol{\lambda})]^2}\right]\left[2\gamma + \frac{d \ln \eta}{d \ln V}\right]\right\}$$

Where:

- B – the bulk modulus
- $\gamma = -\frac{d\ln\langle\omega\rangle}{d\ln V}$ - Gruneisen parameter
- $\eta = N(E_f)\langle I^2\rangle$, and $\langle I^2\rangle$ is the average squared electronic matrix element

Experimental studies show that for most elemental *s*, *p* metals, the T_c most often decrease with pressure inceasing (Figure 1.15). Transition metals have a *d* character superconductivity and electronic structure of thease metals is more complicated. Complexity of electronic struture leads to different response of T_c on pressure increase. For some transition metals T_c increases (V, La) with pressure increasing, for some decreases.

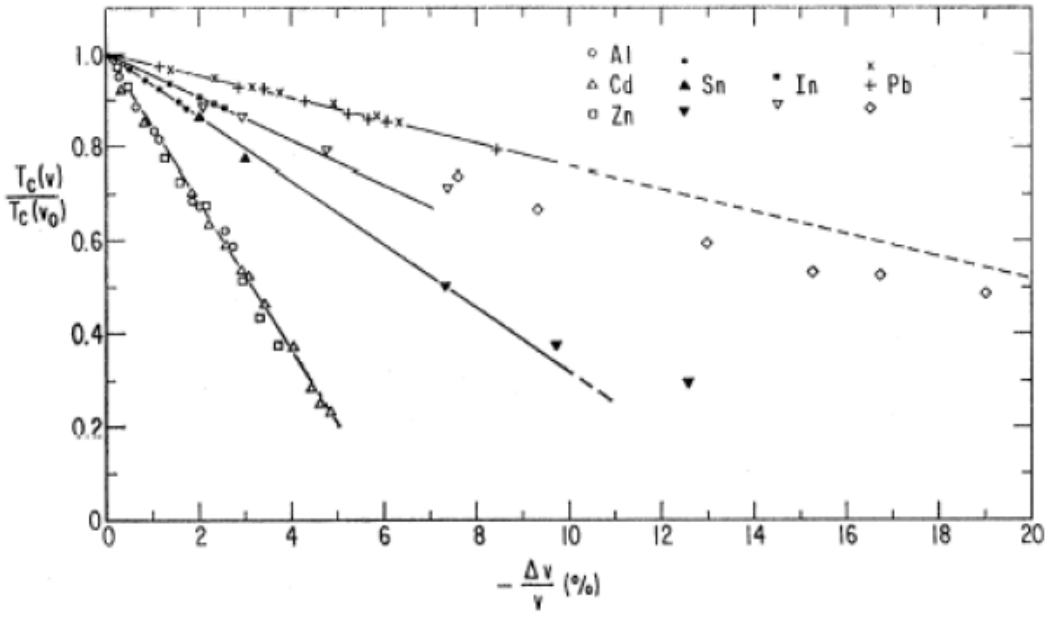

Figure 1.15 - The relative pressure shift of T_c as a function of the relative volume change for a large number of superconducting metallic elements. T_c decreases with increasing of the pressure.

For the non-metal material increase of the pressure can lead to transformation to metal and appearing of superconductivity.

30 elemental materials exhibit superconducting properties at ambient pressure. Applying of pressure increases the number of superconductors among elemental materials to 52 (Figure 1.16).

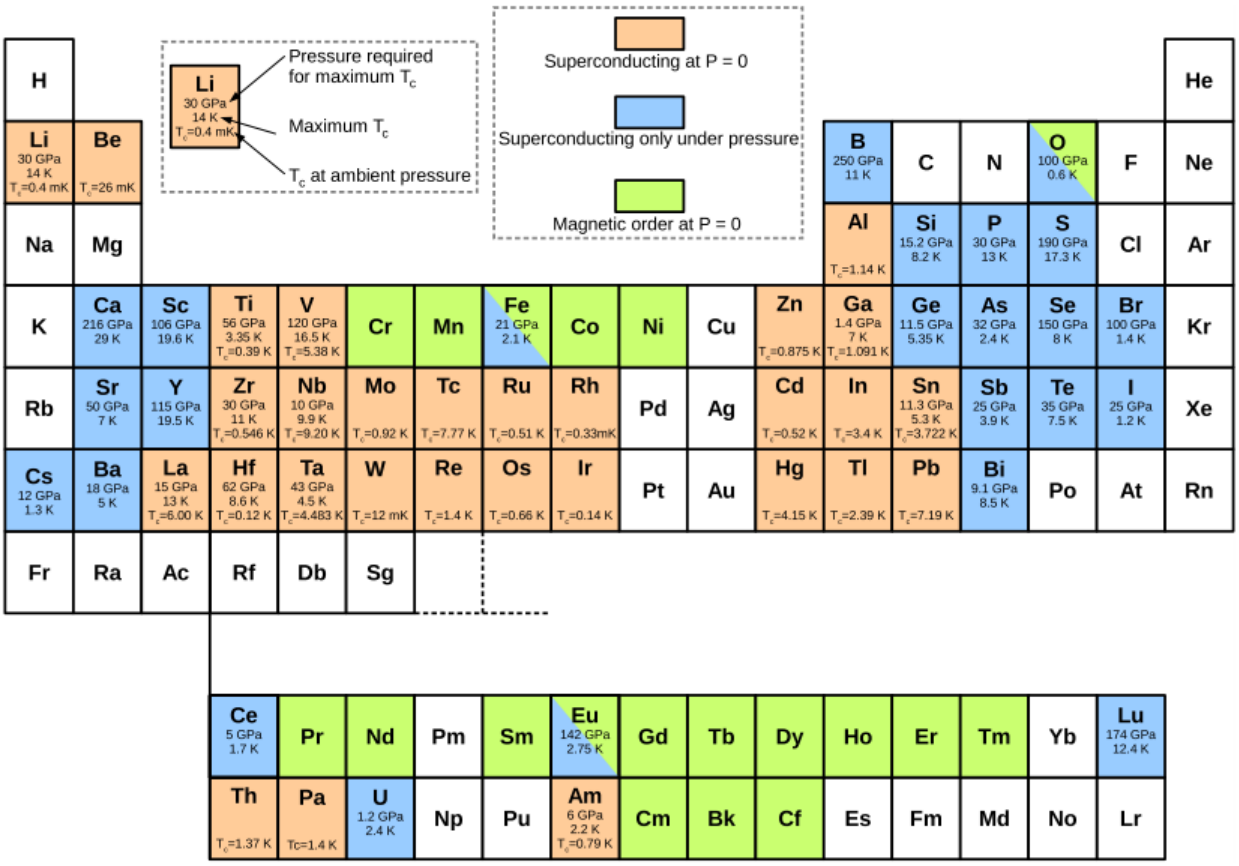

Figure 1.16 - Periodic Table of superconducting elements ([44]Hamlin 2015)

1.4 Superconductivity in hydrogen-rich materials

Hydrogen is the lightest element and seems that should be the simplest of all elements. However, it turns out to be one of the hardest for theoretical research under pressure due to significant quantum effects, anharmonicity, and for experimentalists because its adsorption and diffusion in many materials. First-time metallic hydrogen was theoretically predicted at 1935 year and it's experimentally metallization is one of the most important problems is physics. The pressure of metallization was predicted to be 25 GPa. It was very high pressure for 1935 year ([98]Wigner, Huntington 1935), and it is small for 2015 year. Predicted metallization pressure is growing with time and now it is in the range of 400-700 GPa. Recent calculations showed that metallic hydrogen should be a superconductor at a very high critical temperature T_c ~100-240 K ([100]Zhang et al. 2007; [14]Cudazzo et al. 2008) for a molecular hydrogen, and T_c = 300-350 K in atomic phase at 500 GPa ([65]McMahon, Ceperley 2011). It also was predicted to be metastable by Brovman ([21]E. G. Brovman et al. 1972). However, superconductivity in a pure hydrogen has not been found yet while conductive and likely semimetallic state of the hydrogen

has been recently achieved at pressures approaching 300 GPa ([28]Eremets, Troyan 2011). Till the direct metallization of the hydrogen is not achieved hydrogen-rich materials hit the interest of the investigations.

For metallic hydrides, for instance, PdH, there were expectations that they will be a model of metallic hydrogen and have high T_c. However, it turned out that these systems are far from pure hydrogen. In particular, atoms of hydrogen in the metallic lattice of Pd interact weakly with each other. Importantly, anharmonic effects are very large and the resulting T_c is moderate (T_c about 10 K for PdH). PdH also has negative isotope effect due to anharmonicity of hydrogen vibrations ([88]Skoskiewicz et al. 1974; [30]Errea et al. 2013). N. Ashcroft came with an idea that superconductivity in covalent hydrides can be expected to have high T_c because of very high Debye temperature (high vibrational frequencies due to a light hydrogen atom) and strong electron-phonon interaction. The covalent hydrides are insulators but can be transformed to metals under pressure. Pressure required for the metallization of the covalent hydrides is much less than that for hydrogen, and is in the accessible range of 1-2 Mbars.

Followed numerous calculations supported the Ashcroft's idea of high T_c in hydrides (Table 1-2). T_c was estimated by using the Allen–Dynes modified McMillan equation or solving Eliashberg equations numerically. But for these calculations the structure should be known. Nowadays there is a big progress in the prediction of structures from ab-initio calculations. Now the structural search of the high-pressure phases with good probability can be done by different methods ([77]Pickard, Needs 2011; [71]Oganov et al. 2011; [93]Wang, Ma 2014). The theoretical searching techniques are quickly developing and improving. However, these techniques cannot guarantee that the found structure is the most stable and even lower energy structure is not missed. There is no obvious criterion or benchmark for completion of the search. Regularly new theoretical results are published where the predicted structures are revised and lower energy structures are found.

A lot of hydrides were already studied theoretically and T_c up to 250 K is predicted in pressures of 100-300 GPa (Table 1-2).

Hydride	Pressure	Tc	Ref
YH6	120	251	([59]Li et al. 2015)
CaH6	150	220	([91]Wang et al. 2012)
Si2H6	275	139	([53]Jin et al. 2010)
AlH3(H2)	250	132	([50]Hou et al. 2015)
H3Se	300	110	([101]Zhang et al. 2015)
SiH4(H2)2	250	98	([57]Li et al. 2010)
GeH4(H2)2	230	92	([102]Zhong et al. 2013)
LiH6	300	82	([99]Xie et al. 2014)
GeH3	300	80	([49]Hou et al. 2015)
H2S	160	80	([58]Li et al. 2014)
GaH3	160	73	([41]Gao et al. 2011)
GeH4	220	64	([39]Gao et al. 2008)
SnH4	200	62	([40]Gao et al. 2010)
KH6	166	60	([104]Zhou et al. 2012)
H5Te2	200	58	([103]Zhong et al.)
NbH4	300	38	([38]Gao et al. 2013)
BeH2	250	38	([94]Wang et al. 2014)
SiH4	220	16	([63]Martinez-Canales et al. 2009)

Table 1-2 – Predicted T_c at different pressures for different hydrides

The estimations of the critical temperature of superconductivity T_c should be considered with precaution. Typically T_c is calculated by using the Allen–Dynes modified McMillan equation. However, the value of estimated T_c might depend on the particular structure and details of the phonon and electron spectrum. A good example is AlH_3 which has been predicted to be superconductive with a transition temperature of 24 K at 110 GPa ([43]Goncharenko et al. 2008), but in fact no superconductivity has been observed in the experiment at least at T>4 K ([43]Goncharenko et al. 2008). A reason for this contradiction is the electron-phonon coupling can be associated with modes that are highly anharmonic ([80]Rousseau, Bergara 2010). Another work suggests that polarizability of AlH_3 is much less than that of many other hydrogen-rich compounds (although it is a covalent hydride) which may result in lower T_c ([95]Wei et al. 2013).

Only experiments can give an answer if the calculations of T_c are correct and confirm the prospects of high T_c in the hydrogen-rich materials. Any feedback from the experiment is very valuable for the theoretical community to improve and correct their calculation methods. However, experimental studies of hydrogen-rich compounds are puzzlingly scarce. Only AlH_3 and SiH_4 were studied with electrical, optical and X-ray diffraction measurements ([27]Eremets et al. 2008; [43]Goncharenko et al. 2008). Metallization and superconductivity in SiH_4 has been found experimentally already at P>60 GPa ([27]Eremets et al. 2008) in contradiction with theory which predicts a metallic phase at 262 GPa ([76]Pickard, Needs 2006), or P>220 GPa in a later calculation ([63]Martinez-Canales et al. 2009).

A reason for the very few experimental works is that the experiments are difficult and challenging, especially electrical measurements. For instance, the most attactuve, hydrides with the highest concentration of the hydrogen, such as CaH_4 , CaH_6, and CaH_{12}, LiH_n, n>1, KH_6 and other should be synthesized. This should be done at the conditions of their stability, i.e. at high pressure in a reaction of hydrogen with starting materials such as Ca or CaH_2, Li or LiH. In practice, however, these reactions can be very slow as hydrogen should diffuse into a bulk material. Some of these reactions take very long time. SiH_4, for instance, formed from bulk Si in H_2 during eight months at 124 GPa ([46]Hanfland et al. 2011). Another group of hydrides like SiH_4, HF, PH_3, SH_2, GeH_4 exists at ambient pressure and can be bought. Experiments with these substances reqire however a great care as they are highly toxic, corrosive, flammable, pyrolytic and explosive.

Chapter 2
Experimental techniques

2.1 Diamond anvil cell (DAC)

At the beginning of 20th century, Percy Williams Bridgman introduces anvils to high-pressure technique and pressures up to 10 GPa (100,000 atm) become accessible for experimentalists – much higher than in conventional piston-cylinder apparatus. Anvils in the presses were made from a tungsten carbide (WC).

Diamond is known as the strongest material on the Earth, and it is quite an obvious idea to use it in high-pressure experiments. In a 1959th year, the diamond was fist time used as an anvil by Wier, Van Valkenburg, Bunting and Lippincott ([96]Weir et al. 1959), initially to generate pressures of 10-20 GPa. Pressure above 100 GPa were achieved by Mao et al. ([62]Mao, Bell 1978) by introducing beveled shape of anvils. Now pressures up to 200 GPa can be routinely achieved in the experiments with diamond anvil cell (DAC) and pressures up to 400 GPa can be achieved by few groups. The highest registered pressure with the DAC is about 500-1000 GPa ([20]Dubrovinsky et al. 2015). This was done with a double stage cell so the size of the sample (a metal) is about few micrometers. The pressure achieved in DACs is realy high – it is more than in the center of the Earth (360 GPa).

Diamond anvil cell (DAC) is very universal tool. Figure 2.1 represents a broad range of experimental techniques and measurements which can be performed in DAC. In particular it allows experiments with a temperature range from millikelvins to 7000 K to be performed.

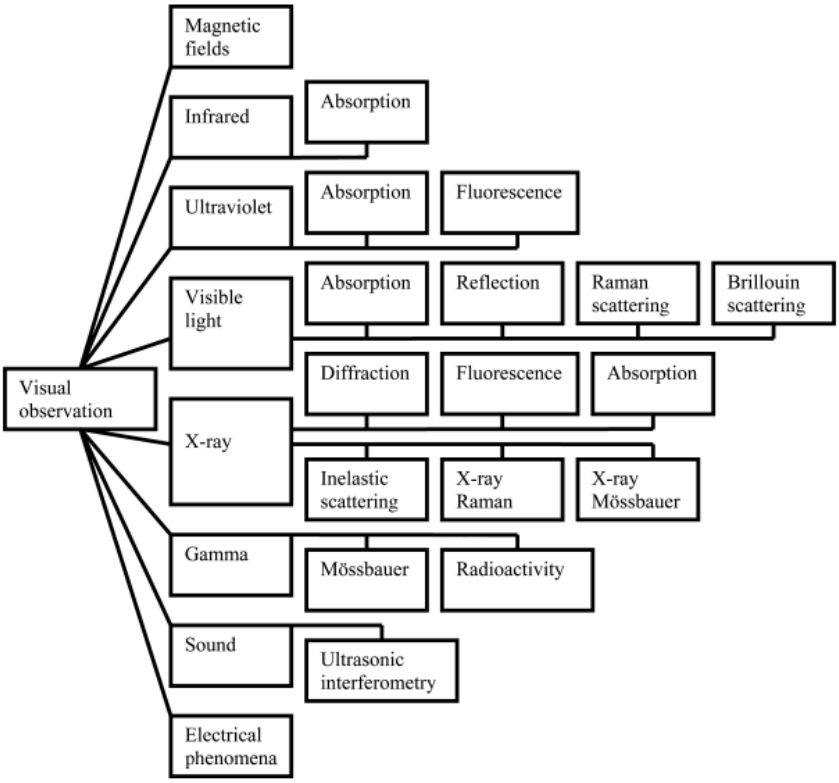

Figure 2.1 - Available experimental techniques in DAC

Figure 2.2 represents the base principle of Diamond Anvil Cell. Sample squeezed between two diamonds and gasket.

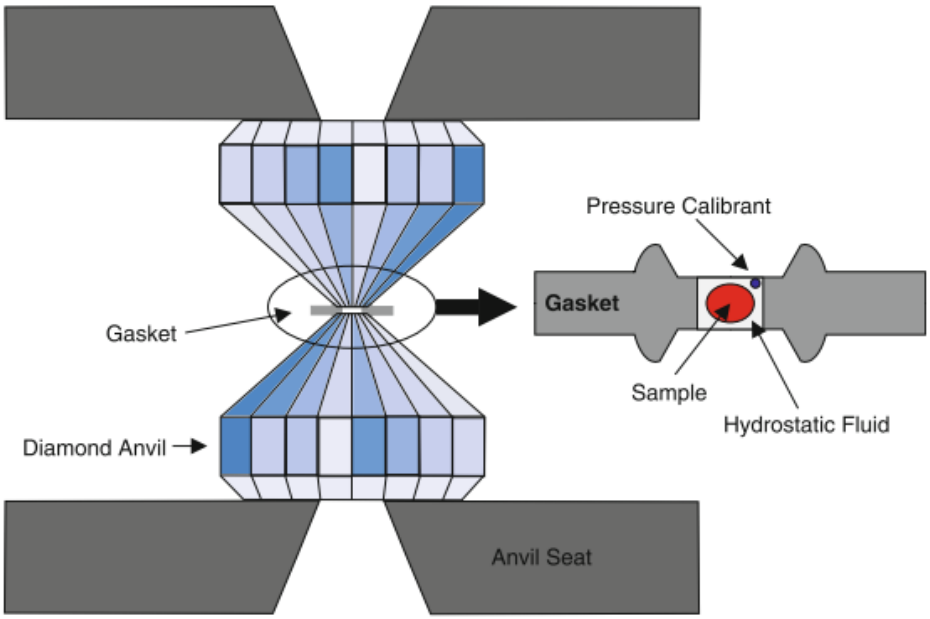

Figure 2.2 –Schema of Diamond Anvil Cell

Basically, Diamond Anvil Cell consists of:

- Body of the cell (Base of the cell, Piston, Cap with screws for pressure increasing and spring)
- Anvil seats
- Diamond anvils
- Gasket

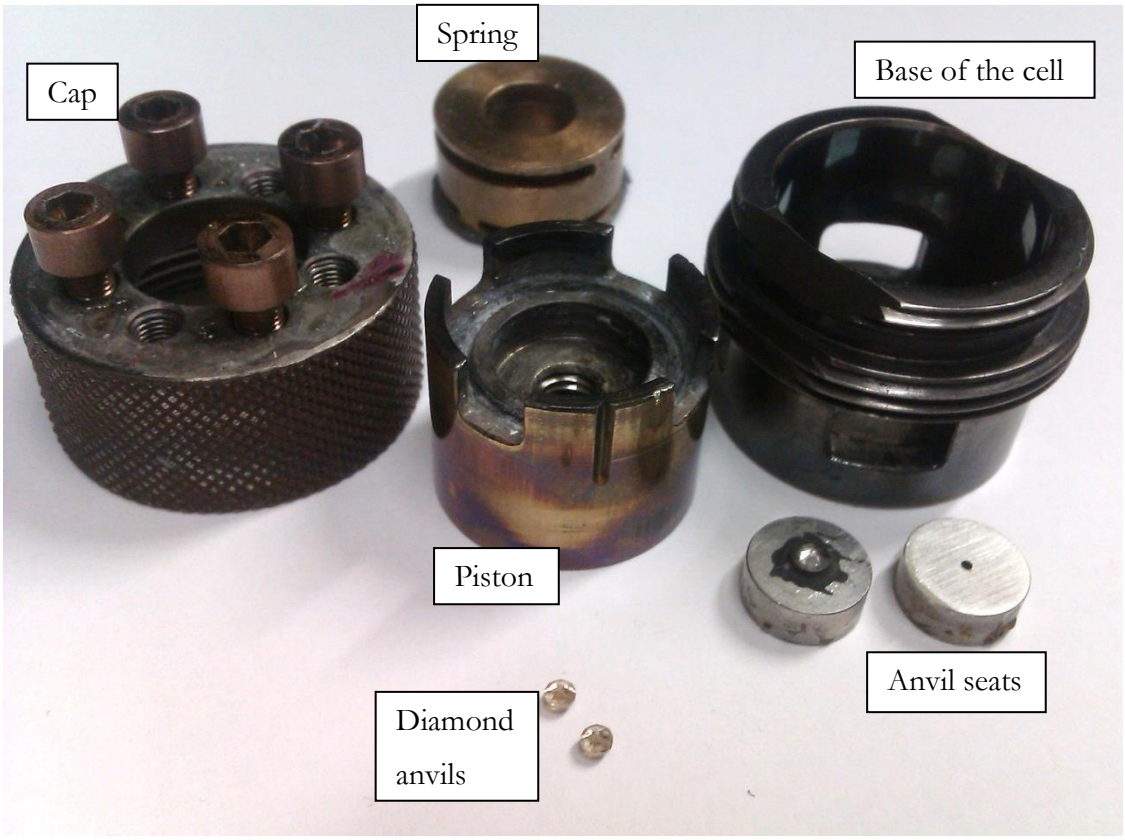

Figure 2.3 Diamond Anvil Cell parts

Diamonds

The heart of DAC is diamond anvils. Diamond serves not only as the hardest material to generate pressures. Diamonds also serves as window to observe the sample and study its properties by probing of electromagnetic radiation from far IR to UV. There is no apparent limit for low frequencies of the radiation. In the UV side diamond is transparent up to ~200 nm- below its band gap E=5.5 eV.

The functioning of DAC strongly depends on the properties of the diamonds used for the anvils.

Diamonds can be characterized by:

- Origin (Natural or Synthetic)
- Amount and type of impurities
- Diamond cut

Origin

Besides natural diamonds are grown inside the Earth at the depth more than 140 km (Fig 2.4) - diamonds can be also synthesized with the aid of high pressures apparatus at P~10 GPa and temperatures of about 2500 degrees (HPHT synthetic diamond). Interestingly, diamonds can also be grown with CVD process without high pressures – from plasma at reduced pressures

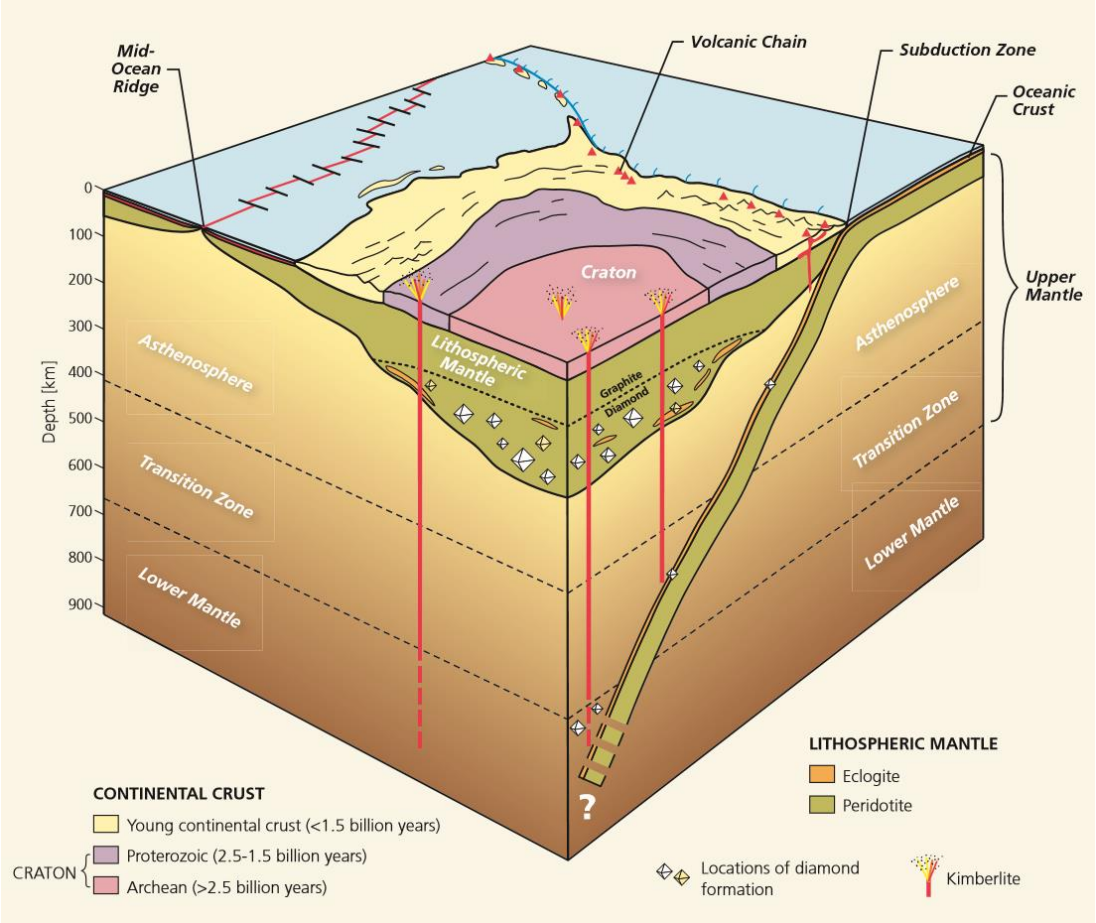

Figure 2.4 Cross-section of the crust and mantle showing the main locations of diamond formation in the Earth's interior ([90]Tappert, Tappert 2011).

Diamonds from all tree sources are used in the high-pressure experiments. The synthetic diamonds (both HPHT and CVD) can be grown very pure, flawless. Such defect free synthetic diamonds are very valuable for IR studies as they have very low absorption and for Raman studies as they have low or negligible luminescence. Synthetic diamonds are considered now as the hardest known materials, but are very brittle. The high pressures of ~300 GPa can be reached

with all kinds of diamonds independently of origin. The highest pressure over 400 GPa was reached with natural diamonds. Probably it can be reached synthetic diamonds too but there is a lack of experiments.

Impurities

All diamonds are classified by an amount and character of impurities. In fact diamond can be doped only with few impurities – with small size atoms. This is hydrogen, lithium, boron and nitrogen. Larger atoms cannot go into the rigid diamond lattice. The main impurity of the natural diamonds is nitrogen. Boron doped diamonds are very rare, they have blue color. There are two major types of diamond which are distinguished by a number of nitrogen per million particles. I type of diamonds contain Nitrogen inclusions more than 10 particles per million (ppm) and II type contains less than 10 ppm. I and II types also sub-divided:

- Ia - diamonds with aggregated impurities of nitrogen (A and B defects) (98% of all natural diamonds).
- Ib – Nitrogen substitute single particles of Carbon (C defects).
- IIa – diamonds with less than 10 ppm of nitrogen impurities (~2% of all natural diamonds)
- IIb - diamonds with less than 10 ppm of nitrogen impurities and with Boron inclusions.

Schematic pictures of A, B, B' and C defects are presented in the Figure 2.5. Yellow circles present Nitrogen atoms and blue circles present carbon atoms. «A» defects are pairs of Nitrogen atoms which substitute carbon atoms. «B» defects are the complex of nitrogen atoms which surrounds a vacancy.

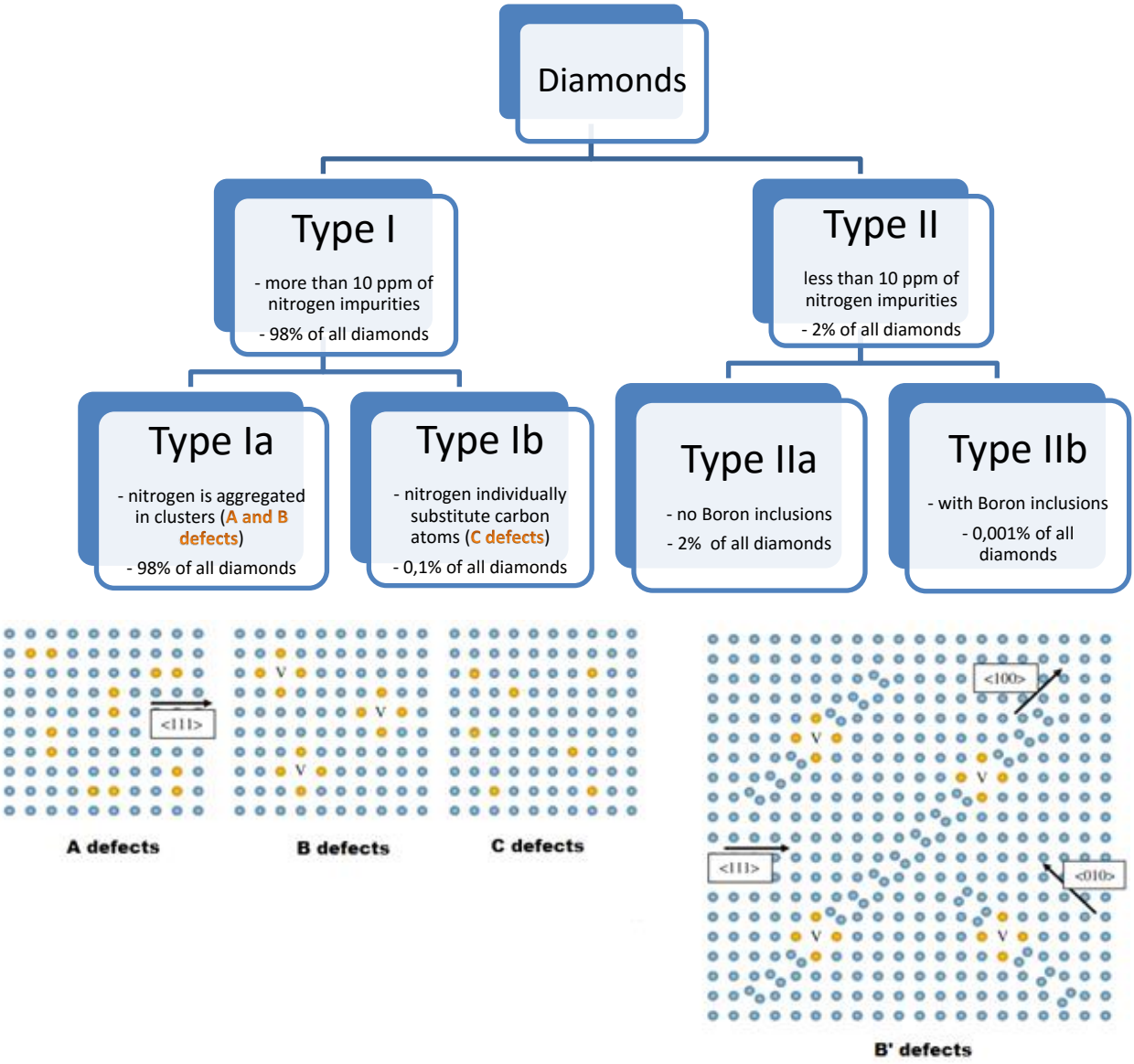

Figure 2.5 Schematic representation of defects in diamonds.

Typically HPHT diamonds have impurities (inclusions) of Nickel, Cobalt or Iron, which are used as a catalyst. CVD diamonds often have an impurity of hydrogen because they are grown from the hydrogen content plasma. Typical Raman spectra of natural (type I) and CVD diamonds are presented in Figure 2.6. The hydrogen-related defects develop in Raman spectra at 3107 cm^{-1}. The nitrogen-vacancy defects can be clearly seen at red spectra as the rising background. All these luminescence spectra complicate spectroscopic measurements.

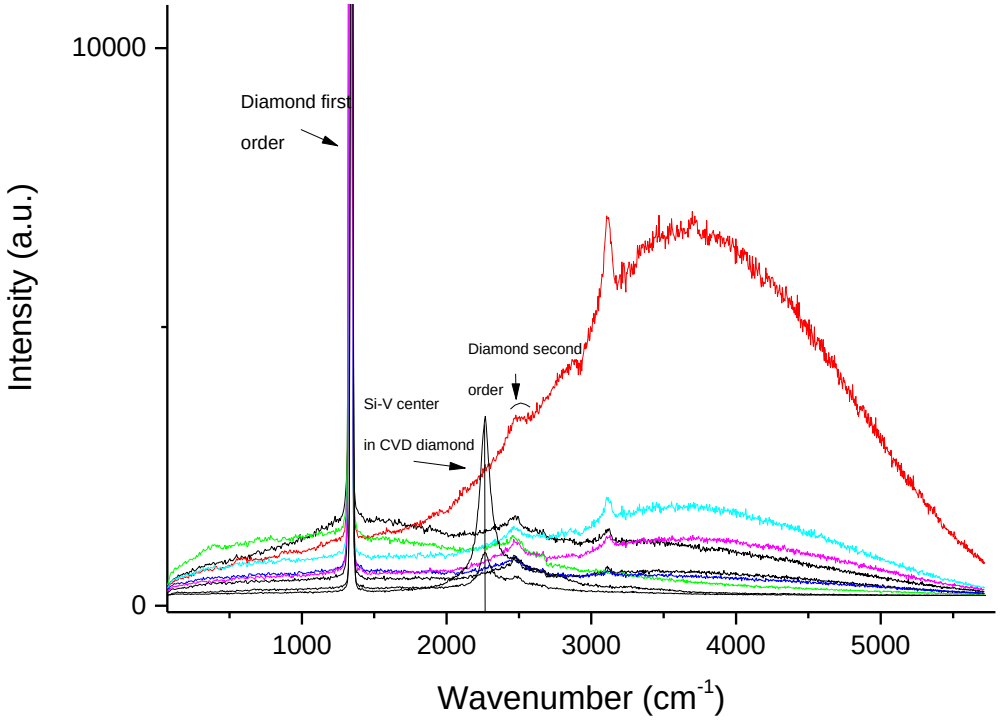

Figure 2.6 – Typical Raman spectra of natural and CVD diamonds

Diamond anvil cell

Diamond is the strongest material and naturally it can generate the highest pressures. Equally important that diamond is transparent for nearly all electromagnetic radiation (with weak absorption in infrared range) up to 5 eV where strong intraband absorption starts. At higher energies diamond is transparent in keV range. Therefore DAC is a very useful tool for various optical, X-ray, electrical and many other studies.

Typical materials for DAC parts are steel or nickel and cobalt containing alloys. These materials have very high mechanical strengths. For magnetic measurements diamond anvil cell can be made of beryllium copper, titanium alloy ([73]Okuchi 2004), NiCrAl alloy (HNU40) ([25]Eremets 1996), silicon aluminum bronze (C64200) ([34]Feng et al. 2014), Cu:Ti or even

from plastic (experimentally was used till 5 GPa). Good review of DAC material properties is presented in the work of X. Wang and K. V. Kamenev ([92]Wang, Kamenev 2014).

This remarkable device is quite simple (Fig. 2.7) however a lot of important details should be known for successful operation.

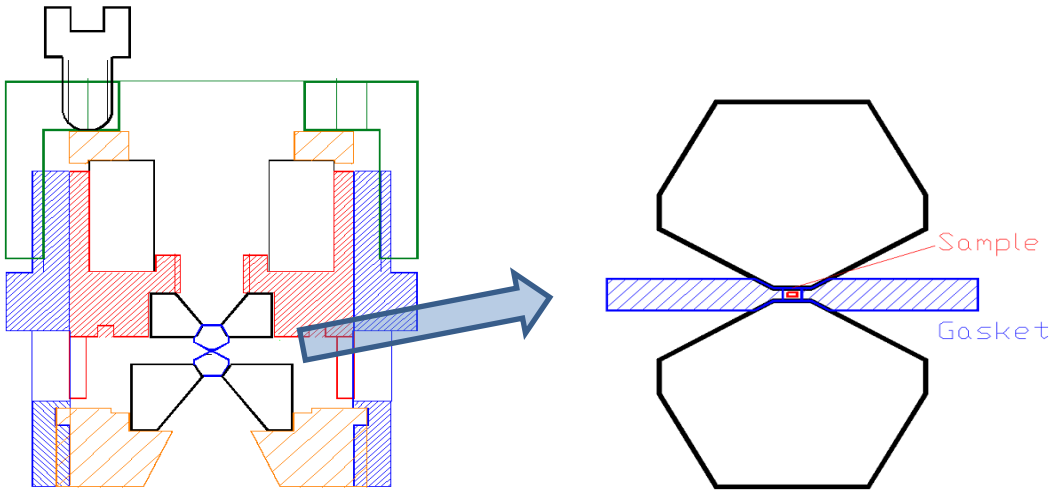

Figure 2.7 Schematic view of DAC

Basically, DAC operates very simply: two diamond anvils are placed on seats and loaded through a piston (Fig. 2.7). But DAC is a precise mechanism which should work with micrometer accuracy because of very small size of culets of diamond anvils- down to 10-20 μm. Therefore the piston-cylinder pair should be well polished, it is crucial to have no play of piston in the cell. Diamond is strong but very brittle material and can be easily damaged.

Anvil Seats

Anvil seats should be made of a strong material because the anvils can be typically loaded more than 1000 kG and produce significant pressure at the table of the anvil. Usually seats are made from tungsten carbide. For X-ray measurements, where large aperture is crucial, seats can be made of boron nitride because it's transparent for X-ray. Initially, seats and diamonds were flat as presented on Figure 2.8a. Diamonds and seats with conical support were introduced by Boehler ([11]Boehler, Hantsetters 2004) (Figure 2.8.b) and have some advantages. They have a larger aperture for optical and X-ray measurements and diamonds are better saved after unloading – they are supported from the sides and do not destroyed completely.

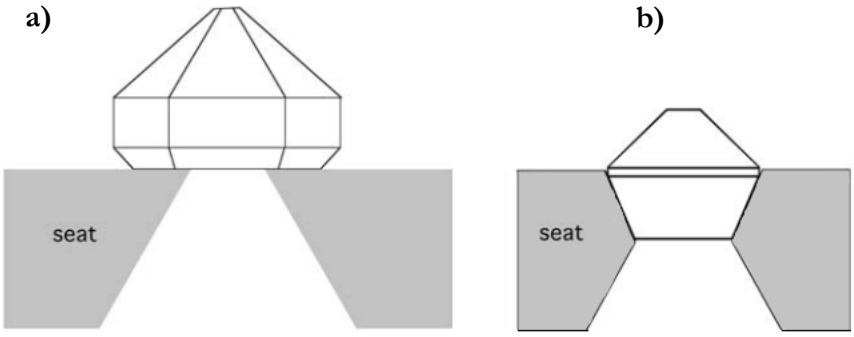

Figure 2.8 - Schematic view of conventional and conical high-pressure anvils and seats

Gasket

DAC was invented in 1958 but at the beginning scientists were working without gasket just pressing the sample between two diamonds. Such technique allows working only with solid samples. In 1962, Van Valkenburg introduced a gasket to the high-pressure DAC technique. The gasket is a piece of metal sheet with a drilled hole for sample loading. Most often steel or rhenium is used as a material for the gasket. It also helped to avoid pressure inhomogeneity across the sample by confine a sample in the chemical inert He medium.

2.2 Pressure measurements

It could be expected that pressure in the diamond anvil cell can be calculated by knowing an applied force, the area to which force is applied and area of a culet. However it does not work because the pressure over diamond tip is very nonuniform. It distributes over diamond tip and gasket from zero at the edge to maximum pressure in the center (where the sample is located), and this distribution strongly dependence on particular diamond-gasket configuration. The problem is that some force is dissipated by the gasket and the friction between the piston and the cylinder, so this method is very inaccurate.

The only reliable way to measure a pressure is to determine a unit cell size of known material and use the equation of state (EoS). EoS of NaCl or some metals (Au, Pt, Re) have been reliably determined from shock-wave experiments and can be used as a primarily pressure scale. This method requires a X-ray probe to be placed together with the sample, and synchrotron radiation. It is not convenient for experimentalist because it require X-Ray source in laboratory and a long time accumulation.

Much more convenient technique for pressure measurement using small ruby was introduced by Forman et al. ([35]FORMAN et al. 1972) using a small ruby. It was found that R1 – line of a ruby fluorescence shifts with pressure and this dependence was calibrated against EoS

in X-ray diffraction measurements. It turned out that the ruby luminescence method is very convenient; in particular, Ruby is chemically inert and micrometer-size can produce a good signal. Ruby scale was a real breakthrough in pressure measurement and make possible to conduct researches under high pressures with DAC for many laboratories.

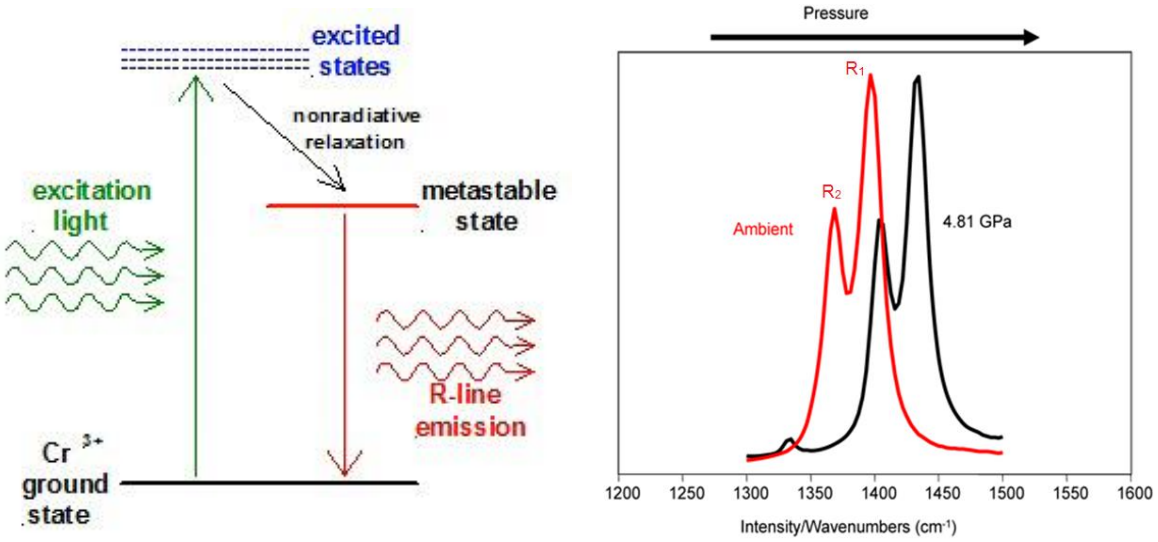

Figure 2.9 – Example of pressure dependency of ruby fluorescence

Ruby scale has limits on pressure and temperature range. For the pressures higher than one Megabar R1 – line broadens and its intensity become comparable with the increasing intensity of diamond. Also for temperatures more than 700 Kelvins R1 – line also broadens and using the ruby scale becomes inaccurate. Spectra of the ruby luminescence at 220 GPa presented on Figure 2.10. Therefore practically only X-ray diffraction of a pressure gauge worked at megabar pressures.

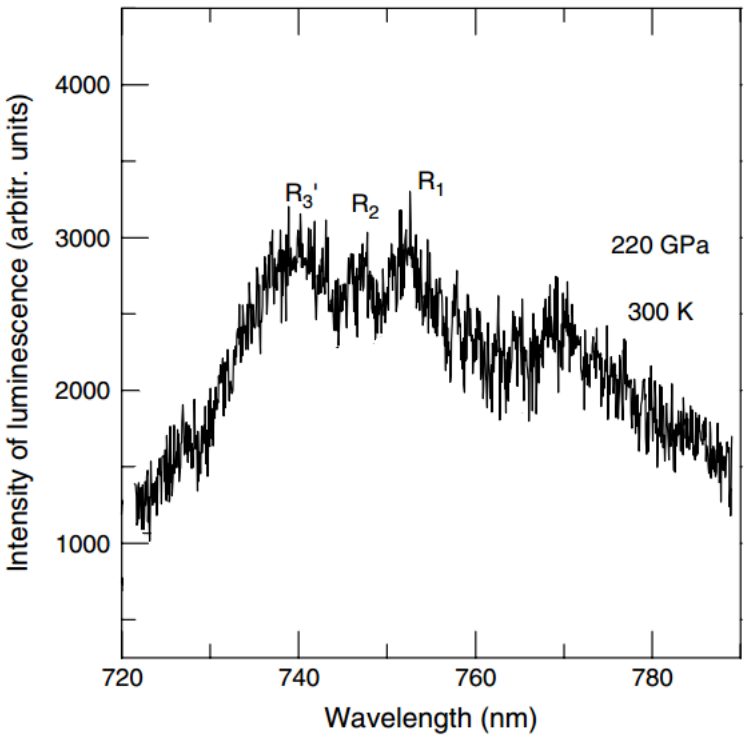

Figure 2.10 Spectra of ruby luminescence at high pressures

Diamond edge scale

For a long time it was known that the Raman spectrum of diamond anvil changes with pressure. Hanfland and Sayassen (1985) reported that high-frequency diamond edge has a linear dependence on the pressure till 300 kbar (0.3 GPa) ([45]Hanfland, Syassen 1985). However they concluded that this shift would be hardly used for determination of pressure mainly because the stresses at the tip of the loaded anvils are highly nonuniform and should strongly depend on the geometry of the anvils, particular gasket etc. However the accumulated experience showed that in fact the pressure dependence of the diamond edge is surprisingly universal and can be used for a reliable estimation of pressure. This pressure scale was introduced by Eremets ([26]Eremets 2003) and then extended for pressures up to 410 GPa ([3]Akahama, Kawamura 2010).

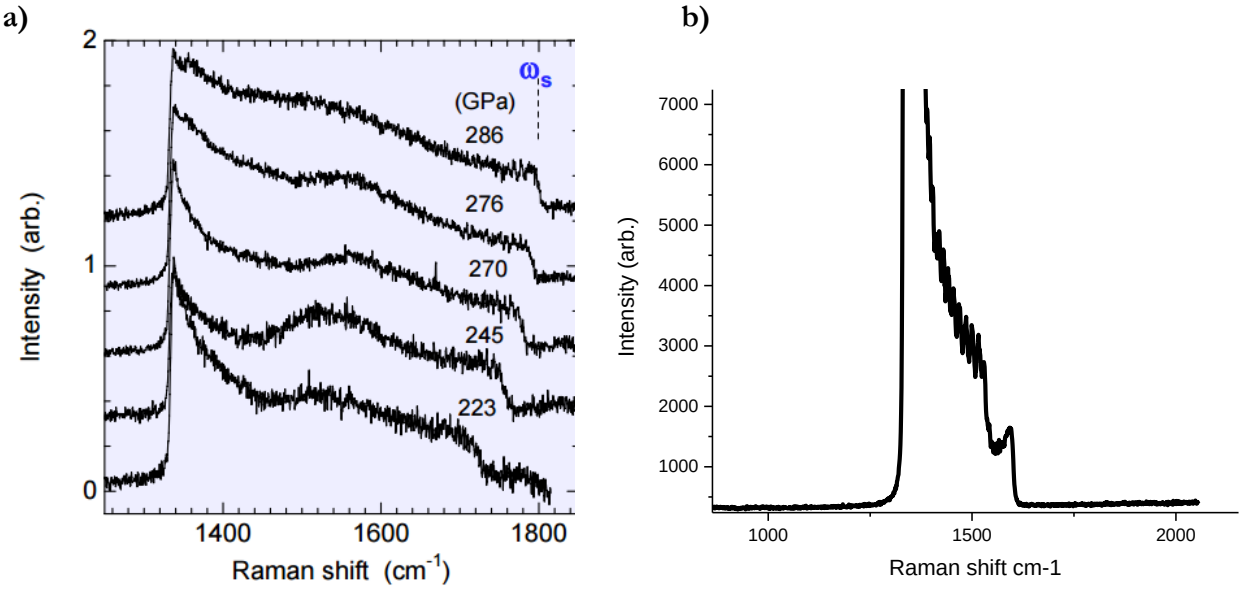

Figure 2.11 - Raman spectra Raman spectra of [001] anvil

Akahama also analyzed differently oriented diamonds: not only typical 001 orientation of the anvil axis but also 111 and 110 ([2]Akahama, Kawamura 2007). This scale is important for determination of pressure with synthetic CVD diamonds which are typically 110 oriented and the diamond edge spectrum is complicated (Fig. 2.11b).

Chapter 3

Experiment preparation

Experiment preparation with resistivity measurements can be divided into the following steps:

- Diamond polishing and alignment
- Gasket preparation
- Electrodes preparation

For the low-temperature loading, a special technique of loading in a cryostat can be applied.

- Low-temperature cryostat loading

3.1 Diamond polishing

Already polished diamond anvils are typically commercially available. We prefer to polish the tip of diamonds by our own. This takes some time but in fact not so long: it is needed about couple of hours to make the most complicated shape with double bevels and culet 10-20 μm. But it gives many advantages: anvils can be done quickly of any desired form, repairmen is also quick. All stages of diamond processing are controlled and this is most important for interpretation of failures of the high pressure experiments as the polishing process can introduce defects. In fact the process of diamond polishing is very interesting and still not well understood. We spent a lot of efforts and studies on polishing of diamonds.

In traditional technology diamond is polished on a specially prepared rotating cast disk (Figure 3.1). The disk is embedded with a diamond grit which is produced by rubbing a mixture of olive oil and diamond powder of specific size into a cast-iron disk. The process of diamond polishing is still not clearly understood. Likely carbon in a diamond experience sp3-sp2 transformation and then is removed mechanically or reacts with oxygen in the air ([75]Pastewka et al. 2011).

Achievement of ultrahigh pressures requires flawless preparation of the diamond surface. In our work, we tried to use a different type of disks for polishing diamonds. We have used:

- standard cast iron disk embedded with diamond
- cast iron disk covered by a mixture of diamond powder and polyvinyl butyral phenol-formaldehyde adhesive (Russian "BF-2" adhesive)
- clean cast iron disk
- stainless steel disk

Each polishing disk has its advantages and disadvantages which will be further described.

Figure 3.1 Diamond Polishing machine

Using clean cast iron disk for diamond polishing

Disk preparation: Polishing of the cast-iron disk can be performed with silicon carbide abrasive. Initially, polishing starts from coarse 120 grit and ends with fine 1200 grit. After the disk polishing, it should be few times cleaned in the ultrasonic cleaning machine. It's important to note that cast-iron has cavities on its surface, and these cavities are full of the polishing abrasive (Figure 3.2). For cleaning a disk from the polishing abrasive the ultrasonic cleaning machine should be used. It's effective to remove residual abrasive from cavities. The abrasive particles can harm diamond during polishing.

Time of one disk polishing is about one day.

Diamond polishing process:

Time of polishing one anvil on clean iron cast disk is around 1-2 hours.

Figure 3.2 Cast Iron disk with cavities which are partially full of silicon carbide abrasive

Cast iron disk embedded with diamond

Disk preparation: Cast-iron disk is initially polished with the silicon carbide cap wheel. Then polishing disk should be cleaned in the ultrasonic cleaning machine to remove possible abrasive. Then a mixture of 1-micron diamond powder and olive oil is rubbed into the disk.

Time of preparation of the disk is about one day.

Diamond polishing process: Using of such disk is a traditional way of diamond polishing. According to current knowledge, diamonds charged into the disk are polished so that they form a flat surfaces parallel to the surface of the disk (Figure 3.3). During diamond polishing carbon in the diamond most probably undergoes sp3-sp2 transformation and then removed mechanically or by oxidation.

Time of the one anvil polishing on the cast disk embedded with diamond is much faster than on the steel disk and it is around 30 minutes.

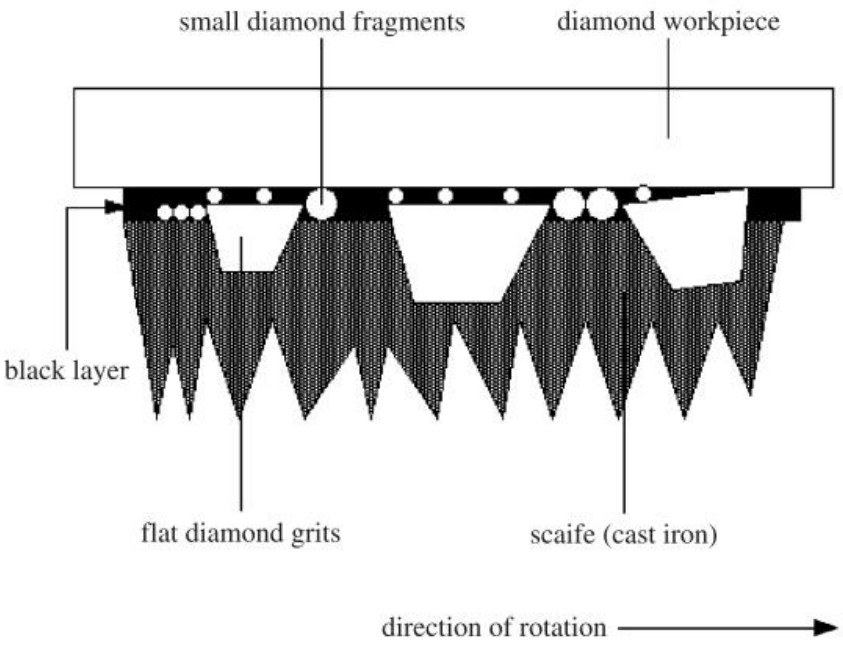

Figure 3.3 Schematic showing the postulated action of the diamond-polishing process. The flat diamond grit particles act as 'anvils' and allow smaller diamond fragments present in the black layer to exert high pressures on the diamond workpiece. The flat diamond grit particles can also pivot to present sharp edges to the oncoming diamond workpiece ([47]Hird, Field 2004).

Cast iron disk covered with mixture of diamond powder and Russian "BF-2" adhesive

Disk preparation: Cast iron disk is polished with the silicon carbide cap wheel and cleaned in ultrasonic cleaning machine. Then a mixture of 1-micron diamond powder, "BF-2" adhesive and alcohol should be sprayed on the surface of the disk, and disk is placed at a temperature of 200 °C for a few hours. Then polymerized mixture should be grind into the disk with diamond crystal.

Diamond polishing process: The polishing process on such disk is similar to polishing on a standard disk made with olive oil.

Using of clean stainless steel disk for diamond polishing

Disk preparation: Polishing of the stainless steel disk is performed with a diamond paste and special rotating microfiber cloth laps. Typically polishing starts from the rough 30 microns diamond paste. Then the size of diamond paste decreases by steps, and lower size particle removes scratches from the previous one. By accurately examining the surface of the stainless steel disk after polishing we detected some diamond inclusions on the disk (Figure 3.4). We checked the presence of the diamond by Raman spectra.

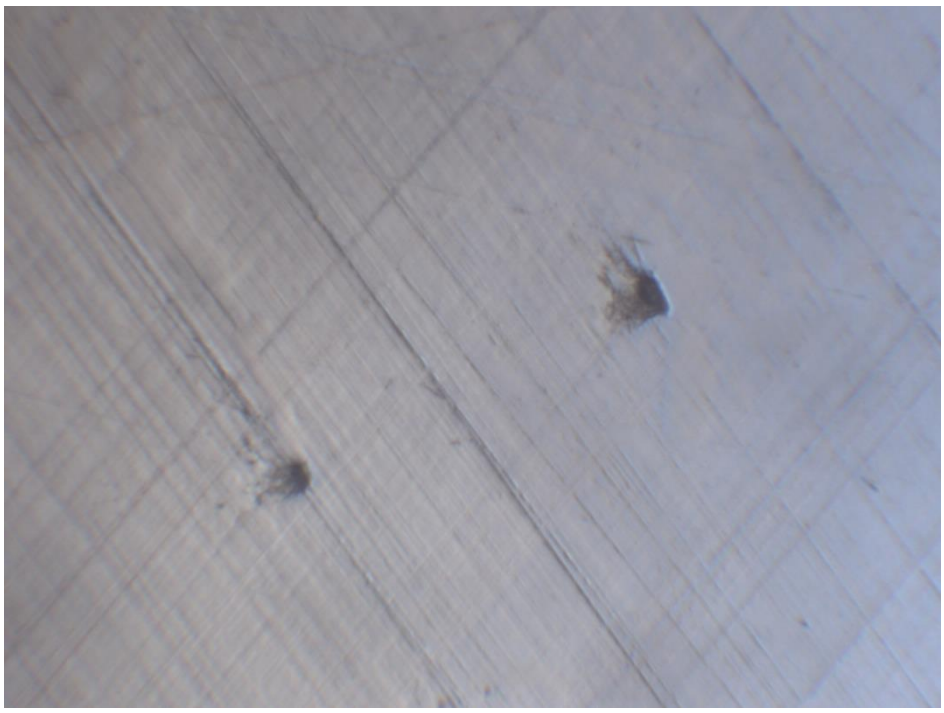

Figure 3.4 Rare diamond inclusions on stainless steel disk after disk re-polishing with 3 micron paste.

Diamond polishing process: Process of diamond polishing on the clean stainless steel disk is not fully understood. The hardness of the diamond is much higher than the hardness of the stainless steel, and diamond should make scratches on disk without any effects on the diamond. The polishing process on the stainless steel likely differs from the polishing on the cast-iron embedded with diamond. We didn't notice any dependence of the diamond anvil orientation on the polishing speed which is well known for the standard scaife. The speed of disk rotation is much higher than in the case of cast-iron disk, and diamond holder heats a lot. It can be supposed that first layer of the diamond reacts with iron and iron carbide forms on the disk surface. Then iron carbide works like an abrasive. During the diamond polishing, stainless steel disk becomes covered with some yellow powder and in the Raman spectra there is a lot of carbon on it. The speed of diamond polishing on the steel disk is very slow compared to the standard cast iron disk embedded with diamonds.

One of the main disadvantages of steel disk is its fast spoiling. The hardness of the diamond is much higher, and it sometimes leaves very big deep scratches on the disk (Figure 3.4). Very soon whole disk become covered with scratches, and it should be repolished.

Polishing of one disk takes at least one day. In case of very deep scratches on disk it can take up to three days.

Time of polishing of one diamond anvil on stainless steel disk can be about 2-4 hours.

Discussion of results of polishing on different disks

Which type of disk is better for polishing is not very clear. Cast iron disk with diamond powder (prepared with olive oil) has the best speed of diamond anvil polishing and lowest speed of spoiling. Important to note that hardness of the cast iron disks can be different and for the good result the hardness should be maximal. During diamond polishing on soft disk big grooves appears on it (like on the clean steel disk) and very fast in becomes unusable.

In our experiments, a pressure near 400 GPa was reached with each type of disks, but more important that these pressure results were not fully reproducible for all kind of disk.

Cast-iron disk prepared with a mixture of diamond powder and olive oil is specially charged with diamonds. Charged diamonds allow perform very fast diamond anvil polishing. During polishing process diamond anvil leaves big scratches on the disk and it's reasonable to assume that diamond anvil not just slide over a surface, but go inside the disk in some depth and unavoidable bumps up against the charged diamonds on the big speed. Subsurface damage can occur after such collisions.

3.2 DAC preparation

We consider the following steps of preparation of DAC.

First, diamond anvil is glued into a seat with the following appliance (Fig 3.5).

Figure 3.5 A process of diamond gluing into the seat

After that culet is cut so that it is parallel to table of the seat. Therefore diamond's culets are automatically parallel each other in the DAC and no tilting mechanisms for alignment are required. Diamonds only should be translated to match culets.

The first step is to put the culet at the axis of DAC. This is important for symmetric loading, and also because culet will not move out of the center (and from another anvil) at small rotation of piston. To align, we place the seat on piston of DAC on a layer of epoxy, touch anvil against glass plate covered with a thin color film (it can be a trace of marker), Figure 3.6. After rotation, culet makes a ring on the surface (Figure 3.6). After that culet is pushed by a stick towards the center of this ring, then rotated once again – smaller ring is created – and finally the culet can be precisely centered. In this position, anvil is slightly pressed and whole DAC is placed in oven for solidification of epoxy.

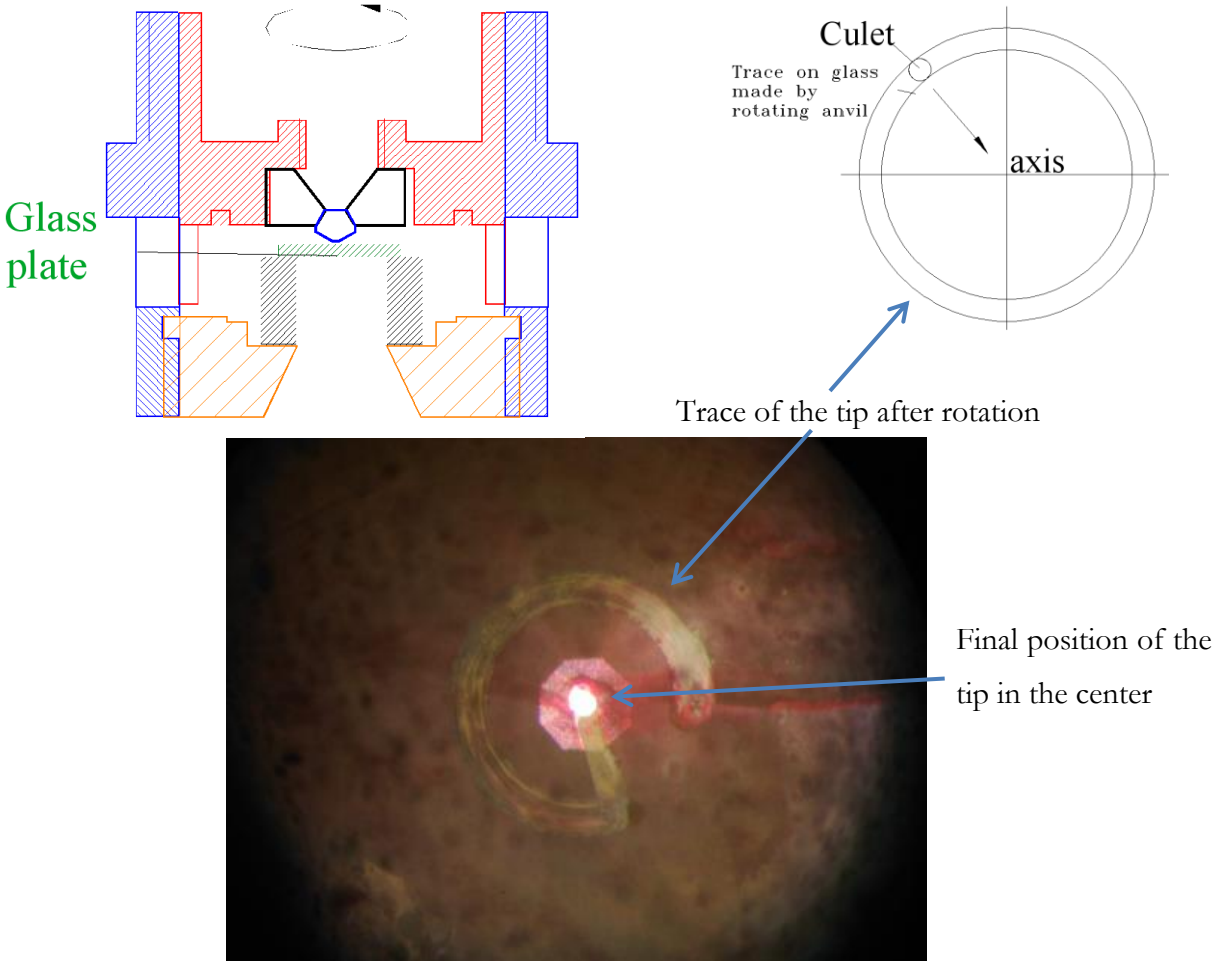

Figure 3.6 Alignment of anvil at axis of DAC. At the beginning the anvil is an arbitrary position (off the axis). At rotation of the piston the anvil tip describes a circle and leaves a trace on the glass plate covered with a very thin layer of paint (e.g. made my marker) (right). This circle is seen through microscope and it gives idea where anvil should move to bring it to the axis. The seat moves by pushing it with a stick through DAC widows. If necessary, this procedure can be repeated when the ring will be closer to the axis, and the anvil can be moved to the axis precisely.

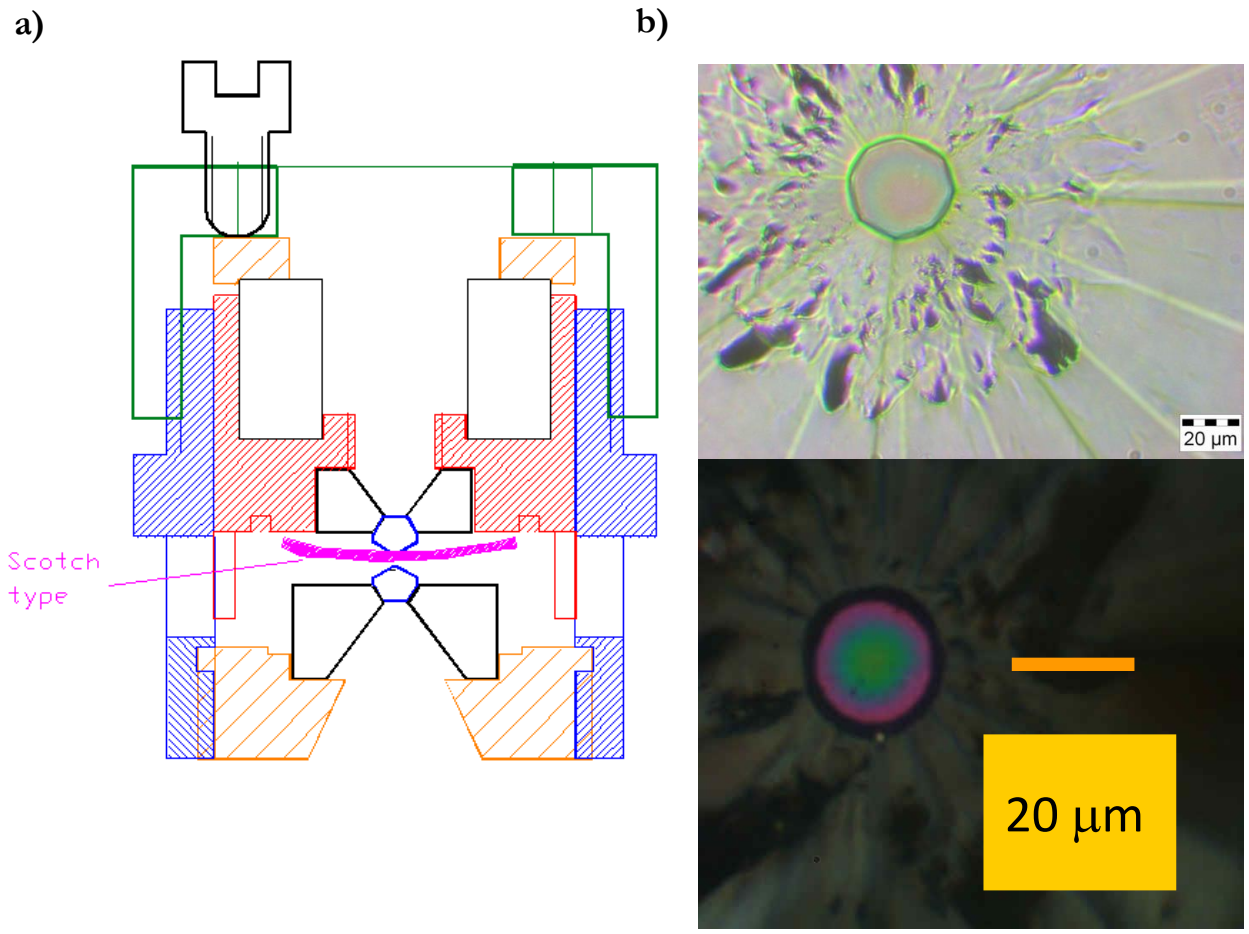

Figure 3.7 Alignment of the base anvil against the anvil placed at piston. It is made by translation of the seat at observing both culets through the Scotch film separating the anvils. Right – images of small culets at final stages of alignment

Then the second anvil (placed on base of the DAC on a layer of epoxy) can be aligned against the first anvil. This is more delicate procedure because anvils can be seriously damaged, if even slightly touch each other - this is of obvious for very small culet 20-50 μm. To prevent this, it is very useful to put a film (a. g. both side Scotch tape) in between anvils. In this case anvils do not touch directly and process of alignment is well controlled.

The base seat is situated on liquid epoxy and therefore very weakly bonded to the DAC body. For this reason, DAC first should be placed vertically so that anvils are observed through piston (Fig. 3.7). At the beginning the base seat can be roughly positioned at the axis by pushing it with a stick through widows of DAC. Then piston is gently moved towards the anvils situated at the base so that piston anvil touches the film. After this, images of culets become clear and they can be precisely aligned by translation of the base seat (pushing it with a stick). After further approaching anvils, a view drastically changes (Fig. 3.7b): it looks as if diamond anvils crack, but

in fact this is a result of extrusion of the film when culets approach each other. At further very gentle pushing of the piston the culets image again becomes clear and at this stage the culets can be finally aligned. The separation between culets is few μm at this stage anvils and can be glued (epoxy solidify). This final stage should be controlled very carefully as pressure >30 GPa can be easily generated and small circular cracks produced. It is better to stop before the "explosion region" (Fig. 3.7b). Gluing can be done in oven but all parts should be made of the same material. If use spring made of BeCu, it will expand stronger that the body and will break diamonds. Alternatively, faster epoxy can be used which solidifies in few hours at room temperature.

After gluing, anvils should be very carefully separated applying only pulling force. Then the gasket should be prepared. It will protect anvils from direct contact at all subsequent procedures. Gasket can be made of different materials. Mostly we use T301 steel, rhenium, or tungsten.

3.3 Gasket preparation

In our experiments, we mostly use steel or rhenium as gasket material. Steel gasket should be pre-indented up to 15-20 GPa. Then hole of the appropriate size is drilled in the middle of the gasket for sample loading. For electrical measurements steel gasket should be insulated from wires. Different materials can be used as an insulator. A cubic boron nitride (cBN) mixed with epoxy can be used for this purpose. It forms a thick layer and has a good adhesion with steel or rhenium. We tried to use different materials: cBN/epoxy, Teflon, $CaSO_4$, NaCl, Al_2O_3/epoxy, MgO/epoxy – but there is no much difference what to use. Some materials as Teflon or NaCl forms an insulating layer which is much thinner, and it can lead to the shortening of the electrodes on the metal gasket. On the other hand, they are transparent, and it's much easier to work with them.

Metallic gasket

We place a piece of metal on the supporting ring (Fig. 3.8). This ring helps to hold gasket perpendicular to DAC axis and imprint gasket symmetrically. The ring should be slightly lower than the level of culet (more than half of the gasket thickness). Ideally, it should rest on the ring after indentation. If ring is too high, the gasket will bend under loading, then lift due to elastic deformations – this is bad. The gasket should "hang" on the culet– this is important because in this case the gasket can freely move between diamond culets and find the right position reproducibly.

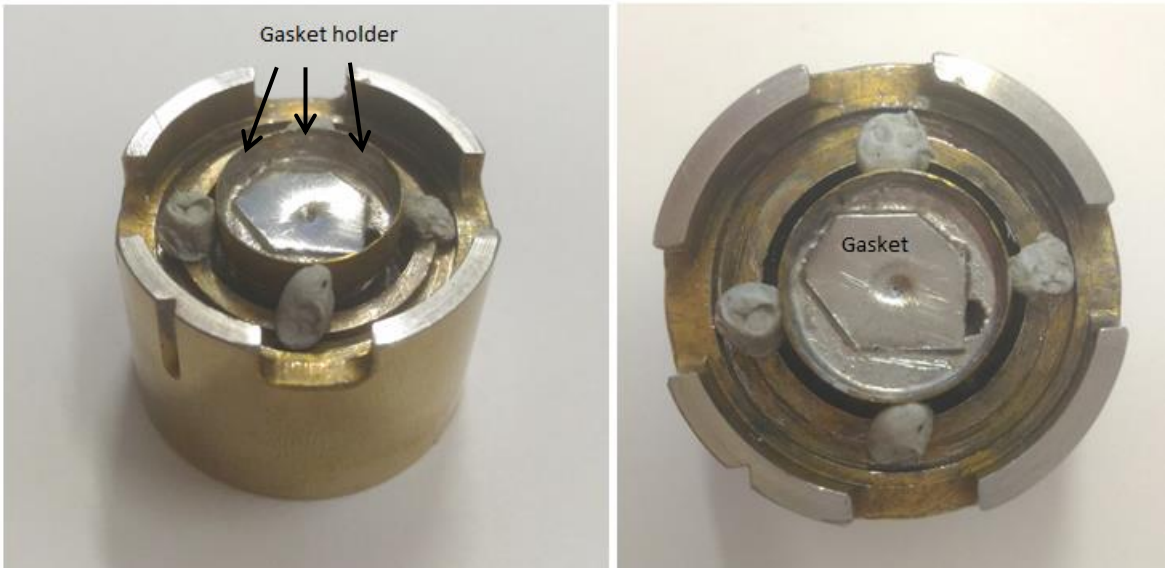

Figure 3.8 Gasket alignment on the diamond

Thickness of the gasket

Certain gasket thickness is very important for good loading and reaching of high pressures. Optimal thickness depends on the culet size and sample. Gaseous samples are very compressible from 0 to 20 GPa and hole in the thick gasket will be clamped before loading of the sample. The solid and fluid sample under the pressure can become harder than the gasket material, and gasket will not be stable. In general - thinner the gasket – better the loading. On the other hand, the thin gasket effects on the limit maximum possible pressure. Large thickness of the gasket is required for the high pressure. Therefore the ideal thickness should be found depending on the sample characteristic and diamond anvil geometry (especially culet size).

The first step is to pre-indent gasket up to 10-20 GPa to form initial thickness. For reproducible placement of the gasket on the diamond, it should be marked relatively piston or cylinder. Then a hole is drilled in the center of the gasket, the gasket is placed between two anvils and clamped. Hole in the gasket begins to clamps and thickness reduces.

The thickness of the gasket is measured by the interference which appears when diamond anvil cell is lighted with white light. Two diamonds form Fabry–Perot interferometer.

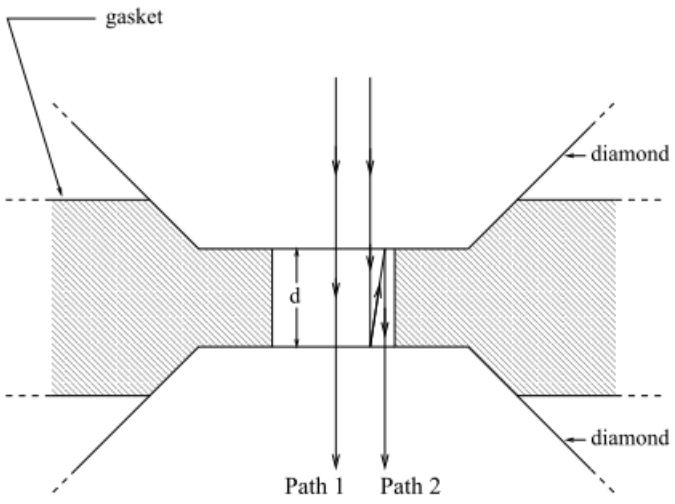

Figure 3.9 Diamonds form Fabry-Perot interferometer

Transmittance function is determined by the equation ([25]Eremets 1996):

$$T = \frac{n^2}{n^2 + (n^2 - 1)^2 \sin^2 \gamma}$$

Where $\gamma = 2\pi ndv$

d – is the distance between two anvils

ν – wavenumbers

n – refractive index

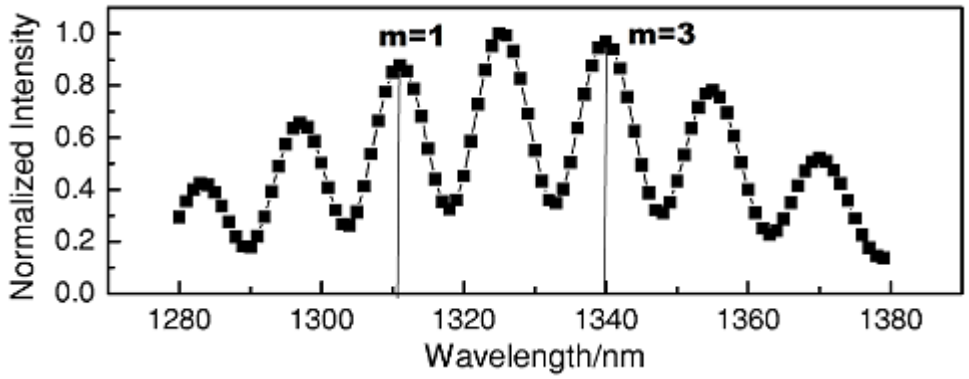

Figure 3.10 Interference maximum on the transiotion spectra

When the transmission is equal to 1, we can observe interference maximum on the Raman spectra. Typical Raman spectra can be seen in Figure 3.10. Condition of maximum in the interference is:

$$2\pi ndv = \pi m \quad (m = 1,2,3 \dots)$$

$$2ndv = m \quad (m = 1,2,3 \dots)$$

To eliminate *m* from the equation and calculate the distance between anvils the difference between two interference maximums can be calculated from Raman spectra. We measure the distance between anvils in the hole in the gasket, so refractive index n is equal to 1.

$$d = \frac{\Delta m}{2\Delta \nu}$$

Insulating gasket preparation

To prepare an insulating layer for electrical measurements the bottom of steel gasket should be drilled out. Then steel gasket should be well cleaned. After that, the full crater of the steel gasket is filled by a cBN and gasket should be indented to 3-5 GPa. As a result, one gets a steel gasket which is isolated with cBN. At the edges of the steel gasket's crater cBN layer can easily be broken. So it's useful to glue it with epoxy by putting a small drop of epoxy on the steel gasket far away from the crater and carefully moving it to cBN. After polymerization of the epoxy, cBN is firmly glued to the steel, and it should be again indented to ~10-15 GPa. Formation of the hole in the insulating gasket is similar to the formation in the steel gasket.

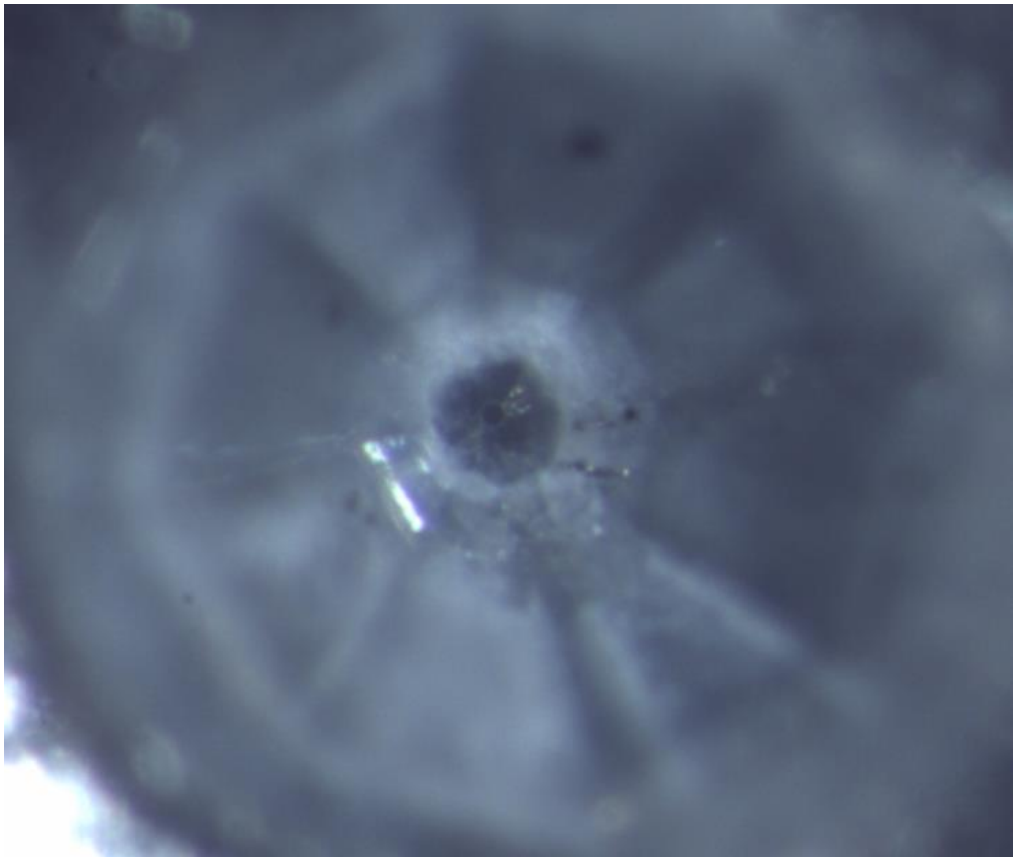

Figure 3.11 NaCl gasket with hole in the center

After the hole is formed electrodes can be prepaid. Then gasket is placed on the anvil and hole is filled with the sample. The solid or fluid sample can be placed in the hole and clamped by diamonds. To load a gaseous sample anvils are moved close to each other until both of them will touch the gasket. Then anvils should be separated a little to allow gas to flow into the hole. The initial gas pressure during the loading is about 0.2 GPa.

3.4 Preparation of electrodes

Electrical measurements in the high-pressure experiments are very complicated. Preparation of the insulating gasket and making of wires is not a common and well-established technology. Each experimental group uses its own techniques.

Manually crafted electrodes

Frequently used technology for the culets more than 100 micron is to make electrodes from platinum strips or other metallic foil and lay them by hands. This method was first introduced by Mao and Bell ([61]Mao 1981) and Shimizu ([87]Shimizu et al. 2002). Disadvantage of this method is a big constraint on the size of culet and sample. It's very complicated technique to place tiny strip by hand inside the culet around 20-30 micron while it is possible ([29]Eremets et al. 2001). But this size of culet is required for an experiment with pressure more than 200 GPa.

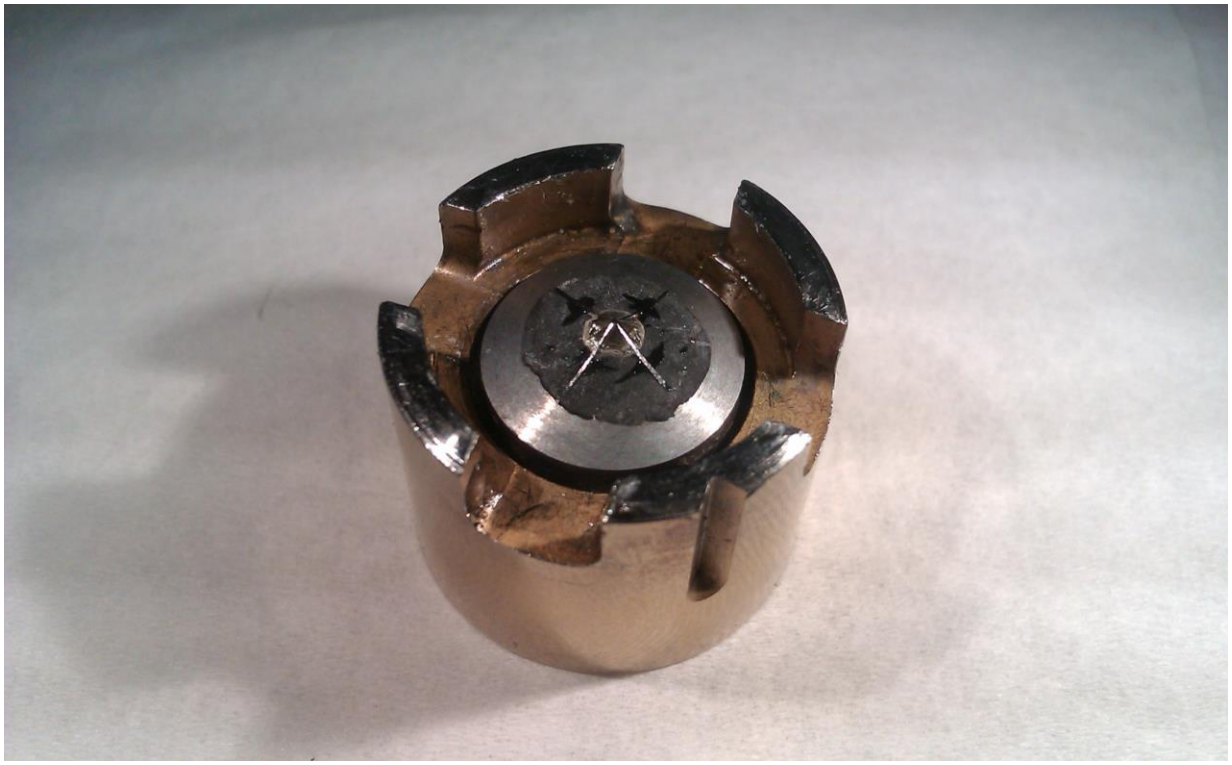

Figure 3.12 Electrodes placed by hands

Focused ion beam lithography

Another method to create electrical contacts on the diamond is to use a focused ion beam ultrathin lithography. Recently work of Rotondu et al. demonstrates good work of lithographic leads up to 240 Gpa ([79]Rotundu et al. 2013). Focused ion beam lithography doesn't have a limitation on the size of the culet. Deposition of the electrodes with this technique can provide precision up to 20 nm. Also the big advantage of this technology is a high robust of the created leads. It's proved in the paper that they can sustain a cleaning with alcohol. Probably such leads can sustain even an indentation of the metal gasket. Unfortunately, a very high cost of focused ion beam system makes this technology inaccessible for major part of laboratories.

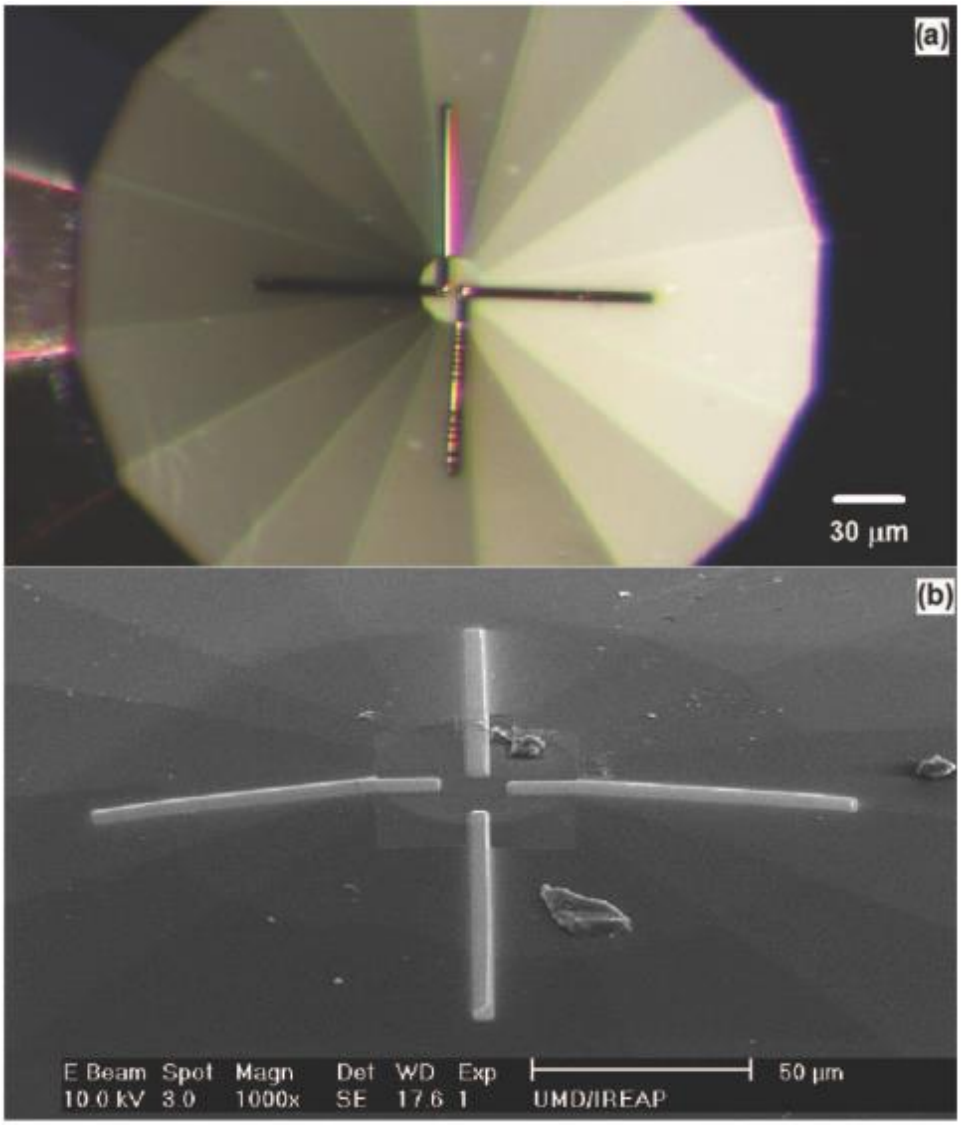

Figure 3.13 - Beveled diamonds with FIB lithographic electrical contacts for multimegabar DAC resistivity measurements ([79]Rotundu et al. 2013).

Sputtered electrodes

Another way to form ohmic contacts on the diamond is a sputtering of Ti, Ta, Al or other metal on the diamond. Technology of the good ohmic contacts formation has been developing for a long time ([15]Das K. et al. 1992; [33]Evans et al. 2009; [97]Werner M. et al. 1995). In our experience, the electrodes are made with the aid of a mask which cover diamond. The mask has four slits through which metal can be sputtered should be manufactured. In our experiments we make a mask from an aluminum foil and place it above the diamond. In sputtering system diamond should be ion etched for 30-40 seconds and without breaking vacuum metal contacts can be sputtered. Ion beam etching is used to clean the surface of diamond once again which can be contaminated during placing a mask. The thickness of sputtered metal is about 0.1 micron. Metal contacts should be covered with gold or platinum to protect electrodes from oxidation. The calculated resistivity of sputtered electrodes is about 10^{-6} Ohm*m. The resisstance of one electrode is about 100 Ohm which is suatable. The sputtered electrodes adher to the diamond surface satisfactory – they can be even cleaned with alcohol, but with time about 2-4 weeks on the open air - resistivity increases dramatically, and electrodes show a semiconductors behavior. Sputtered electrodes can be connected to the copper wires with platinum foil or silver paint. Schematic picture of this design can be seen in Figure 3.14 and photo is on the Figure 3.15.

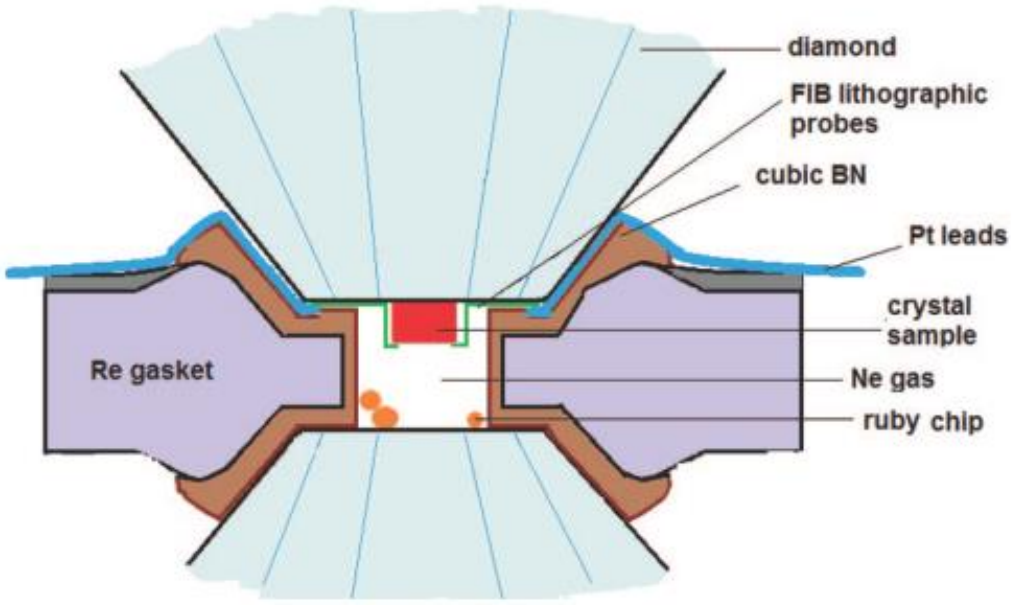

Figure 3.14 Schematic drawing of electric measurements in DAC ([79]Rotundu et al. 2013)

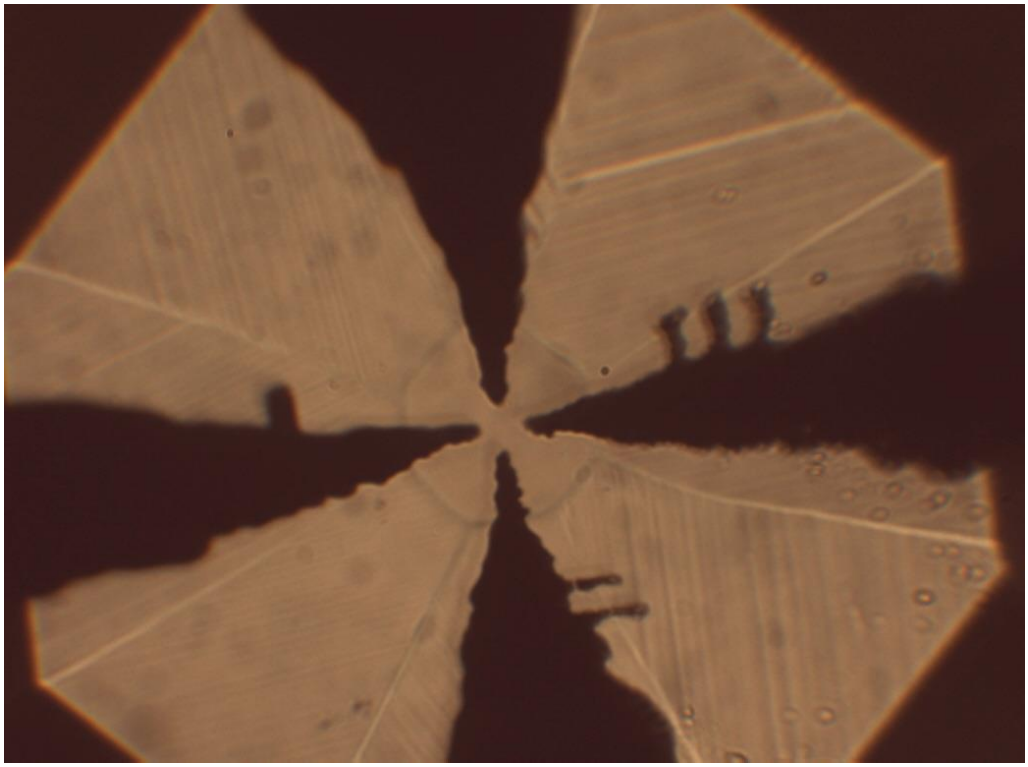

Figure 3.15 Sputtered electrodes

The gasket should also be connected to the fifth wire to have the possibility to check shortage between gasket and electrodes.

3.5 Low-temperature loading in the cryostat

Some samples can decompose under the high pressure and high temperature. To prevent the decomposition a loading at low temperatures can be implemented. A diamond anvil cell can be placed into a cryostat and cooled down to a temperature at which sample become liquid. Then gas can be put into a rim around diamond anvil through a capillary. Schematic drawing of such loading can be seen in Figure 3.16.

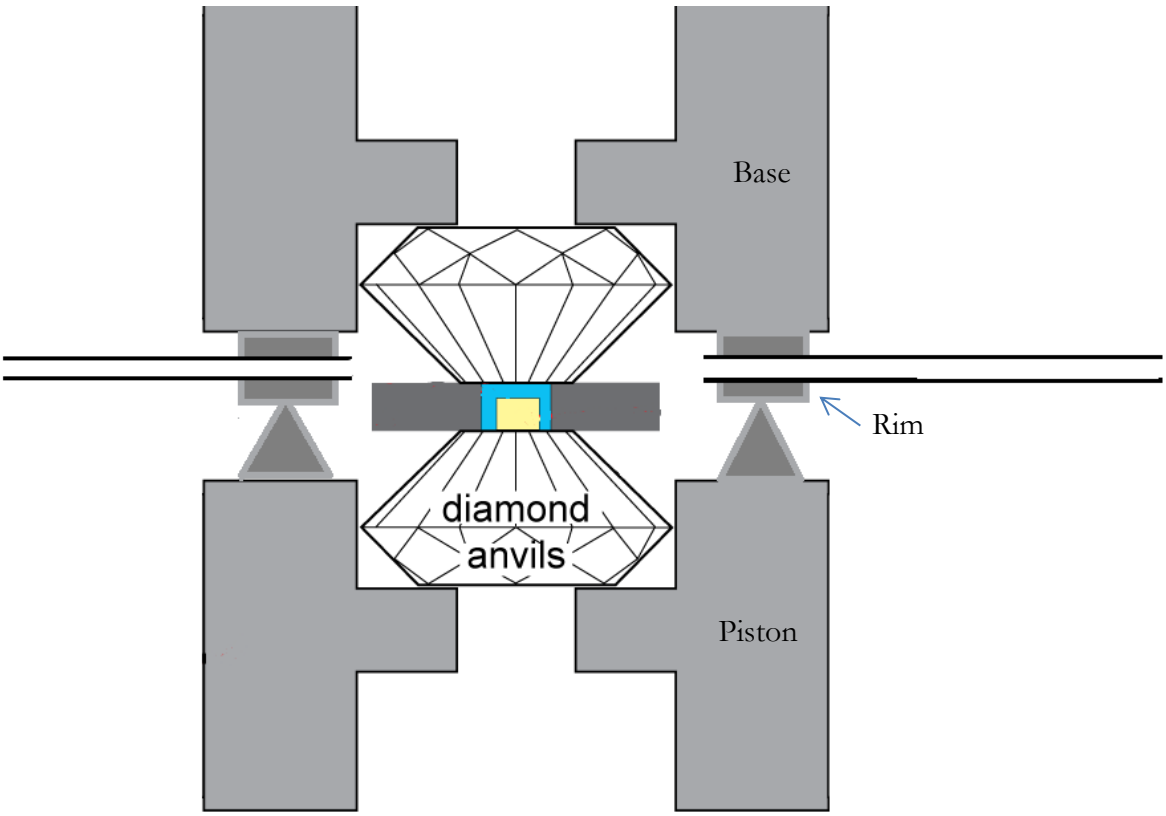

Figure 3.16 Low-temperature cryostat loading

The rim is glued with epoxy on the piston. It is full of indium in the middle and has holes for capillaries and wires. The blade is glued on the base. For a good sealing at the low temperatures Stycast 2850 FT epoxy and catalyst 9 is used. At the room temperature piston is moved close to the base on the distance about 100 microns between two anvils. Blade penetrates into the indium and forms closed space near the anvils. Air from this space should be pumped out through capillaries. At the low temperatures small leaks may appear between the indium and the blade due to different temperature expansion coefficient of the indium and the blade. To close the leaks at the low temperature piston should be moved closer to base on the distance about 20-50 microns between anvils. At temperature lower than the boiling point gaseous sample is put into the rim where it become liquid and completely fills space inside the rim including a hole in the gasket. After this sample can be clamped between anvils and gasket.

Chapter 4

Superconductivity at Sulphur hydride (H_xS)

4.1 Motivation and Previous Results

We have selected H_2S for our experiment for several reasons. First, this is predictions which was made in 2014 ([58]Li et al. 2014). It becomes metal at a low pressure of 100 GPa and has relatively high T_c of 80 K at 160 GPa. From experimental point of view H_2S is available and well-known gas which one do not need to be synthesized in contrast, for instance to KH_6 or CaH_6 ([104]Zhou et al. 2012; [91]Wang et al. 2012). H_2S is not explosive and flammable (in small concentration) like some other hydrides, although it is still corrosive, high reactive and toxic. Leaks of H_2S are easily detectable by the smell in very small, not dangerous concentrations.

H_2S is known as a typical molecular compound with a rich phase diagram ([37]Fujihisa et al. 2004). Infrared studies of H_2S under pressure show that hydrogen sulfide transforms to a metal at the pressures about 96 GPa ([81]Sakashita et al. 1997). The transformation is complicated by the partial dissociation of H_2S and the appearance of elemental sulfur at P>27 GPa at room temperature, and higher pressures at lower temperatures ([81]Sakashita et al. 1997; [37]Fujihisa et al. 2004). Therefore, the metallization of hydrogen sulfide can be explained by elemental sulfur which is known to become metallic above 95 GPa ([55]Kometani et al. 1997). No experimental studies of hydrogen sulfide are known above 100 GPa.

Hydride	Pressure	Tc
CaH6	150	220
KH6	60	166
Si2H6	275	139
AlH3(H2)	250	132
H3Se	300	106
GeH3	180	100
SiH4(H2)2	250	98
LiH6	300	82
H2S	160	80
GeH4(H2)2	250	76
GaH3	160	73
GeH4	220	64
SnH4	200	62
H5Te2	200	57
NbH3	300	38
BeH2	200	30
AlH3	110	24
SiH4	260	16

Recent theoretical work ([58]Li et al. 2014) revised the phase diagram of H_2S, and a number of new stable structures has been found. In Li's work it is predicted that at pressures P>130 GPa – higher pressures than experimentally observed – hydrogen sulfide was predicted to become a metal and a superconductor with a maximal transition temperature of ~80 K at 160 GPa. Precipitation of sulfur has been found to be very unlikely, in apparent contradiction to the experiments ([86]Shimizu et al. 1995; [37]Fujihisa et al. 2004).

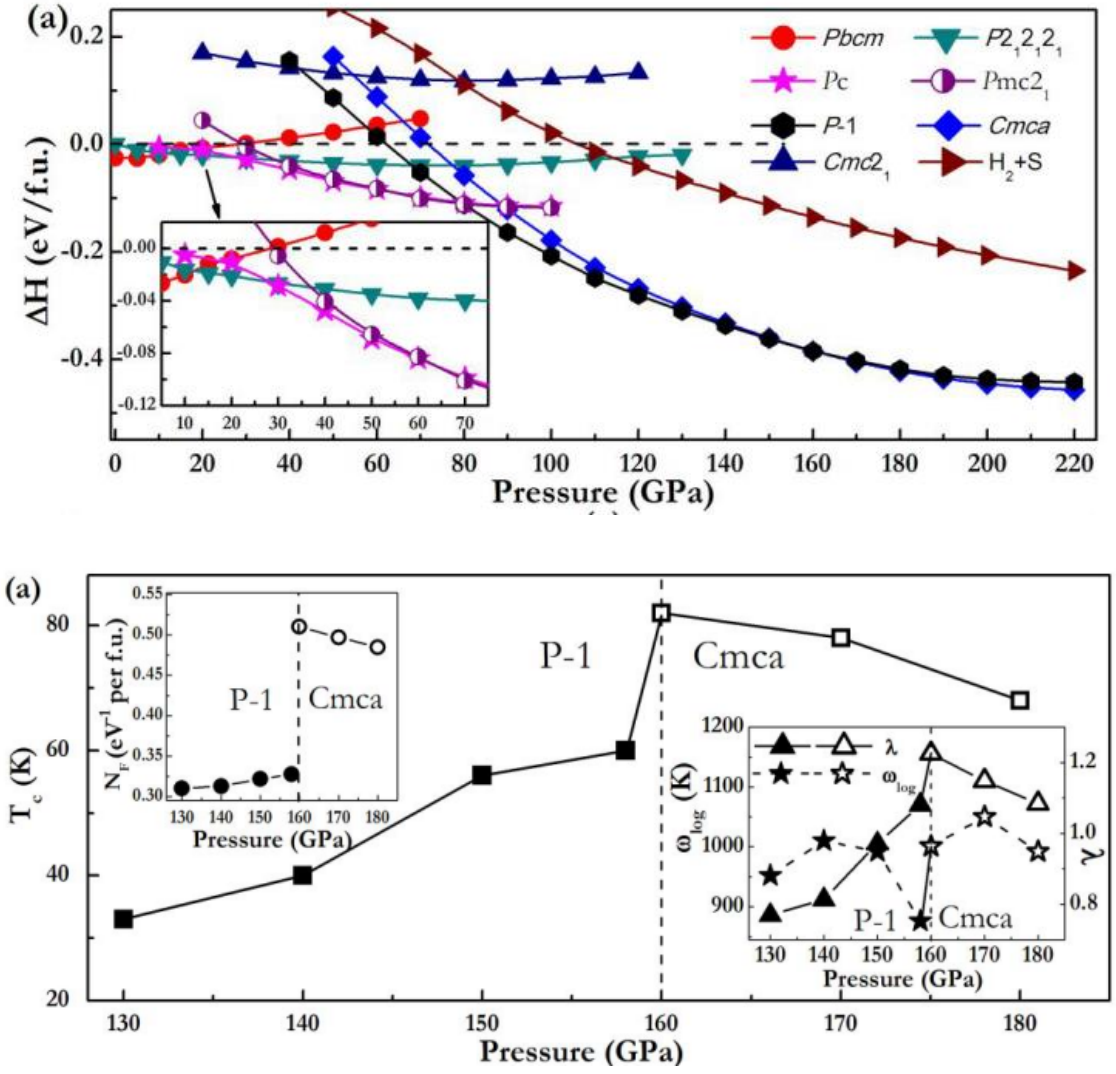

Figure 4.1
a) Enthalpy curves of various structures with respect to the previously predicted Ibca structure. The results of some previously proposed structures are not shown since their enthalpies are extremely high, out of comparison range in the figure. The enthalpies of S + H_2 with respect to the Ibca structure were also plotted to examine the thermodynamical stability of H_2S at high-pressure
b) Pressure dependence of T_c within P-1 and Cmca phases ([58]Li et al. 2014).

4.2 Experimental Results

In our typical experiment, we perform loading in a cryostat at temperatures of liquid hydrogen sulfide. The DAC was placed into a cryostat and cooled down to 191-213 K (within the temperature range of liquid H_2S) and then H_2S gas was put through a capillary into a rim around diamond anvil where it liquified. H_2S of 99,5% and D_2S of 97% purity have been used. The filling was monitored visually (Fig. 4.2) and the sample was identified by measuring Raman spectra.

Video of loading process is available online here: https://vimeo.com/131914556

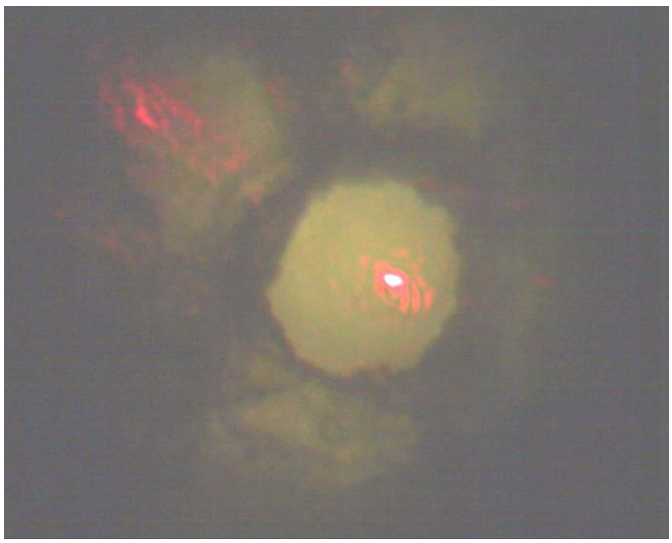

Figure 4.2 – Loading of H_2S sample at 191-213 K temperatures

Then liquid H_2S was clamped in the gasket hole by pushing the piston of the DAC with the aid of screws outside the cryostat. The thickness of the sample can be estimated to be few microns as measured from interference spectra through the clamped transparent sample. The thickness might be ~1 μm in if the sample expanded over the culet. After the clamping, DAC was heated to ~220 K to evaporate the rest of the H_2S, and then the pressure was further increased typically at this temperature. The pressures remained stable during the cooling within ±5 GPa. The low-temperature loading seems to be required to prepare samples with high T_c. If H_2S was loaded at room temperature in the gas loader, for example, only sulfur was detected in Raman and X-ray scattering.

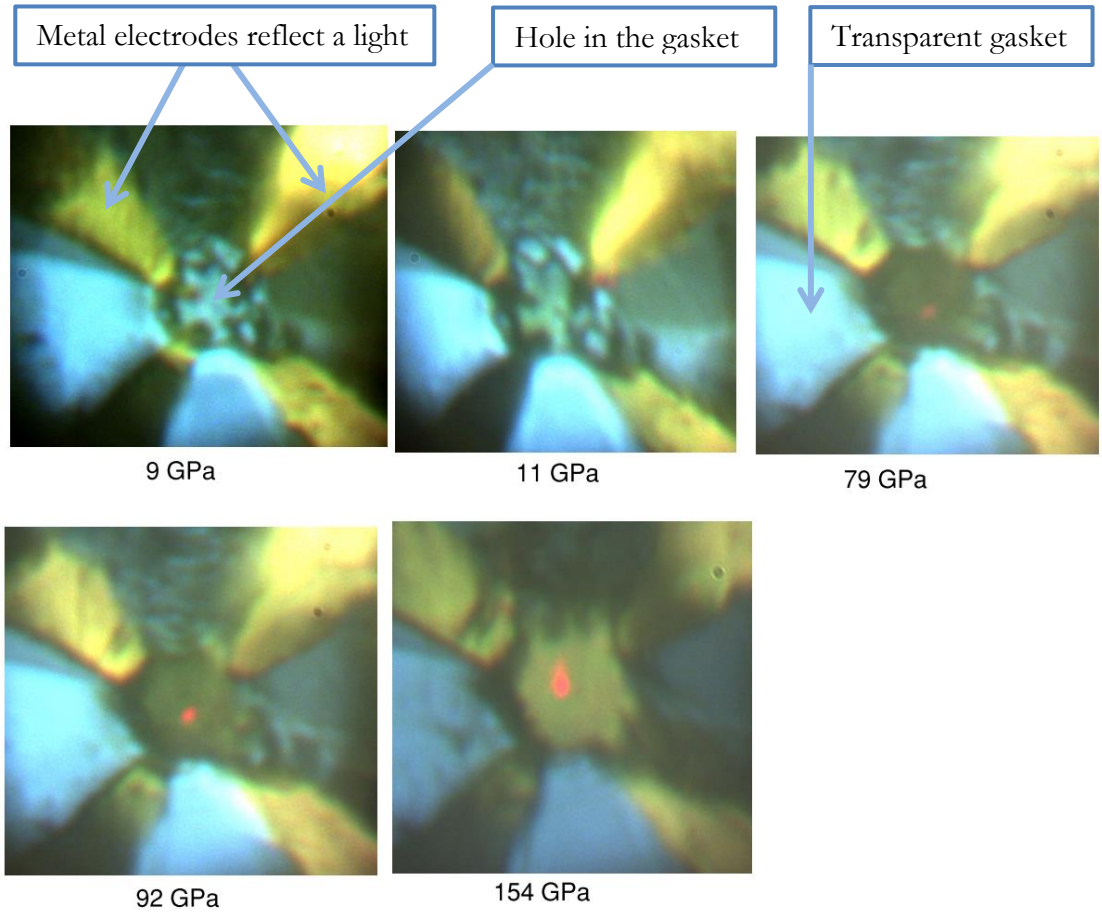

Figure 4.3 Sample's transformation during pressure increase.

Figure 4.3 shows sample's transformation during pressure increasing. Pictures are made with transmitting and reflective light simultaneously. Blue parts of the pictures are the transparent gasket. Yellow is a reflection from the metal electrodes. The sample is transparent at 9 GPa. Darkening begins at about 11 GPa and sample become opaque at about 30-40 GPa. Very weak reflection appears at 79 GPa. Reflection of the sample becomes comparable with electrode's reflection at about 150 GPa.

Raman measurements

For optical measurements, a Raman spectrometer was equipped with a nitrogen-cooled CCD and notch filters. The 632.8 nm line of a He-Ne laser was used to excite the Raman spectra and to determine pressure. The pressure was determined by a diamond edge scale ([26]Eremets 2003) at room and low temperatures.

The Raman spectra of H_2S and D_2S were measured as the pressure increased and were in general agreement with the literature data ([85]Shimizu et al. 1992; [86]Shimizu et al. 1995).

Hydrogen sulfide lost their molecular identity at a pressure of 50 GPa as the vibrons vanish (Figure 4.4). Above this pressure only a broad band at 1900 cm^{-1} remains. Vibron modes disappear in D_2S at a higher pressure about 100 GPa. Lattice modes in H_2S disappear above 150 GPa.

Raman spectrum is complicated by the decomposition of H_2S with precipitation of elemental sulfur. In our Raman measurements, precipitation of sulfur can be observed at a pressure about 70 GPa and temperature of 200 K. Raman peaks at 160 cm^{-1} and 600 cm^{-1} appeared in H_2S and D_2S. Stronger peaks of elemental sulfur in Raman spectra can be observed in the samples which were exposed at room temperature at low pressures. If the sample is cooled at the temperature about 200 K sulfur likely is in small amounts, only weak Raman peak is seen at the highest pressures which can be assigned to sulfur. Raman spectra of sulfur were measured separately at the room and low temperatures.

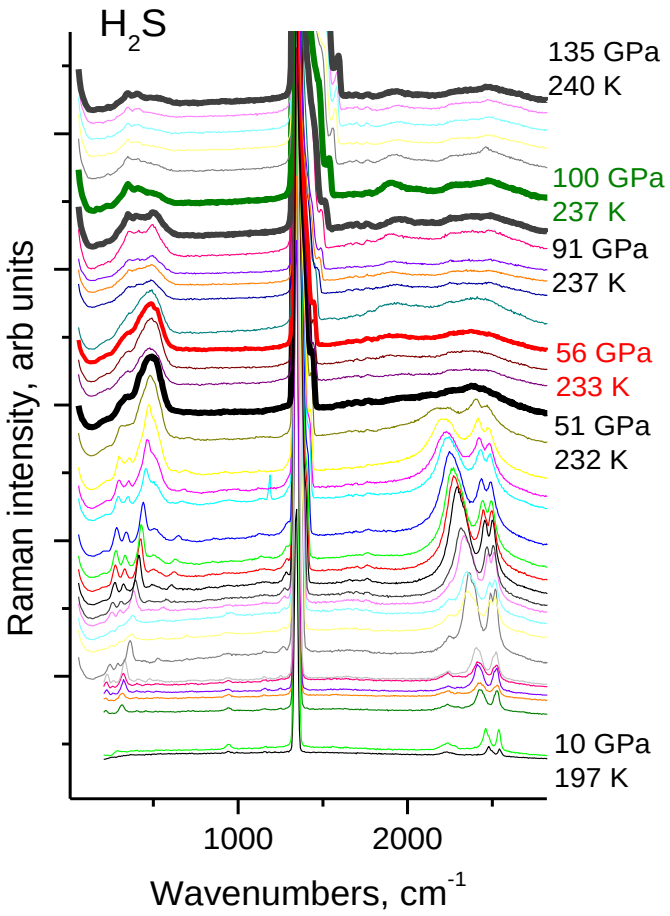

Figure 4.5 H_2S Raman spectra

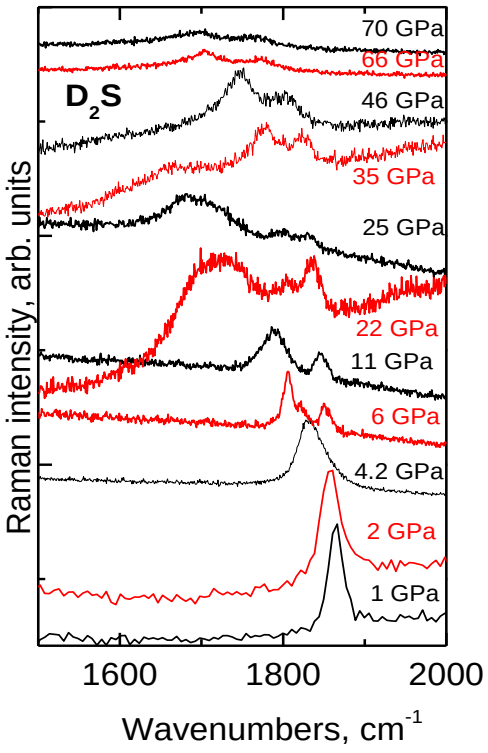

Figure 4.4 - Raman spectra of D_2S measured at T~170 K.

In contrast to the clear evidence of sulfur even traces of hydrogen vibron were never observed despite the use of the ultralow luminescence synthetic diamond anvils. No hydrogen vibron has been found even after 1 hour of accumulation ([37]Fujihisa et al. 2004).

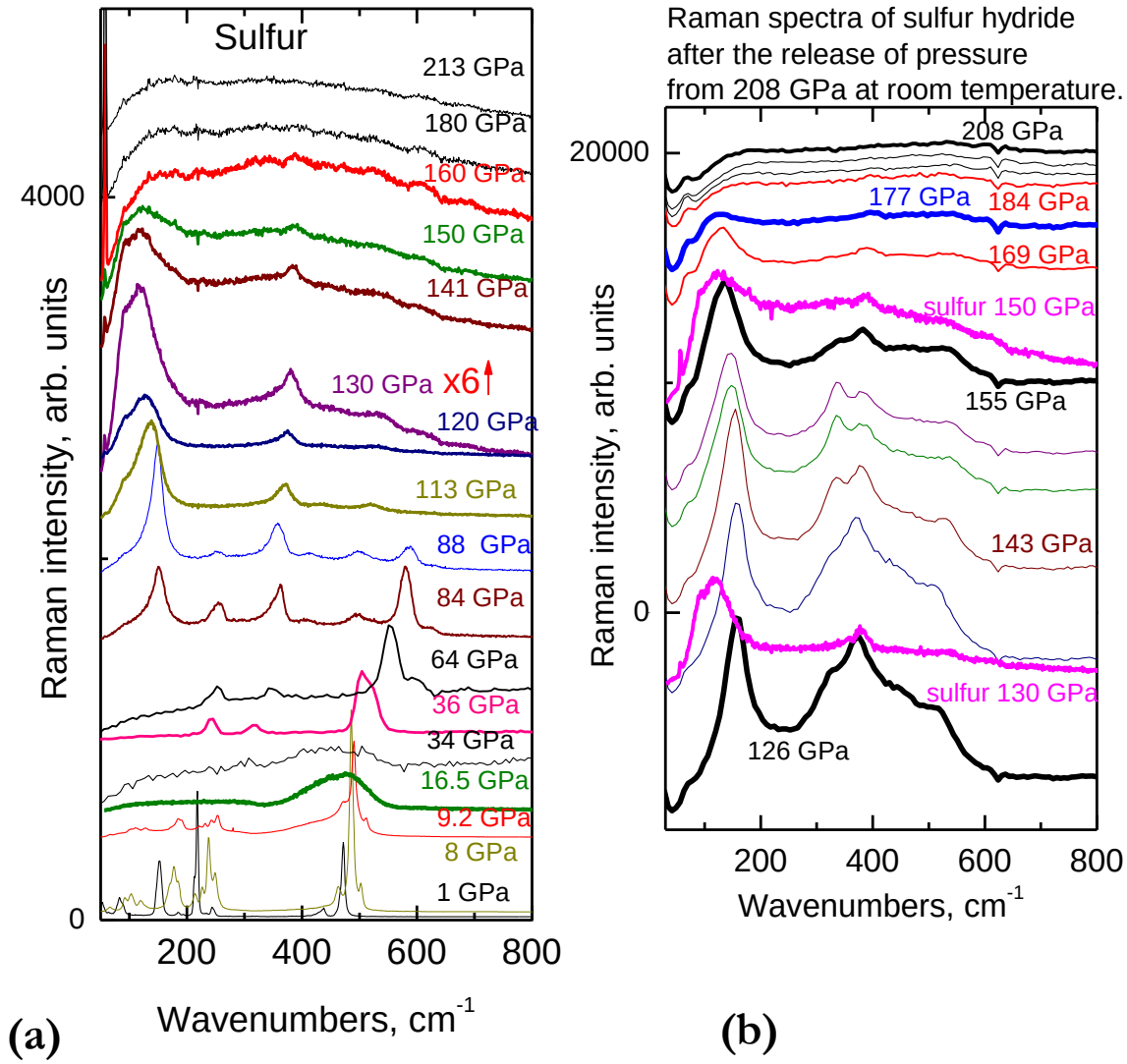

Figure 4.6 - Raman spectra of sulfur hydride compared with elemental sulfur.

Ultralow luminescence synthetic diamond anvils allowed us to record the Raman spectra at high pressures in the metallic state.

Figure 4.6 shows a Raman spectra of the elemental sulfur at different pressures measured at the room temperature over a wide pressure range. At the low pressures, the Raman signal is very strong but above ~10 GPa the intensity dramatically decreases, and a reflected signal appears. Above 80 GPa a new phase appeared which persists to 150 GPa in the metallic state. At 160 GPa the Raman spectrum disappears, likely because of transformation to the β-Po phase.

Figure 4.6b shows Raman spectra of sulfur hydride after the release of pressure from 208 GPa at room temperature. The spectra are much stronger than those from sulfur in the metallic state at high pressures. There can be a phase transition at ≈180 GPa.

There is an apparent difference in the Raman spectra of sulfur hydride (a) and sulfur (b): the peaks at ~100 cm^{-1} shift relative to each other, the phase transformation are at different pressures: 160 GPa for sulfur and 180 GPa for sulfur hydride. Finally, the Raman spectra of sulfur hydride are significantly stronger.

Electrical Measurements

Methods

The resistance were measured using the four-probe Van der Pauw method with Tantalum electrodes sputtered on the diamond (Chapter 3.4). Current of 10-10000 μA was supplied by a Keithley 6220 current source. Voltage was measured by a Keithley 2000 multimeter. Electrical measurements were reproduced in the PPMS6000 Quantum Design physical property device.

The insulating gasket was prepared from either Teflon, NaCl or CaSO4 as these materials do not react with H_2S. To check a possible contribution of the diamond surface to the conductivity we prepared once a configuration with pair of electrodes on the one diamond and another pair on the another diamond anvil similar to Ref.28 ([28]Eremets, Troyan 2011).

The temperature was determined by slow (warming rate of ~1 K/min) and allowing the DAC to equilibrate with attached thermometer. Temperature also was checked with PPMS setup.

Sample behavior during pressure increasing

The sample starts to conduct at P ~ 50 GPa. At this pressure, it is a semiconductor as shown by the temperature dependence of the resistance and a pronounced photoconductivity. At 90-100 GPa, the resistance drops further, and the temperature dependence becomes metallic. No photoconductive response is observed in this state. It is a poor metal – its resistivity at 100 K is ≈ $3x10^{-5}$ Ohm m at 110 GPa and ≈$3x10^{-7}$ Ohm m at ~200 GPa (Figure 4.7).

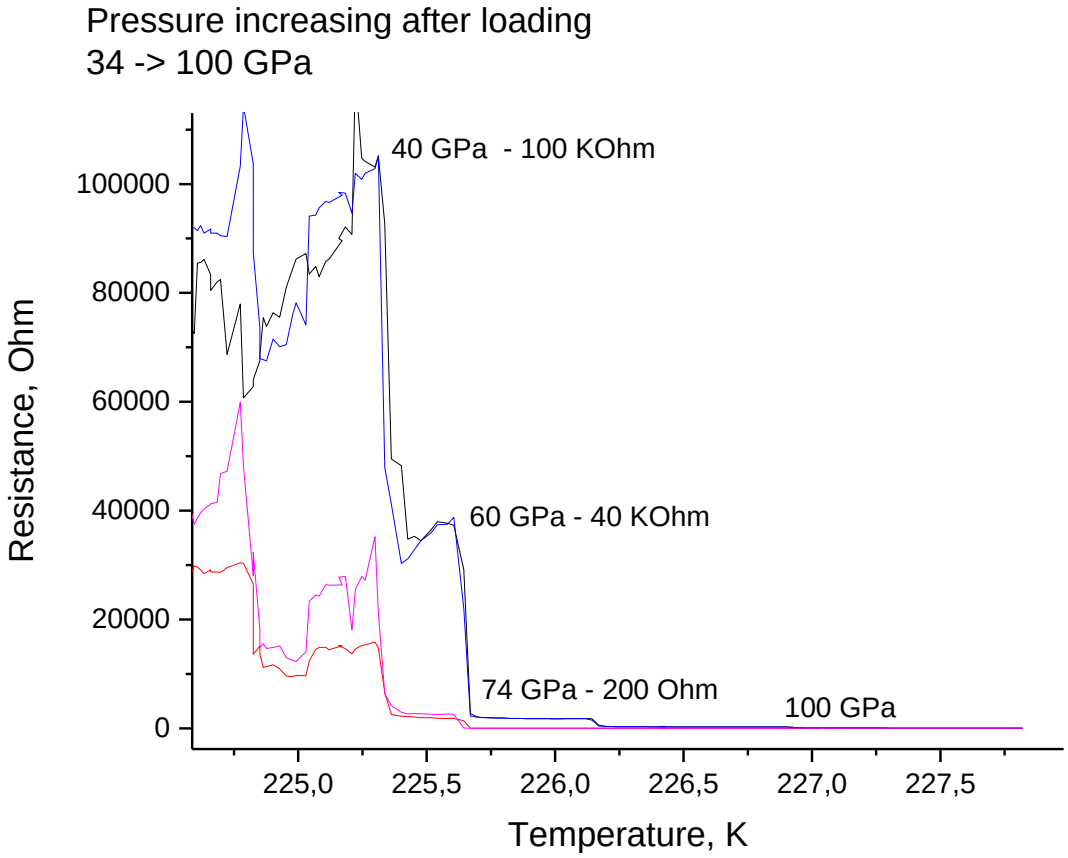

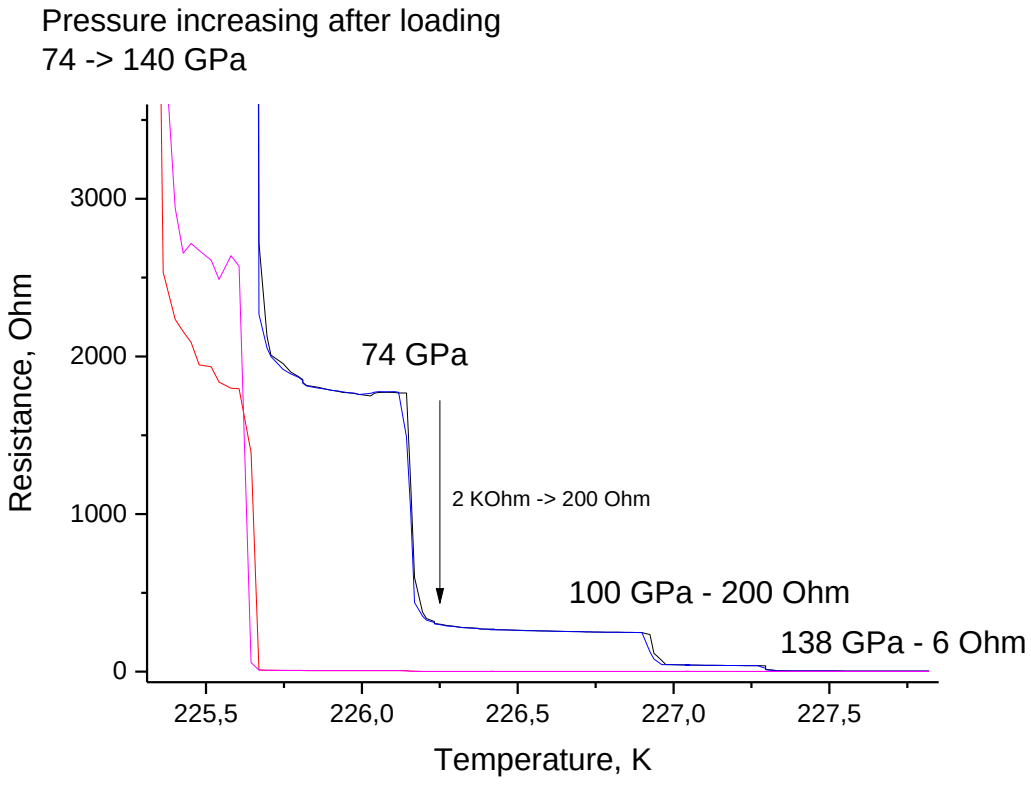

Figure 4.7 – Resistance drop during pressure increasing

Sample behavior during cooling and warming cycles

During the cooling of the sample at pressures of about 100 GPa (Figure 4.8), the resistance abruptly drops by three to four orders of magnitude indicating a transition to the superconducting state. At the next increase of pressure at low temperatures of T<100 K T_c steadily increases with pressure. However at the pressures of ~ 160 GPa T_c increases sharply (Fig. 4.8b).

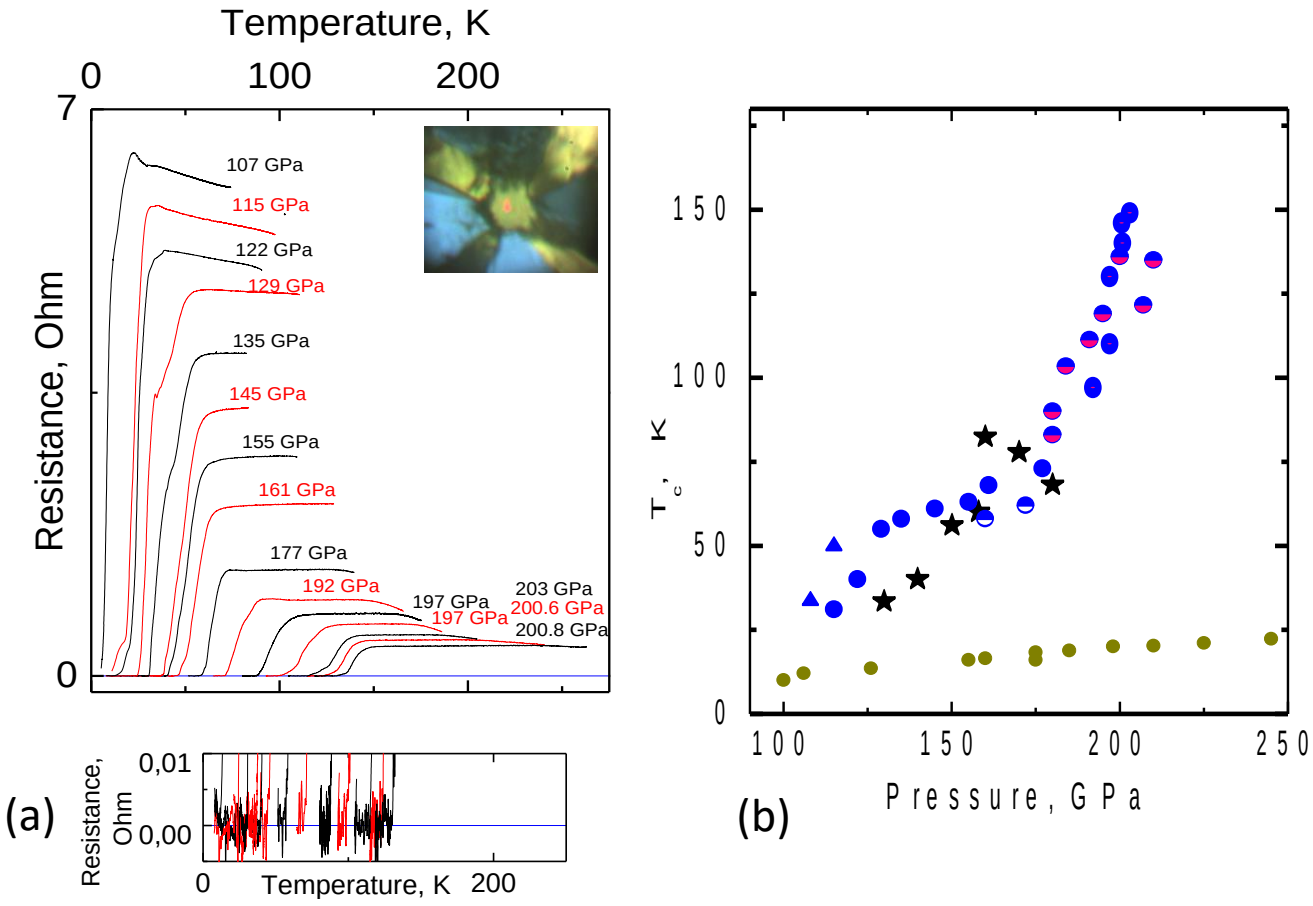

Figure 4.8 – Temperature dependence of the resistance of sulfur hydride measured at different pressures.

Figure 4.8a shows temperature dependence of resistance of sulfur hydride for different pressures. The pressure values are indicated near the corresponding plots. In this run, the sample was clamped at T~220 K and the pressure was increased to ~100 GPa, and then the sample was cooled down. Plots at pressures <135 GPa were scaled (reduced 5-10 times) for easier comparison with the higher pressure steps. The resistance was measured with a current of 10 μA. Bottom: the resistance plots near zero. The resistance was measured with four electrodes

deposited on a diamond anvil that touched the sample (inset). The diameters of the samples were ~25 μm and the thickness ~1 μm.

Figure 4.8b - Blue round points represent a critical temperatures determined from Fig. 4.8a. Other blue points were obtained in the similar runs. Measurements at P>~160 GPa revealed a sharp increase in T_c. In this pressure range the R(T) measurements were performed over a larger temperature range up to 260 K, the corresponding experimental points are indicated by adding pink color. These points likely reflect a transient state for these particular pressure/temperature conditions. Black stars are calculations from Ref. 58. Dark yellow points are T_c's of pure sulfur obtained with the same four-probe electrical measurement method. They are consistent with literature data (susceptibility measurements) but have higher values up to 22 kelvin at P>200 GPa.

Warming of the sample to the room temperature at the stable pressure leads to decreasing of the resistivity in 1-2 order (Figure 4.9).

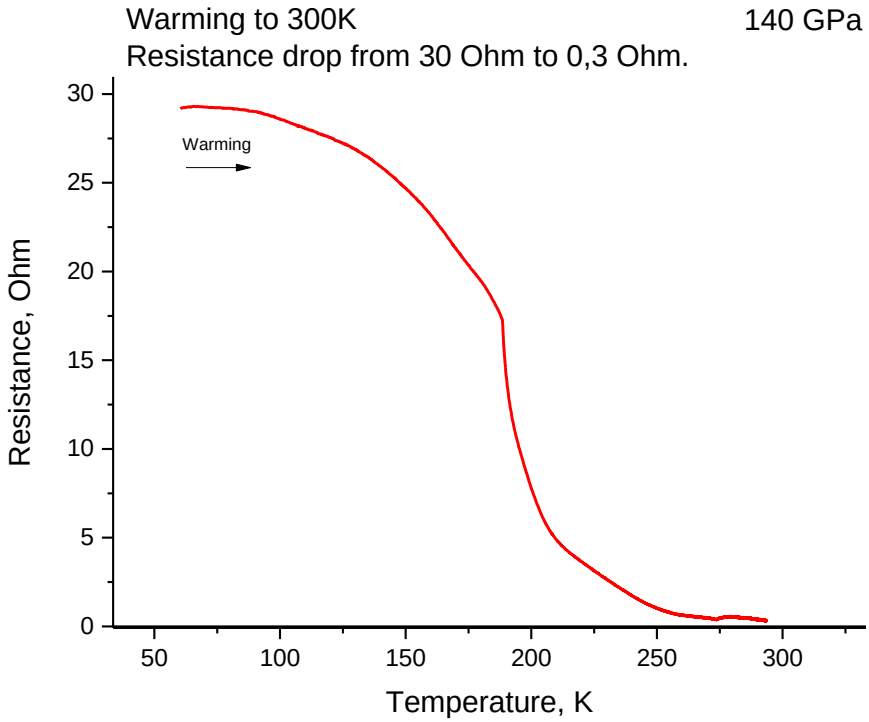

Figure 4.9 – Resistance drop during warming of the sample

Higher temperatures of 150-250 K lead to the increase of T_c and the decrease of sample resistance. It can indicate a possible kinetics transformation. Therefore in further experiments we anneal all samples by heating them to room or higher temperatures. Such sample preparation allowed us to obtain stable results, compare different isotopes, obtain the dependence of T_c on the pressure and magnetic field.

The sample should be annealed at the pressure more than 100 GPa. Low pressure and high temperature possibly lead to sample decomposition.

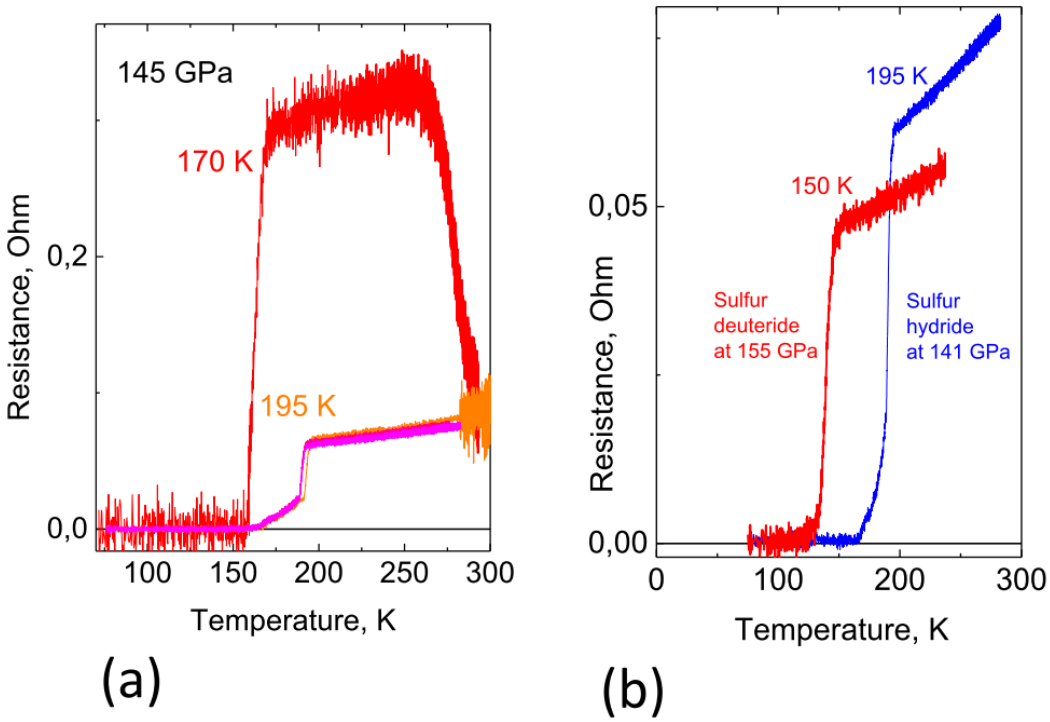

Figure 4.10 Pressure and temperature effects on T_c in sulfur hydride and sulfur deuteride.

Figure 4.10a shows the difference of resistance and critical temperature (T_c) of the sulfur hydride before and after warming to room temperature. The sample was pressurized to 145 GPa at 220 K and then cooled to 100 K. During next slow warming ~1 K/min T_c =170 K was determined. At temperatures above ~250 K the resistance dropped sharply, and at the next temperature run T_c increased to ~195 K. This T_c remained nearly the same for next two runs.

Isotope effect

Superconductors should experience a shift of critical temperature for its isotope. To check this property of superconductors we measure an electrical resistance of D_2S.

Figure 4.10b shows typical superconductive steps for sulfur hydride and sulfur deuteride. The data are acquired during slow warming within several hours. The critical temperature T_c is defined here as the sharp kink in the transition to normal metallic behavior. These curves were obtained after annealing at room temperature as shown in Fig. 4.10a.

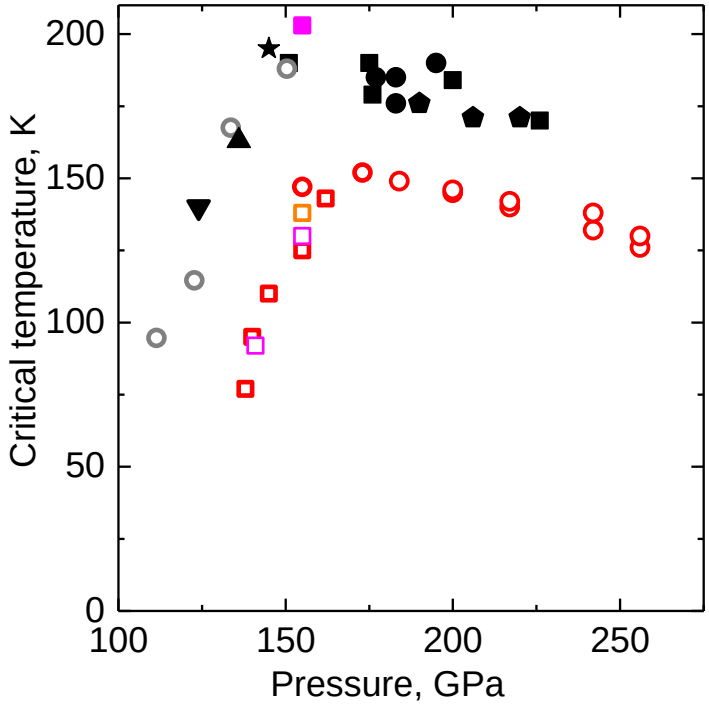

Figure 4.11 Dependence of T_c on pressure.

Figure 4.11 shows a summary for critical temperature dependence on pressure for sulfur hydride (H_xS) and sulfur deuteride (D_xS). The data on annealed samples are presented. Open color points refer to sulfur deuteride and filled points to sulfur hydride. Highest measured T_c for sulfur hydride is 203 K.

Electrical Measurements in Magnetic Field

The presence of an isotopic effect is a sign that zero resistance is due to superconductivity, but not a some mistake in measurement. Another property of superconductors is a shift of critical temperature in the presence of magnetic field.

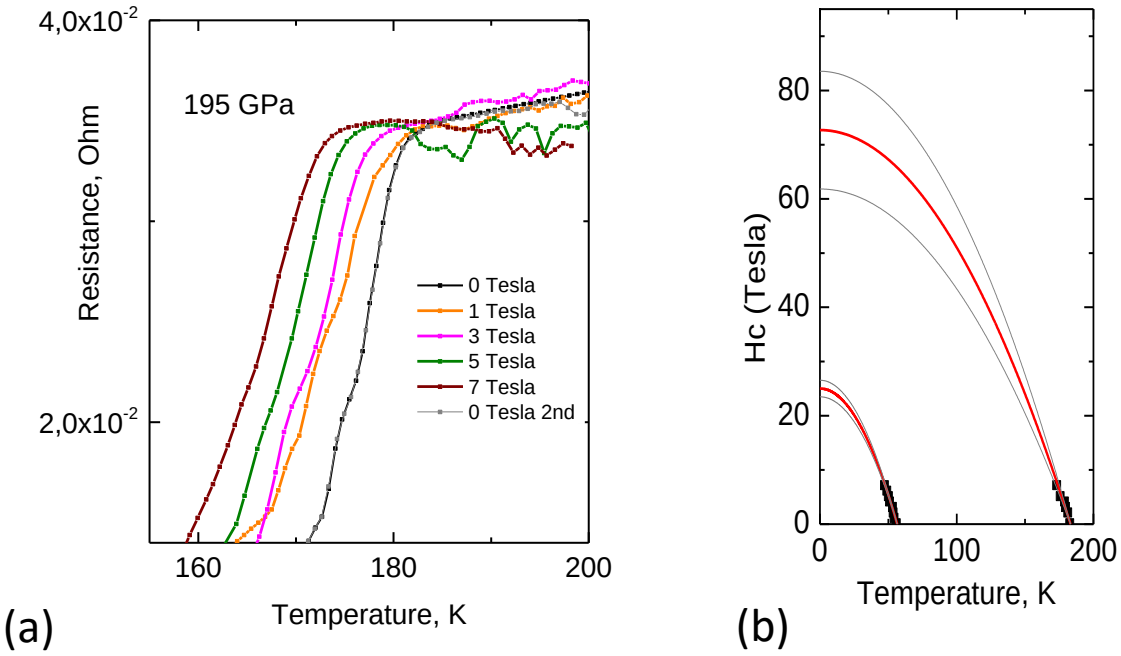

Figure 4.12 – Temperature dependence of the resistance of sulfur hydride in different magnetic fields.

Figure 4.12 shows the shift of the ~60 K superconducting transition in the 0-7 T magnetic fields. The upper and low parts of the transition are shown enlarged in the insets. The temperature dependence of the resistance without magnetic field was measured three times: before applying the field, after applying 1,3,5,7 Tesla and finally after applying 2,4,6 Tesla (black, grey and dark grey colors).

Figure 4.13a shows the same measurements but with the 185 K step.

Figure 4.13b shows the shift of the critical temperature of the superconducting transition T_c

with magnetic field. To estimate the critical magnetic field H_c, the plots were extrapolated to high magnetic fields using $H_c(T)=H_{c0}(1-(T/T_c)^2)$ formula. The extrapolation has been done with 95% confidence (band shown as grey lines).

Magnetic susceptibility measurements

One of the main property of superconductors is a Meissner - Ochsenfeld effect – expelling of the magnetic field from the superconductor.

Magnetic susceptibility measurements were performed in MPMS Quantum Design setup. For this measurements a miniature nonmagnetic cell made of Cu:Ti alloy working up to 200 GPa was designed (Fig. 4.14b). Samples of the diameter of ~50-100 μm and thickness of few micrometers were prepared to provide a sufficient signal. During the measurements the

background signal of the high-pressure cell measured at T = 220 K has been automatically subtracted that essentially improved a signal to noise ratio.

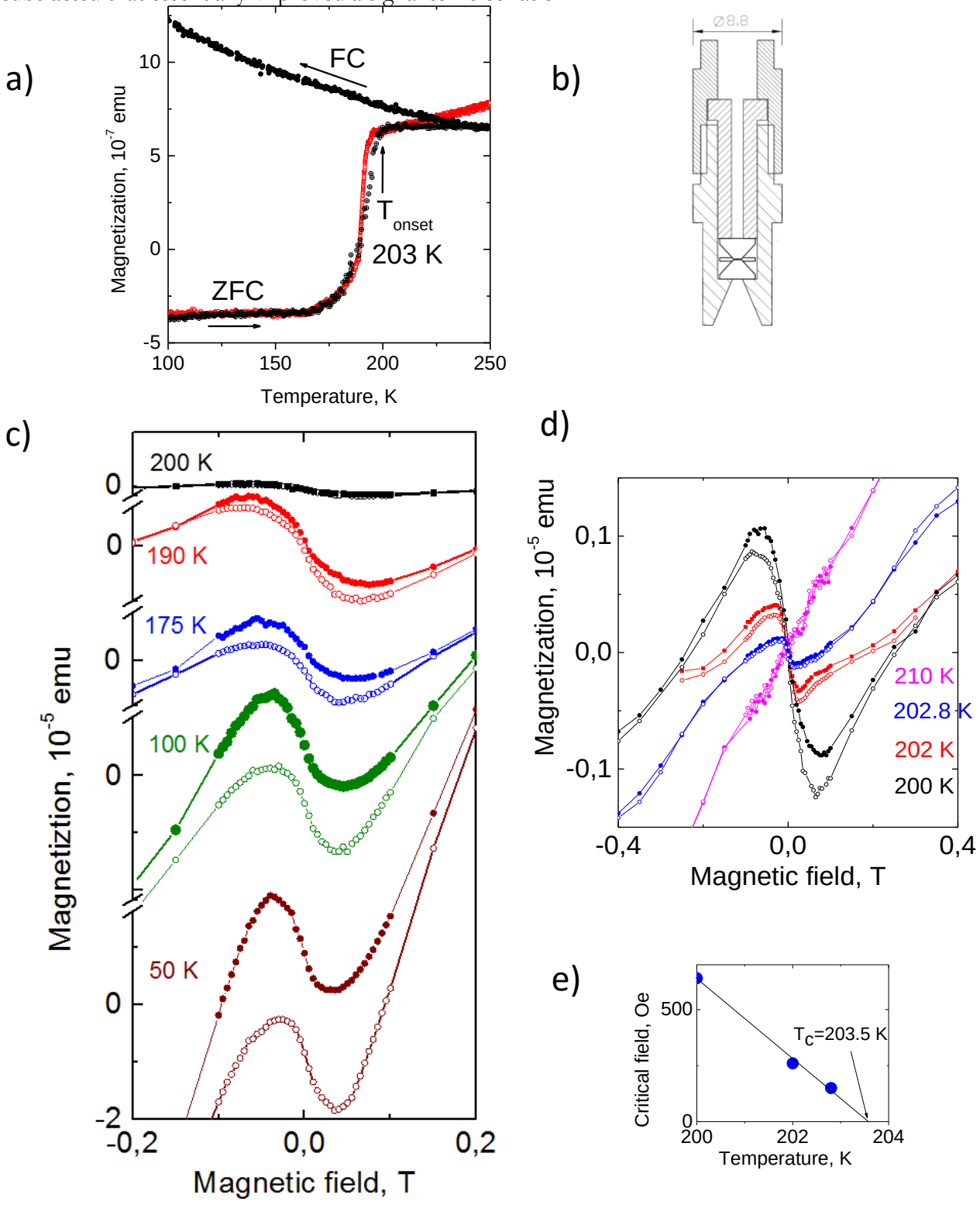

Figure 4.13 – Magnetization measurements.

Figure 4.14a shows the temperature dependence of the magnetization of sulfur hydride at a pressure of 155 GPa in a the zero-field-cooled (ZFC) and 20 Oe field cooled (FC) modes. ZFC curve demonstrates a rather sharp transition from the diamagnetic to the paramagnetic state which could be classified as a superconducting one. The onset temperature is T_{onset} = 203 K. For comparison, the superconducting step obtained for sulfur hydride from electrical measurements at 145 GPa is shown by red color. Resistivity data (T_{onset} = 195 K) were scaled and settled vertically to compare with the magnetization data. The insert shows a sulfur hydride sample at 140 GPa in a Re gasket.

The superconducting transition with T_{onset} = 203 K is confirmed by the magnetization M(H) measurements at different temperatures. Figure 4.14c shows magnetization measurements M(H) of sulfur hydride at a pressure of 155 GPa. Diamagnetism in the Meissner phase is responsible for the initial decrease of the magnetization until the first critical field H_{C1} of 300 Oe is attained. Afterward, a subsequent increase of the magnetization as external field increases is explained by penetration of magnetic vortexes which confirms the assignment to the hard Type II superconductors. As the sign of the field change reverses, the magnetic flux in the Shubnikov state remains trapped, and the returning branch of the magnetic cycle runs above the direct one providing the irreversibility of the magnetization curve. Hysteretic behavior of the magnetization becomes more clearly visible as temperature decreases.

The magnetization curves show hysteresis indicating the type II superconductor.

Magnetic hysteresis measurements were also performed using a subtraction of a background which was determined in the normal state at T = 250 K. The magnetization curves however are distorted by obvious paramagnetic input (observed in other superconductors too). In our case, the paramagnetic signal is likely from the DAC. Further study of the origin of this input is required. The paramagnetic background increases with a temperature decrease. The minima at the magnetization curves (~ 350 Oe) are the result of the diamagnetic input from superconductivity and the paramagnetic background. The first critical field H_{C1}~300 Oe can be roughly estimated as a point where magnetization deviates from the linear behavior. At higher fields, magnetization increases due to the penetration of magnetic vortexes. As the sign of the field change reverses (full points), the magnetic flux in the Shubnikov phase remains trapped and therefore the back run is irreversible - returning branch of the magnetic cycle runs above the direct one. Hysteretic behavior of the magnetization becomes more clearly visible as the temperature decreases.

Figure 4.14d shows at high temperatures T>200 K the magnetization decreases sharply.

Figure 4.14e shows extrapolation of the pronounced minima at the magnetization curves to higher temperatures gives the onset of superconductivity at T = 203.5 K.

Prove of superconducting transition

(1) There is a sharp drop in resistivity with cooling indicating a phase transformation. The measured minimum resistance is at least as low ~10^{-11} Ohm m – about two orders of magnitude less than for pure copper measured at the same temperature.

(2) A strong isotope effect: T_c shifts to lower temperatures for sulfur deuteride indicating phonon-assisted superconductivity. The BCS theory gives dependence of critical temperature on the atomic mass M as $T_c \sim M^{-\alpha}$ where α ~0.5. Comparison T_c's in the pressure range P>170 GPa gives α ~0.3.

(3) T_c shifts to lower temperatures with the available magnetic field up to 7 Tesla. Much higher fields are required to destroy the superconductivity: extrapolation of $T_c(B)$ gives an estimate of a critical magnetic field as high as 70 T.

(4) Magnetic susceptibility measurements show a sharp transition from the diamagnetic to the paramagnetic state at the zero-field-cooled (ZFC) curve. The critical temperature of the superconducting state T_c = 203 K. The width of the superconducting transition is nearly the same as in electrical measurements (Fig. 4.14a). Magnetization measurements M(H) at different temperatures (Fig. 4.14c) revealed a pronounced hysteresis indicating type II superconductivity. The magnetization decreases sharply at temperatures above 200 K indicating the onset of superconductivity at 203.5 K in agreement with the susceptibility measurements (Fig. 4.14a).

Discussion

We have presented pure experimental evidence of superconductivity in the sulfur hydride.

However the compound responsible for the high T_c is not obvious. The superconductivity measured in the low temperature runs (Fig. 4.8a) likely relates to H_2S as it is consistent with calculations for H_2S ([58]Li et al. 2014) both the value of T_c ~ 80 K and its pressure behavior. However, superconductivity with T_c ~ 200 K does not follow from these calculations. It can relates to the decomposition of H_2S as high temperatures are involved to reach the high T_c (Fig. 4.10a). Precipitation of elemental sulfur upon the decomposition could be expected (which is well known at low pressures of P<100 GPa) ([37]Fujihisa et al. 2004), however superconducting transition in elemental sulfur occurs at significantly lower temperatures (Fig. 4.8). Another expected product of the decomposition of H_2S is hydrogen. However, the strong characteristic vibrational stretching mode from H_2 molecule was never observed in our Raman spectra as well as in Ref. 37. Therefore we suppose that the dissociation of H_2S is different with the creation of higher hydrides such as $3H_2S \rightarrow H_6S + 2S$ or $2H_2S \rightarrow H_4S + S$. It is

natural to expect these reactions as the valency of sulfur is not only 2 but can also be 4, and 6. In fact calculations in Ref.54 indirectly support this hypothesis as the dissociation $H_2S \rightarrow H_2 + S$ was shown to be energetically very unfavorable. We found further theoretical support in Ref. 19 ([19]Duan et al. 2014). In this work the van der Waals compound $(H_2S)_2H_2$ has been considered and shown that at pressures above 111 GPa H_3S a molecular unit with R3m structure is built, and above 180 GPa H_6S units with Im-3m structure are formed. The predicted T_c's are respectively ~ 160 K and 190 K and the pressure dependencies for these two phases are close to our experimental values. The phase transition between R3m and Im-3m structures is predicted at ~180 GPa. This likely relates to the changes in Raman spectra observed in the 170-180 GPa (Fig. 4.6b). Hypothesis on the transformation H_2S to H_6S (H_3S stoichiometry) is fully supported by further calculations ([31]Errea et al. 2015; [9]Bernstein et al. 2015). All further works based on the Im-3m structure and others are consistent in prediction of T_c >200 K ([4]Akashi et al. 2015; [31]Errea et al. 2015; [74]Papaconstantopoulos et al. 2015; [56]Lev P. Gor'kov, V. Z. Kresin 2015; [52]Ion Errea et al. 2015) with the hydrogen sublattice giving the main contribution to superconductivity. Inclusion of zero-point vibrations and anharmonicity in the calculations corrected the calculated T_c to ~190 K, and the isotope coefficient from α=0.5 to α=0.35 – both in agreement with the present work. Experimental measurements of X-ray data ([22]Einaga et al.) show that the superconducting phase is in good agreement with theoretically predicted hexagonal and body-centred cubic (bcc) structure and coexists with elemental sulfur. This the high-temperature superconductivity of 203 K can be explained by the formation of H_3S ($3H_2S \rightarrow 2H_3S + S$) under compression.

Key features of H_xS superconductor

Here are some important key features of the new high-T_c sulfur hydride superconductor:

(1) The new superconductor is of type II. This fact is clearly supported by (i) a difference in temperature-dependent ZFC and FC magnetization, which is due to the Meissner effect (ZFC) and magnetic flux capture when the sample is cooled down from its normal state (FC); and (ii) the magnetic hysteresis curves. The magnetic hysteresis curves also have all the features of typical type II superconductors with a mixed state between H_{c1} and H_{c2}.

(2) A typical value of the coherence length ξ in the framework of the Ginzburg–Landau theory can be estimated on the basis of the measured upper critical fields from conductivity measurements. Using the experimental estimation 60 T < H_{c2} < 80 T and the relation

$$\xi_{GL} = \frac{1}{2}\sqrt{\frac{h}{\pi e H_{c2}}}$$

Limits for the coherence length: 2.3 nm > ξ > 2.0 nm. We note that this relatively short coherence length is of the same order as, for instance, the values for superconducting YBa2Cu3O7 (1.3 nm) and Nb3Sn (3.5 nm).

(3) The London penetration depth λL can be estimated from the known relation of the lower critical field H_{c1} to the upper critical field H_{c2} for a type II superconductor

$$\frac{H_{c1}}{H_{c2}} \approx \frac{\ln \kappa}{2\sqrt{2}\kappa^2}$$

in the limit $\varkappa >> 1$ of the Ginzburg–Landau parameter $\kappa = \frac{\lambda_L}{\xi_{GL}}$. Considering the experimental value of the first critical field of 3 × 10−2 T and the above-mentioned relation 60 T < Hc2 < 80 T, we can obtain the following estimate for the London penetration depth: λ ≈ 125 nm.

(4) According to Bean's model, the magnetic critical current density of the superconductor can be estimated from the distance between the direct and the returning branches of the magnetic hysteresis loop at a given magnetic field. Provided grain radii are about 0.1 μm, the intra-grain critical current J_c is about 107 A cm^{-2}.

Chapter 5
Superconductivity above 100 K in PH_3 at high pressures

5.1 Motivation and Previous Results

The finding of superconductivity in H_xS system at 200 K under pressure ([18]Drozdov et al. 2015) experimentally supports a statement of BCS theory in Eliashberg extension that there is no apparent limit for the critical temperature (T_c) of superconductivity ([12]Carbotte 1990), and it stimulates the search for even higher transition temperatures. A lot of theoretical simulations yielding very high superconducting temperatures were done after that. Experimentally superconductivity was found in SiH_4 with T_c = 17 K ([27]Eremets et al. 2008), in $BaReH_9$ ([67]Muramatsu et al. 2015) with T_c ~ 7 K, and finally at 203 K in sulfur hydride. Other hydrogen containing materials such as AlH_3 ([43]Goncharenko et al. 2008), $B_{10}H_{14}$ ([24]Eremets 2003) however did not reveal superconductivity. Thus, there is still the question whether the high-temperature superconductivity in sulfur hydride system is a unique phenomenon among hydrogen containing materials.

PH_3 was selected for the present study because this material with its covalent bonding is similar to H_2S. Few experimental studies were performed on this compound such as infrared absorption and Raman scattering ([51]Huang et al. 1977). There are no studies under pressure both in experiment and theory.

5.2 Experimental results

Phosphine gas (99,999% from Air Liquide) was liquified in a diamond anvil cell (DAC) at 170 K (Fig. 1a) using the same technique as described in Chapter 3.5. The presence of the sample was controlled visually and by measuring Raman spectra showing the characteristic peak of PH_3 at ~2300 cm^{-1} ([51]Huang et al. 1977). After clamping the sample, it was pressurized at low temperatures of T < 200 K to avoid possible decomposition. Electrical measurements were performed with four electrodes in the Van der Pauw geometry with the same technique as in Chapter 3.4. Under pressure the P-H stretching mode of phosphine at 2300 cm^{-1} shifts to higher

frequencies. The Raman intensity decreases with pressure and the signal vanishes, with the sample darkening at pressure >25 GPa.

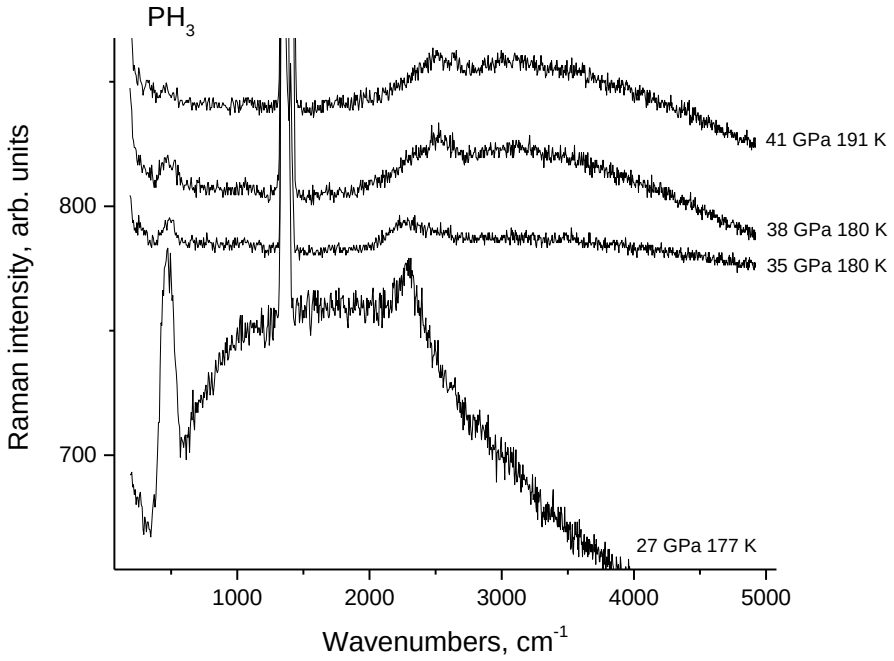

Figure 5.1 - Raman spectra of phosphine at different pressures and temperatures

The sample becomes opaque and starts to conduct at ~30 GPa (measured at 180 K), and weakly visible reflection appears at 35 GPa. The sample is apparently semiconducting because a strong photoconducting response.

The photoconductivity was not observed at P~40 GPa, indicating that at this pressure the sample is already metallic. We did not measure the temperature dependence of resistance at this pressure to check if the sample is metallic and possibly superconducting. Temperature scans were measured at pressures P>80 GPa.

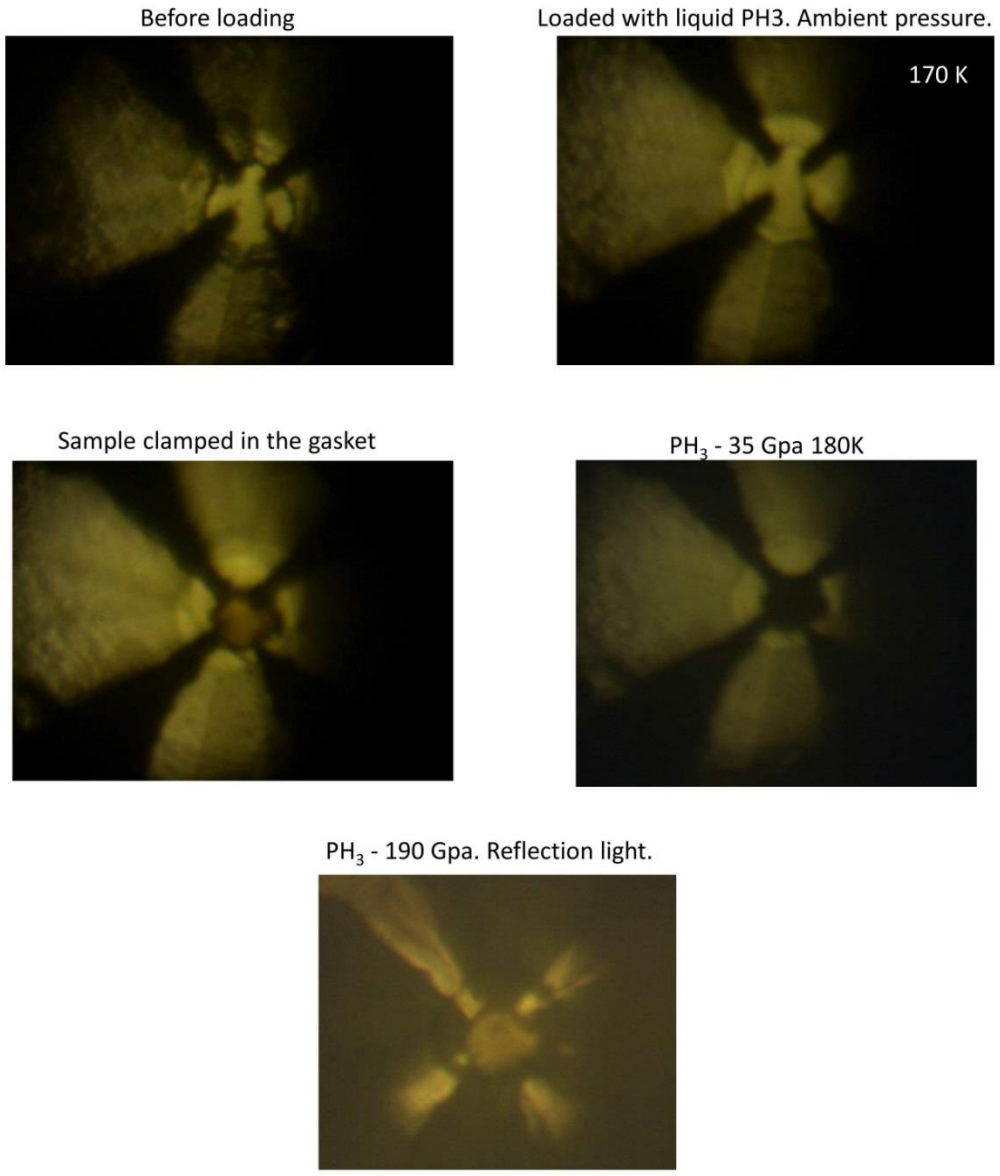

Figure 5.2 – Images of loading and pressure increase of PH_3 sample.

At the first cooling at 83 GPa, we observed a signature of a superconducting transition: the resistance abruptly dropped to "zero" at the critical temperature (T_c) of 30 K, Fig. 1b. Probably superconductivity exists also at lower pressures. The resistivity of the sample below the transition temperature is about 10^{-9} Ohm m which is the limit of our measurement device (Figure 5.4). Next pressure increasing to P=117 GPa was performed at T< 200 K and then the sample was cooled down. The critical temperature T_c increased with pressure up to 103 K at 207 GPa (Figure 5.7). This pressure run was reproduced twice at similar temperature conditions of loading.

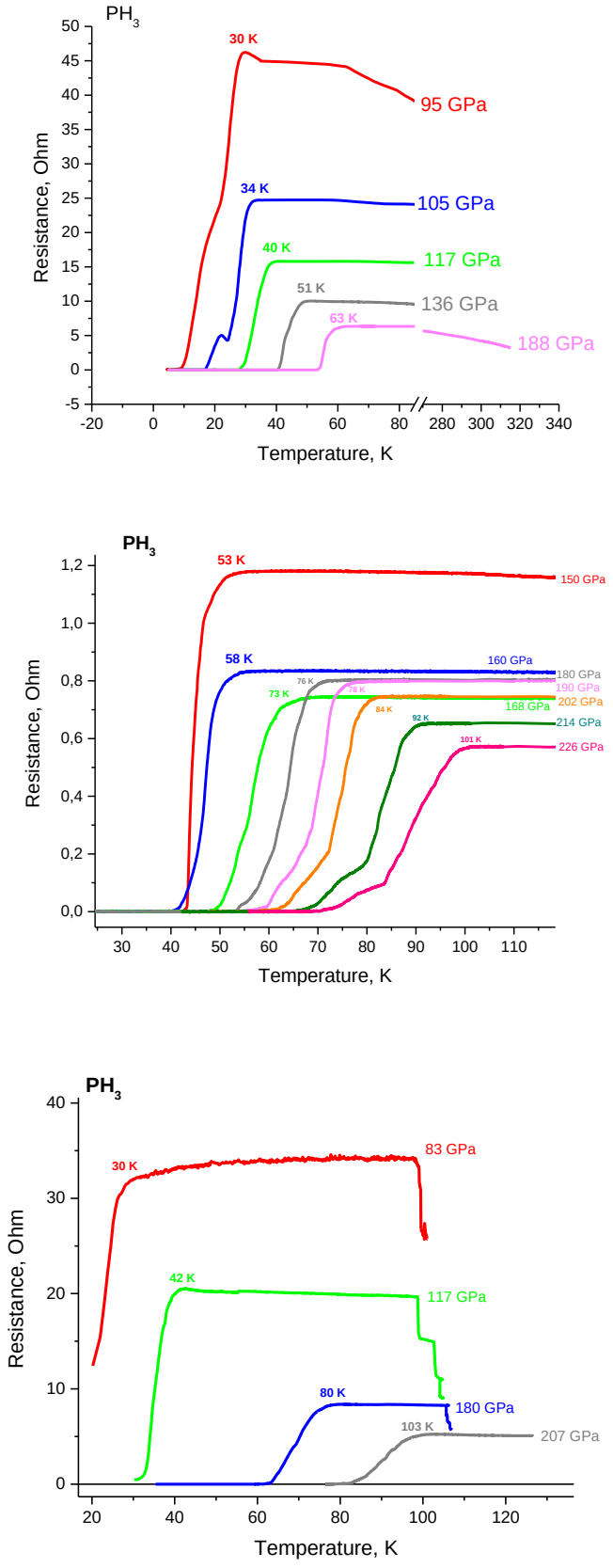

Figure 5.3 Electrical measurements of phosphine at high pressures.

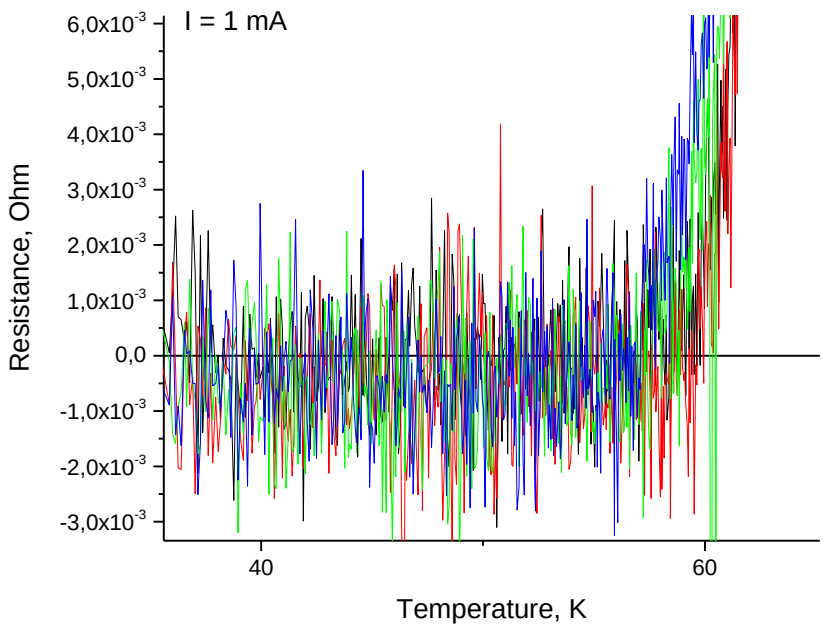

Figure 5.4 – Zero resistance of sample with dimensions 20x20x1 mcm.

Similar to H_2S sample we observed that the resistance of the sample starts to decrease during the warming to the room temperature which could be a sign of the decomposition or phase transition (Figure 5.5). However, after warming to the room temperature, critical temperature becomes about 40 K at a pressure of 210 GPa and the second step appears on the R-T dependence near 24 kelvins. After second warm to room temperature critical temperature becomes ~22 kelvins at 251 GPa.

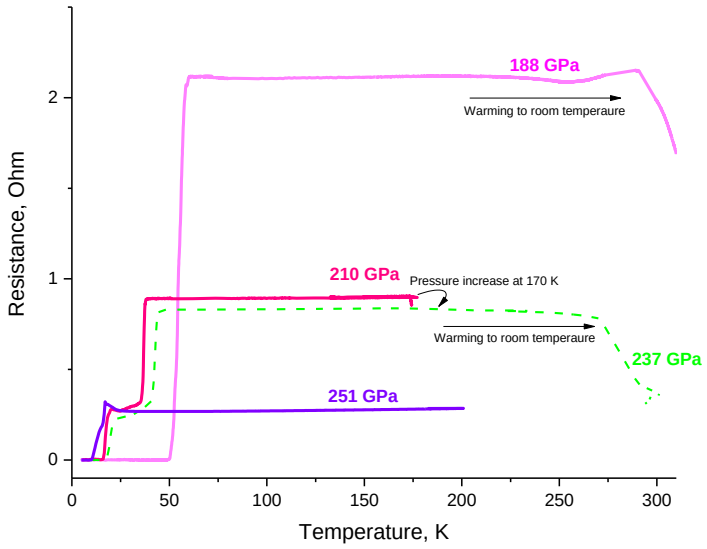

Figure 5.5 Resistance decrease during warming

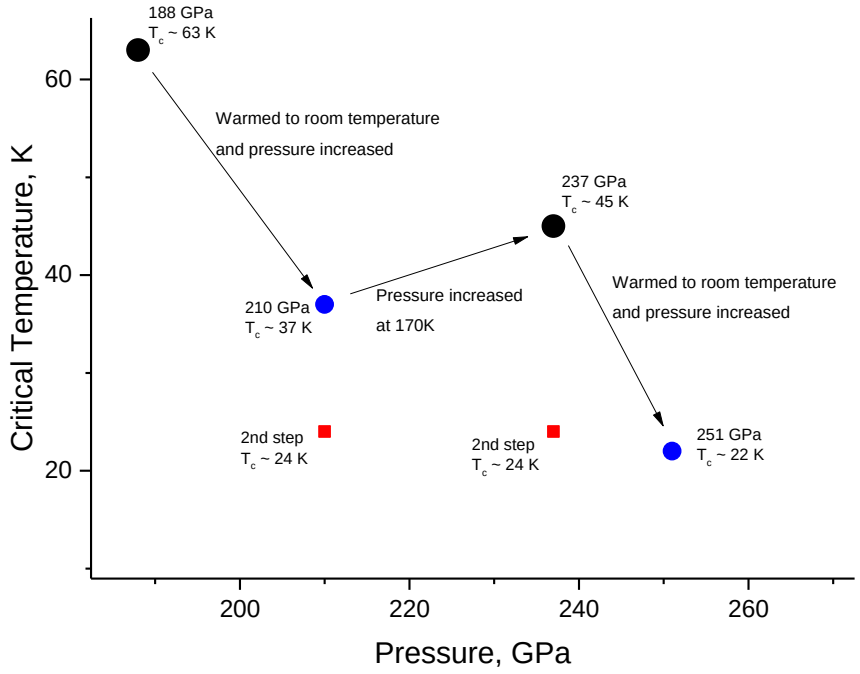

Figure 5.6 – Critical temperature behavior after warming to room temperature

The dependence of the critical temperature T_c on the pressure is plotted in Figure 5.7.

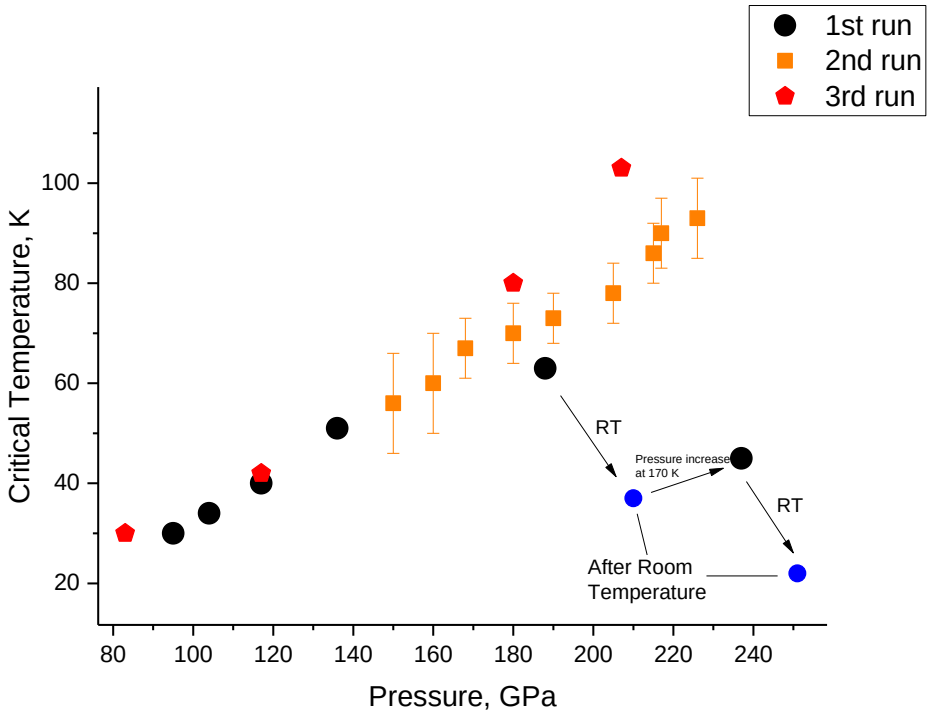

Figure 5.7 - Critical temperature dependence on pressure

These first experimental data clearly evidence another (besides sulfur hydride) hydride with very high T_c. It is likely conventional superconductor. Obviously the experiments should be extended to studies of the isotope effect in PD_3 and of magnetic susceptibility. In contrast to H_3S the phase with high T_c apparently is metastable. After warming it transforms to a stable phase with lower T_c. Interestingly, independent theoretical calculations ([54]José A. Flores-Livas et al. 2015; [83]Shamp et al. 2016; [60]Liu et al. 2016) indeed has found that not PH_3 but PH_2 is most stable phase at 150-200 GPa pressure range. Decreased critical temperature after warming to room temperature can be associated with PH_2 phase or elemental phosphorous which is not investigated experimentally at this pressure.

Chapter 6

Summary

Pressure is a great tool for changing material properties and synthesis of new materials. Materials once obtained under pressure sometimes can be synthesized at ambient pressure. Diamond synthesis is a celebrity example.

At this high pressure work superconductivity with critical temperature above liquid nitrogen (high-temperature superconductivity) was found in two hydrides:

- H_3S – critical temperature about 203 K at 150 GPa
- PH_3 – critical temperature about 100 K at 200 GPa

This work confirms an idea of high-temperature superconductivity in the hydrogen rich systems. A big variety of hydrogen containing systems opens a venue for future studies and search for even higher, room temperature superconductivity.

Chapter 7 Publication bibliography

[1]. Abrikosov, A. A. (1957): The magnetic properties of superconducting alloys. In *Journal of Physics and Chemistry of Solids* 2 (3), pp. 199–208. DOI: 10.1016/0022-3697(57)90083-5.

[2]. Akahama, Yuichi; Kawamura, Haruki (2007): Diamond anvil Raman gauge in multimegabar pressure range. In *High Pressure Research* 27 (4), pp. 473–482. DOI: 10.1080/08957950701659544.

[3]. Akahama, Yuichi; Kawamura, Haruki (2010): Pressure calibration of diamond anvil Raman gauge to 410 GPa. In *J. Phys.: Conf. Ser.* 215, p. 12195. DOI: 10.1088/1742-6596/215/1/012195.

[4]. Akashi, Ryosuke; Kawamura, Mitsuaki; Tsuneyuki, Shinji; Nomura, Yusuke; Arita, Ryotaro (2015): First-principles study of the pressure and crystal-structure dependences of the superconducting transition temperature in compressed sulfur hydrides. In *Phys. Rev. B* 91 (22). DOI: 10.1103/PhysRevB.91.224513.

[5]. Allen, P. B.; Dynes, R. C. (1975): Transition temperature of strong-coupled superconductors reanalyzed. In *Phys. Rev. B* 12 (3), pp. 905–922. DOI: 10.1103/PhysRevB.12.905.

[6]. Ashcroft, N. W. (1968): Metallic Hydrogen. A High-Temperature Superconductor? In *Phys. Rev. Lett.* 21 (26), pp. 1748–1749. DOI: 10.1103/PhysRevLett.21.1748.

[7]. Ashcroft, N. W. (2004): Hydrogen dominant metallic alloys: High temperature superconductors? In *PHYSICAL REVIEW LETTERS* 92 (18). DOI: 10.1103/PhysRevLett.92.187002.

[8]. Bednorz, J. G.; Muller, K. A. (1986): Possible highT c superconductivity in the BaLaCuO system. In *Z. Physik B - Condensed Matter (Zeitschrift fur Physik B Condensed Matter)* 64 (2), pp. 189–193. DOI: 10.1007/BF01303701.

[9]. Bernstein, N.; Hellberg, C. Stephen; Johannes, M. D.; Mazin, I. I.; Mehl, M. J. (2015): What superconducts in sulfur hydrides under pressure and why. In *Phys. Rev. B* 91 (6). DOI: 10.1103/PhysRevB.91.060511.

[10]. Blevins, Gilbert S.; Gordy, Walter; Fairbank, William M. (1955): Superconductivity at Millimeter Wave Frequencies. In *Phys. Rev.* 100 (4), pp. 1215–1216. DOI: 10.1103/PhysRev.100.1215.

[11]. Boehler, Reinhard; Hantsetters, Koen de (2004): New anvil designs in diamond-cells. In *High Pressure Research* 24 (3), pp. 391–396. DOI: 10.1080/08957950412331323924.

[12]. Carbotte, J. P. (1990): Properties of boson-exchange superconductors. In *Rev. Mod. Phys.* 62 (4), pp. 1027–1157. DOI: 10.1103/RevModPhys.62.1027.

[13]. Corak, W. S.; Goodman, B. B.; Satterthwaite, C. B.; Wexler, A. (1954): Exponential Temperature Dependence of the Electronic Specific Heat of Superconducting Vanadium. In *Phys. Rev.* 96 (5), pp. 1442–1444. DOI: 10.1103/PhysRev.96.1442.2.

[14]. Cudazzo, P.; Profeta, G.; Sanna, A.; Floris, A.; Continenza, A.; Massidda, S.; Gross, E. K. U. (2008): Ab initio description of high-temperature superconductivity in dense molecular hydrogen. In *PHYSICAL REVIEW LETTERS* 100 (25). DOI: 10.1103/PhysRevLett.100.257001.

[15]. Das K.; V. Venkatesan; K. Miyata; D.L. Dreifus (1992): A review of the electrical characteristics of metal contacts on diamond. In *Thin Solid Films: Diamond Films and Related Materials* Volume 212, Issues 1–2, 15 May 1992, Pages 19–24. Available online at 10.1016/0040-6090(92)90494-V.

[16]. Deaver, Bascom S.; Fairbank, William M. (1961): Experimental Evidence for Quantized Flux in Superconducting Cylinders. In *Phys. Rev. Lett.* 7 (2), pp. 43–46. DOI: 10.1103/PhysRevLett.7.43.

[17]. Doll, R.; Näbauer, M. (1961): Experimental Proof of Magnetic Flux Quantization in a Superconducting Ring. In *Phys. Rev. Lett.* 7 (2), pp. 51–52. DOI: 10.1103/PhysRevLett.7.51.

[18]. Drozdov, A. P.; Eremets, M. I.; Troyan, I. A.; Ksenofontov, V.; Shylin, S. I. (2015): Conventional superconductivity at 203 kelvin at high pressures in the sulfur hydride system. In *Nature* 525 (7567), p. 73-+. DOI: 10.1038/nature14964.

[19]. Duan, Defang; Liu, Yunxian; Tian, Fubo; Li, Da; Huang, Xiaoli; Zhao, Zhonglong et al. (2014): Pressure-induced metallization of dense (H2S)(2)H-2 with high-T-c superconductivity. In *SCIENTIFIC REPORTS* 4. DOI: 10.1038/srep06968.

[20]. Dubrovinsky, L.; Dubrovinskaia, N.; Bykova, E.; Bykov, M.; Prakapenka, V.; Prescher, C. et al. (2015): The most incompressible metal osmium at static pressures above 750 gigapascals. In *Nature* 525 (7568), p. 226-+. DOI: 10.1038/nature14681.

[21]. E. G. Brovman; Yu. Kagan; A. Kholas (1972): Properties of Metallic Hydrogen Under Pressure. In *JOURNAL OF EXPERIMENTAL AND THEORETICAL PHYSICS* 35.

[22]. Einaga, M.; Sakata, M.; Ishikawa, T.; Shimizu, K.; Eremets, M.; Drozdov, A. et al.: Crystal Structure of 200 K-Superconducting Phase of Sulfur Hydride System. In *arXiv:1509.03156*.

[23]. Eliashberg G.M. (1960): Interactions between electrons and lattice vibrations in a superconductor. In *Sov. Phys. JETP* 11, 696.

[24]. Eremets, M. (2003): Exploring superconductivity in low-Z materials at megabar pressures. In *Physica B: Condensed Matter* 329-333, pp. 1312–1316. DOI: 10.1016/S0921-4526(02)02138-5.

[25]Eremets, M. I. (1996): High pressure experimental methods. Oxford, New York: Oxford University (Oxford science publications).

[26]. Eremets, M. I. (2003): Megabar high-pressure cells for Raman measurements. In *J. Raman Spectrosc.* 34 (7-8), pp. 515–518. DOI: 10.1002/jrs.1044.

[27]. Eremets, M. I.; Trojan, I. A.; Medvedev, S. A.; Tse, J. S.; Yao, Y. (2008): Superconductivity in hydrogen dominant materials: Silane. In *SCIENCE* 319 (5869), pp. 1506–1509. DOI: 10.1126/science.1153282.

[28]. Eremets, M. I.; Troyan, I. A. (2011): Conductive dense hydrogen. In *NATURE MATERIALS* 10 (12), pp. 927–931. DOI: 10.1038/NMAT3175.

[29]. Eremets, M. L.; Hemley, R. J.; Mao, H.; Gregoryanz, E. (2001): Semiconducting non-molecular nitrogen up to 240 GPa and its low-pressure stability. In *Nature* 411 (6834), pp. 170–174.

[30]. Errea, Ion; Calandra, Matteo; Mauri, Francesco (2013): First-Principles Theory of Anharmonicity and the Inverse Isotope Effect in Superconducting Palladium-Hydride Compounds. In *PHYSICAL REVIEW LETTERS* 111 (17). DOI: 10.1103/PhysRevLett.111.177002.

[31]. Errea, Ion; Calandra, Matteo; Pickard, Chris J.; Nelson, Joseph; Needs, Richard J.; Li, Yinwei et al. (2015): High-Pressure Hydrogen Sulfide from First Principles: A Strongly Anharmonic Phonon-Mediated Superconductor. In *PHYSICAL REVIEW LETTERS* 114 (15). DOI: 10.1103/PhysRevLett.114.157004.

[32]. Errea, Ion; Calandra, Matteo; Pickard, Chris J.; Nelson, Joseph; Needs, Richard J.; Li, Yinwei et al. (2015): High-Pressure Hydrogen Sulfide from First Principles: A Strongly Anharmonic Phonon-Mediated Superconductor. In *PHYSICAL REVIEW LETTERS* 114 (15). DOI: 10.1103/PhysRevLett.114.157004.

[33]. Evans, D. A.; Roberts, O. R.; Williams, G. T.; Vearey-Roberts, A. R.; Bain, F.; Evans, S. et al. (2009): Diamond-metal contacts: interface barriers and real-time characterization. In *JOURNAL OF PHYSICS-CONDENSED MATTER* 21 (36). DOI: 10.1088/0953-8984/21/36/364223.

[34]. Feng, Yejun; Silevitch, D. M.; Rosenbaum, T. F. (2014): A compact bellows-driven diamond anvil cell for high-pressure, low-temperature magnetic measurements. In *REVIEW OF SCIENTIFIC INSTRUMENTS* 85 (3). DOI: 10.1063/1.4867078.

[35]. FORMAN, R. A.; BLOCK, S.; BARNETT, J. D.; PIERMARI.GJ (1972): PRESSURE MEASUREMENT MADE BY UTILIZATION OF RUBY SHARP-LINE LUMINESCENCE. In *SCIENCE* 176 (4032), p. 284-&.

[36]. Fröhlich, H. (1950): Theory of the Superconducting State. I. The Ground State at the Absolute Zero of Temperature. In *Phys. Rev.* 79 (5), pp. 845–856. DOI: 10.1103/PhysRev.79.845.

[37]. Fujihisa, Hiroshi; Yamawaki, Hiroshi; Sakashita, Mami; Nakayama, Atsuko; Yamada, Takahiro; Aoki, Katsutoshi (2004): Molecular dissociation and two low-temperature high-pressure phases of H2S. In *Phys. Rev. B* 69 (21). DOI: 10.1103/PhysRevB.69.214102.

[38]. Gao, Guoying; Hoffmann, Roald; Ashcroft, N. W.; Liu, Hanyu; Bergara, Aitor; Ma, Yanming (2013): Theoretical study of the ground-state structures and properties of niobium hydrides under pressure. In *Phys. Rev. B* 88 (18). DOI: 10.1103/PhysRevB.88.184104.

[39]. Gao, Guoying; Oganov, Artem R.; Bergara, Aitor; Martinez-Canales, Miguel; Cui, Tian; Iitaka, Toshiaki et al. (2008): Superconducting high pressure phase of germane. In *PHYSICAL REVIEW LETTERS* 101 (10). DOI: 10.1103/PhysRevLett.101.107002.

[40]. Gao, Guoying; Oganov, Artem R.; Li, Peifang; Li, Zhenwei; Wang, Hui; Cui, Tian et al. (2010): High-pressure crystal structures and superconductivity of Stannane (SnH4). In *PROCEEDINGS OF THE NATIONAL ACADEMY OF SCIENCES OF THE UNITED STATES OF AMERICA* 107 (4), pp. 1317–1320. DOI: 10.1073/pnas.0908342107.

[41]. Gao, Guoying; Wang, Hui; Bergara, Aitor; Li, Yinwei; Liu, Guangtao; Ma, Yanming (2011): Metallic and superconducting gallane under high pressure. In *PHYSICAL REVIEW B* 84 (6). DOI: 10.1103/PhysRevB.84.064118.

[42]. Gao, L.; Xue, Y. Y.; Chen, F.; Xiong, Q.; Meng, R. L.; Ramirez, D. et al. (1994): Superconductivity up to 164 K in HgBa2Cam−1CumO2m+2+δ (m =1, 2, and 3) under quasihydrostatic pressures. In *Phys. Rev. B* 50 (6), pp. 4260–4263. DOI: 10.1103/PhysRevB.50.4260.

[43]. Goncharenko, Igor; Eremets, M. I.; Hanfland, M.; Tse, J. S.; Amboage, M.; Yao, Y.; Trojan, I. A. (2008): Pressure-induced hydrogen-dominant metallic state in aluminum hydride. In *PHYSICAL REVIEW LETTERS* 100 (4). DOI: 10.1103/PhysRevLett.100.045504.

[44]. Hamlin, J. J. (2015): Superconductivity in the metallic elements at high pressures. In *Physica C: Superconductivity and its Applications* 514, pp. 59–76. DOI: 10.1016/j.physc.2015.02.032.

[45]. Hanfland, M.; Syassen, K. (1985): A Raman study of diamond anvils under stress. In *J. Appl. Phys.* 57 (8), p. 2752. DOI: 10.1063/1.335417.

[46]. Hanfland, Michael; Proctor, John E.; Guillaume, Christophe L.; Degtyareva, Olga; Gregoryanz, Eugene (2011): High-Pressure Synthesis, Amorphization, and Decomposition of Silane. In *PHYSICAL REVIEW LETTERS* 106 (9). DOI: 10.1103/PhysRevLett.106.095503.

[47]. Hird, J. R.; Field, J. E. (2004): Diamond polishing. In *Proceedings of the Royal Society A: Mathematical, Physical and Engineering Sciences* 460 (2052), pp. 3547–3568. DOI: 10.1098/rspa.2004.1339.

[48]. Hirsch, J. E.; Maple, M. B.; Marsiglio, F. (2015): Superconducting materials classes. Introduction and overview. In *Physica C: Superconductivity and its Applications* 514, pp. 1–8. DOI: 10.1016/j.physc.2015.03.002.

[49]. Hou, Pugeng; Tian, Fubo; Li, Da; Zhao, Zhonglong; Duan, Defang; Zhang, HuaDi et al. (2015): Ab initio study of germanium-hydride compounds under high pressure. In *RSC Adv* 5 (25), pp. 19432–19438. DOI: 10.1039/c4ra13183e.

[50]. Hou, Pugeng; Zhao, Xiusong; Tian, Fubo; Li, Da; Duan, Defang; Zhao, Zhonglong et al. (2015): High pressure structures and superconductivity of AlH 3 (H 2) predicted by first principles. In *RSC Adv* 5 (7), pp. 5096–5101. DOI: 10.1039/c4ra14990d.

[51]. Huang, T.-H.; Decius, J. C.; Nibler, J. W. (1977): Raman and IR spectra of crystalline phosphine in the γ phase. In *Journal of Physics and Chemistry of Solids* 38 (8), pp. 897–904. DOI: 10.1016/0022-3697(77)90128-7.

[52]. Ion Errea; Matteo Calandra; Chris J. Pickard; Joseph Nelson; Richard J. Needs; Yinwei Li et al. (2015): Quantum Hydrogen-Bond Symmetrization and High-Temperature Superconductivity in Hydrogen Sulfide. In *arXiv:1512.02933v1*. Available online at http://arxiv.org/abs/1512.02933v1.

[53]. Jin, Xilian; Meng, Xing; He, Zhi; Ma, Yanming; Liu, Bingbing; Cui, Tian et al. (2010): Superconducting high-pressure phases of disilane. In *PROCEEDINGS OF THE NATIONAL ACADEMY OF SCIENCES OF THE UNITED STATES OF AMERICA* 107 (22), pp. 9969–9973. DOI: 10.1073/pnas.1005242107.

[54]. José A. Flores-Livas; Maximilian Amsler; Christoph Heil; Antonio Sanna; Lilia Boeri; Gianni Profeta et al. (2015): Superconductivity in metastable phases of phosphorus-hydride compounds under high pressure arXiv:1512.02132.

[55]. Kometani, Shoji; Eremets, Mikhail I.; Shimizu, Katsuya; Kobayashi, Michihiro; Amaya, Kiichi (1997): Observation of Pressure-Induced Superconductivity of Sulfur. In *J. Phys. Soc. Jpn.* 66 (9), pp. 2564–2565. DOI: 10.1143/JPSJ.66.2564.

[56]. Lev P. Gor'kov; V. Z. Kresin (2015): Pressure and high Tc superconductivity: applications to sulfur hydrides. In *arXiv:1511.06926v2*. Available online at http://arxiv.org/abs/1511.06926v2.

[57]. Li, Yinwei; Gao, Guoying; Xie, Yu; Ma, Yanming; Cui, Tian; Zou, Guangtian (2010): Superconductivity at similar to 100 K in dense SiH4(H-2)(2) predicted by first principles. In *PROCEEDINGS OF THE NATIONAL ACADEMY OF SCIENCES OF THE UNITED STATES OF AMERICA* 107 (36), pp. 15708–15711. DOI: 10.1073/pnas.1007354107.

[58]. Li, Yinwei; Hao, Jian; Liu, Hanyu; Li, Yanling; Ma, Yanming (2014): The metallization and superconductivity of dense hydrogen sulfide. In *JOURNAL OF CHEMICAL PHYSICS* 140 (17). DOI: 10.1063/1.4874158.

[59]. Li, Yinwei; Hao, Jian; Liu, Hanyu; Tse, John S.; Wang, Yanchao; Ma, Yanming (2015): Pressure-stabilized superconductive yttrium hydrides. In *SCIENTIFIC REPORTS* 5. DOI: 10.1038/srep09948.

[60]. Liu, Hanyu; Li, Yinwei; Gao, Guoying; Tse, John S.; Naumov, Ivan Ivanovich (2016): Crystal Structure and Superconductivity of PH 3 at High Pressures. In *J. Phys. Chem. C. DOI:* 10.1021/acs.jpcc.5b12009.

[61]. Mao, H. K. (1981): Electrical resistivity measurements of conductors in the diamond-window, high-pressure cell. In *Rev. Sci. Instrum.* 52 (4), p. 615. DOI: 10.1063/1.1136650.

[62]. Mao, H. K.; Bell, P. M. (1978): HIGH-PRESSURE PHYSICS - SUSTAINED STATIC GENERATION OF 1.36 TO 1.72 MEGABARS. In *SCIENCE* 200 (4346), pp. 1145–1147.

[63]. Martinez-Canales, Miguel; Oganov, Artem R.; Ma, Yanming; Yan, Yan; Lyakhov, Andriy O.; Bergara, Aitor (2009): Novel Structures and Superconductivity of Silane under Pressure. In *PHYSICAL REVIEW LETTERS* 102 (8). DOI: 10.1103/PhysRevLett.102.087005.

[64]. Maxwell, Emanuel (1950): Isotope Effect in the Superconductivity of Mercury. In *Phys. Rev.* 78 (4), p. 477. DOI: 10.1103/PhysRev.78.477.

[65]. McMahon, Jeffrey M.; Ceperley, David M. (2011): High-temperature superconductivity in atomic metallic hydrogen. In *Phys. Rev. B* 84 (14). DOI: 10.1103/PhysRevB.84.144515.

[66]. McMillan, W. L. (1968): Transition Temperature of Strong-Coupled Superconductors. In *Phys. Rev.* 167 (2), pp. 331–344. DOI: 10.1103/PhysRev.167.331.

[67]. Muramatsu, Takaki; Wanene, Wilson K.; Somayazulu, Maddury; Vinitsky, Eugene; Chandra, Dhanesh; Strobel, Timothy A. et al. (2015): Metallization and Superconductivity in the Hydrogen-Rich Ionic Salt BaReH 9. In *J. Phys. Chem. C* 119 (32), pp. 18007–18013. DOI: 10.1021/acs.jpcc.5b03709.

[68]. Nagamatsu, J.; Nakagawa, N.; Muranaka, T.; Zenitani, Y.; Akimitsu, J. (2001): Superconductivity at 39 K in magnesium diboride. In *Nature* 410 (6824), pp. 63–64.

[69]. Nguyen, N.; Studer, F.; Raveau, B. (1983): Oxydes ternaires de cuivre a valence mixte de type K2NiF4 deficitaires en oxygene. Evolution progressive d'un etat semi-conducteur vers un etat semi-metallique des oxydes. In *Journal of Physics and Chemistry of Solids* 44 (5), pp. 389–400. DOI: 10.1016/0022-3697(83)90066-5.

[70]. Nguyen, Ninh; Choisnet, Jacques; Hervieu, Maryvonne; Raveau, Bernard (1981): Oxygen defect K2NiF4-type oxides. The compounds. In *Journal of Solid State Chemistry* 39 (1), pp. 120–127. DOI: 10.1016/0022-4596(81)90310-8.

[71]. Oganov, Artem R.; Lyakhov, Andriy O.; Valle, Mario (2011): How Evolutionary Crystal Structure Prediction Works-and Why. In *ACCOUNTS OF CHEMICAL RESEARCH* 44 (3), pp. 227–237. DOI: 10.1021/ar1001318.

[72]. Ogg, Richard A. (1946): Bose-Einstein Condensation of Trapped Electron Pairs. Phase Separation and Superconductivity of Metal-Ammonia Solutions. In *Phys. Rev.* 69 (5-6), pp. 243–244. DOI: 10.1103/PhysRev.69.243.

[73]. Okuchi, Takuo (2004): A new type of nonmagnetic diamond anvil cell for nuclear magnetic resonance spectroscopy. In *Physics of the Earth and Planetary Interiors* 143-144, pp. 611–616. DOI: 10.1016/j.pepi.2003.07.024.

[74]. Papaconstantopoulos, D. A.; Klein, B. M.; Mehl, M. J.; Pickett, W. E. (2015): Cubic H3S around 200 GPa. An atomic hydrogen superconductor stabilized by sulfur. In *Phys. Rev. B* 91 (18). DOI: 10.1103/PhysRevB.91.184511.

[75]. Pastewka, Lars; Moser, Stefan; Gumbsch, Peter; Moseler, Michael (2011): Anisotropic mechanical amorphization drives wear in diamond. In *NATURE MATERIALS* 10 (1), pp. 34–38. DOI: 10.1038/NMAT2902.

[76]. Pickard, Chris J.; Needs, R. J. (2006): High-pressure phases of silane. In *PHYSICAL REVIEW LETTERS* 97 (4). DOI: 10.1103/PhysRevLett.97.045504.

[77]. Pickard, Chris J.; Needs, R. J. (2011): Ab initio random structure searching. In *JOURNAL OF PHYSICS-CONDENSED MATTER* 23 (5). DOI: 10.1088/0953-8984/23/5/053201.

[78]. Reynolds, C. A.; Serin, B.; Wright, W. H.; Nesbitt, L. B. (1950): Superconductivity of Isotopes of Mercury. In *Phys. Rev.* 78 (4), p. 487. DOI: 10.1103/PhysRev.78.487.

[79]. Rotundu, C. R.; Cuk, T.; Greene, R. L.; Shen, Z.-X.; Hemley, Russell J.; Struzhkin, V. V. (2013): High-pressure resistivity technique for quasi-hydrostatic compression experiments. In *REVIEW OF SCIENTIFIC INSTRUMENTS* 84 (6). DOI: 10.1063/1.4809025.

[80]. Rousseau, Bruno; Bergara, Aitor (2010): Giant anharmonicity suppresses superconductivity in AlH3 under pressure. In *Phys. Rev. B* 82 (10). DOI: 10.1103/PhysRevB.82.104504.

[81]. Sakashita, M.; Yamawaki, H.; Fujihisa, H.; Aoki, K.; Sasaki, S.; Shimizu, H. (1997): Pressure-Induced Molecular Dissociation and Metallization in Hydrogen-Bonded H2S Solid. In *Phys. Rev. Lett.* 79 (6), pp. 1082–1085. DOI: 10.1103/PhysRevLett.79.1082.

[82]. Schilling, A.; Cantoni, M.; Guo, J. D.; Ott, H. R. (1993): Superconductivity above 130 K in the Hg–Ba–Ca–Cu–O system. In *Nature* 363 (6424), pp. 56–58. DOI: 10.1038/363056a0.

[83]. Shamp, A.; Terpstra, T.; Bi, T.; Falls, Z.; Avery, P.; Zurek E. (2016): Decomposition Products of Phosphine UnderPressure: PH2 Stable and Superconducting? J. Am. Chem. Soc.

[84]. Shaplygin et al. (1979): Preparation and Properties of the Compounds Ln2CuO4 (Ln=La, Pr, Nd, Sm, Eu, Gd) and Some of their Solid Solutions. In *Russian Journal of Inor ganic Chem.,* 24, (6), pp 820—824.

[85]. Shimizu, H.; Murashima, H.; Sasaki, S. (1992): High-pressure Raman study of solid deuterium sulfide up to 17 GPa. In *J. Chem. Phys.* 97 (10), p. 7137. DOI: 10.1063/1.463538.

[86]. Shimizu, H.; Yamaguchi, H.; Sasaki, S.; Honda, A.; Endo, S.; Kobayashi, M. (1995): Pressure-temperature phase diagram of solid hydrogen sulfide determined by Raman spectroscopy. In *Phys. Rev. B* 51 (14), pp. 9391–9394. DOI: 10.1103/PhysRevB.51.9391.

[87]. Shimizu, K.; Ishikawa, H.; Takao, D.; Yagi, T.; Amaya, K. (2002): Superconductivity in compressed lithium at 20 K. In *Nature* 419 (6907), pp. 597–599. DOI: 10.1038/nature01098.

[88]. Skoskiewicz, T.; Szafranski, A. W.; Bujnowski, W.; Baranowski, B. (1974): Isotope effect in the superconducting palladium-hydrogen-deuterium system. In *J. Phys. C: Solid State Phys.* 7 (15), pp. 2670–2676. DOI: 10.1088/0022-3719/7/15/015.

[89]. Swift, Robinson M.; White, David (1957): Low Temperature Heat Capacities of Magnesium Diboride (MgB 2) and Magnesium Tetraboride (MgB 4). In *J. Am. Chem. Soc.* 79 (14), pp. 3641–3644. DOI: 10.1021/ja01571a007.

Tappert, R.; Tappert, M. C. (2011): Diamonds in Nature: A Guide to Rough Diamonds. In Ralf Tappert, Michelle C. Tappert, R. Tappert, M. C. Tappert (Eds.): The Origin of Diamonds, pp. 1–142.

[91]. Wang, Hui; Tse, John S.; Tanaka, Kaori; Iitaka, Toshiaki; Ma, Yanming (2012): Superconductive sodalite-like clathrate calcium hydride at high pressures. In *PROCEEDINGS OF THE NATIONAL ACADEMY OF SCIENCES OF THE UNITED STATES OF AMERICA* 109 (17), pp. 6463–6466. DOI: 10.1073/pnas.1118168109.

[92]. Wang, X.; Kamenev, K. V. (2014): Review of modern instrumentation for magnetic measurements at high pressure and low temperature. In *Low Temp. Phys.* 40 (8), pp. 735–746. DOI: 10.1063/1.4892645.

[93]. Wang, Yanchao; Ma, Yanming (2014): Perspective: Crystal structure prediction at high pressures. In *JOURNAL OF CHEMICAL PHYSICS* 140 (4). DOI: 10.1063/1.4861966.

[94]. Wang, Ziwei; Yao, Yansun; Zhu, Li; Liu, Hanyu; Iitaka, Toshiaki; Wang, Hui; Ma, Yanming (2014): Metallization and superconductivity of BeH2 under high pressure. In *JOURNAL OF CHEMICAL PHYSICS* 140 (12). DOI: 10.1063/1.4869145.

[95]. Wei, Yong-Kai; Ge, Ni-Na; Ji, Guang-Fu; Chen, Xiang-Rong; Cai, Ling-Cang; Zhou, Su-Qin; Wei, Dong-Qing (2013): Elastic, superconducting, and thermodynamic properties of the cubic metallic phase of AlH3 via first-principles calculations. In *J. Appl. Phys.* 114 (11), p. 114905. DOI: 10.1063/1.4821287.

[96]. Weir, C. E.; Lippincott, E. R.; van Valkenburg, A.; Bunting, E. N. (1959): Infrared studies in the 1- to 15-micron region to 30,000 atmospheres. In *J. RES. NATL. BUR. STAN. SECT. A.* 63A (1), p. 55. DOI: 10.6028/jres.063A.003.

[97]. Werner M.; Tech. Univ. Berlin, Germany; Dorsch, O.; Baerwind, H.-U.; Obermeier, E.; Johnston, C. et al. (1995): The effect of metallization on the ohmic contact resistivity to heavily B-doped polycrystalline diamond films. In *Electron Devices, IEEE Transactions on* Volume:42 (7). Available online at 10.1109/16.391217.

[98]. Wigner, E.; Huntington, H. B. (1935): On the Possibility of a Metallic Modification of Hydrogen. In *J. Chem. Phys.* 3 (12), p. 764. DOI: 10.1063/1.1749590.

[99]. Xie, Yu; Li, Quan; Oganov, Artem R.; Wang, Hui (2014): Superconductivity of lithium-doped hydrogen under high pressure. In *ACTA CRYSTALLOGRAPHICA SECTION C-CRYSTAL STRUCTURE COMMUNICATIONS* 70, pp. 104–111. DOI: 10.1107/S2053229613028337.

[100]. Zhang, Lijun; Niu, Yingli; Li, Quan; Cui, Tian; Wang, Yi; Ma, Yanming et al. (2007): Ab initio prediction of superconductivity in molecular metallic hydrogen under high pressure. In *Solid State Communications* 141 (11), pp. 610–614. DOI: 10.1016/j.ssc.2006.12.029.

[101]. Zhang, Shoutao; Wang, Yanchao; Zhang, Jurong; Liu, Hanyu; Zhong, Xin; Song, Hai-Feng et al. (2015): Phase Diagram and High-Temperature Superconductivity of Compressed Selenium Hydrides. In *SCIENTIFIC REPORTS* 5. DOI: 10.1038/srep15433.

[102]. Zhong, Guohua; Zhang, Chao; Wu, Guangfen; Song, Jianjun; Liu, Zhuang; Yang, Chunlei (2013): Superconductivity in GeH4(H2)2 above 220GPa high-pressure. In *Physica B: Condensed Matter* 410, pp. 90–92. DOI: 10.1016/j.physb.2012.10.039.

[103]. Zhong, X.; Wang, H.; Zhang, J.; Liu, H.; Zhang, S.; Song, H. et al.: Tellurium Hydrides at High Pressures: High-temperature Superconductors. In *arXiv:1503.00396v3*.

[104]. Zhou, Dawei; Jin, Xilian; Meng, Xing; Bao, Gang; Ma, Yanming; Liu, Bingbing; Cui, Tian (2012): Ab initio study revealing a layered structure in hydrogen-rich KH 6 under high pressure. In *Phys. Rev. B* 86 (1). DOI: 10.1103/PhysRevB.86.014118.